

AD-A267 950 NTATION PAGE

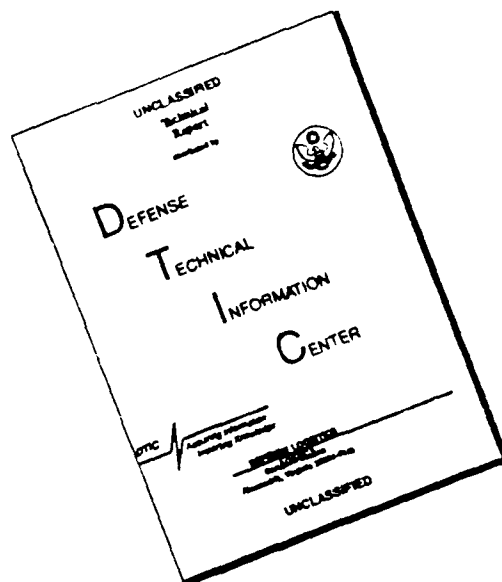
Form Approved
OMB No. 0704-0188



ated to a deadline for response, including the time for reviewing instructions, searching existing data sources, reviewing the collection of information. Send comments regarding this burden estimate or any other aspect of this burden to Washington Headquarters Services, Directorate for Information Operations and Reports, 1215 Jefferson Office Building, Management and Budget, Paperwork Reduction Project (0704-0188), Washington, DC 20503.

1. AGENCY USE ONLY (Leave blank)		2. REPORT DATE 1993		3. REPORT TYPE AND DATES COVERED THESIS/DISSERTATION	
4. TITLE AND SUBTITLE Mesoscale Frontogenesis: An Analysis of Two Cold Front Case Studies.				5. FUNDING NUMBERS	
6. AUTHOR(S) William J. Spendley Jr.					
7. PERFORMING ORGANIZATION NAME(S) AND ADDRESS(ES) AFIT Student Attending: North Carolina State Univ				8. PERFORMING ORGANIZATION REPORT NUMBER AFIT/CI/CIA 93-037	
9. SPONSORING/MONITORING AGENCY NAME(S) AND ADDRESS(ES) DEPARTMENT OF THE AIR FORCE AFIT/CI 2950 P STREET WRIGHT-PATTERSON AFB OH 45433-7765				10. SPONSORING / MONITORING AGENCY REPORT NUMBER	
11. SUPPLEMENTARY NOTES					
12a. DISTRIBUTION / AVAILABILITY STATEMENT Approved for Public Release IAW 190-1 Distribution Unlimited MICHAEL M. BRICKER, SMSgt, USAF Chief Administration				12b. DISTRIBUTION CODE	
13. ABSTRACT (Maximum 200 words)					
<p>DTIC SELECTE S B D AUG 17 1993</p> <p style="text-align: right;">93-19038</p>					
14. SUBJECT TERMS				15. NUMBER OF PAGES 112	
				16. PRICE CODE	
17. SECURITY CLASSIFICATION OF REPORT		18. SECURITY CLASSIFICATION OF THIS PAGE		19. SECURITY CLASSIFICATION OF ABSTRACT	
				20. LIMITATION OF ABSTRACT	

DISCLAIMER NOTICE



THIS DOCUMENT IS BEST
QUALITY AVAILABLE. THE COPY
FURNISHED TO DTIC CONTAINED
A SIGNIFICANT NUMBER OF
PAGES WHICH DO NOT
REPRODUCE LEGIBLY.

ABSTRACT

SPENDLEY, WILLIAM J. JR. Mesoscale Frontogenesis: An Analysis of Two Cold Front Case Studies. (Under the direction of Dr. Allen J. Riordan.)

A comparative analysis of mesoscale- β frontogenesis is presented for two case studies of cold fronts that originated west of the Appalachians and moved across North Carolina during the Genesis of Atlantic Lows Experiment (GALE). The evolution of the fronts is depicted with a detailed three-dimensional analysis. The two cold fronts are compared to the classic model of fronts established by the Norwegian school.

Diagnostic computations of divergence, vorticity, dynamical forces and frontogenesis were performed. The individual contributions of shear, confluence, and diabatic terms were determined to assess their relative importance in frontogenetical forcing.

The diabatic process of differential cloud shading and its thermal impact at the surface contributed significantly to the development of a zone of strong temperature gradient ahead of both wind shift lines. A more extensive cloud free area contributed to more widespread diabatic forcing in case 1 as compared to case 2.

Meteograms, satellite imagery and diagnostic computations of divergence, vorticity and frontogenesis confirm that only the extreme eastern portion of both wind shift lines over the coastal

plain and adjacent waters of North Carolina remained active and well-defined. The confluence term dominated frontogenetical forcing over this region. It is hypothesized that the pre-existing baroclinic zone over the cold Atlantic shelf waters had a pronounced influence on the regeneration of the frontal boundaries along extreme eastern North Carolina. Results of other relevant studies confirm this possibility.

The dynamical force balance and parcel trajectories were computed at selected times. The pressure gradient was the dominant force, and parcel accelerations appeared to be the result of parcels moving from stronger pressure gradient areas into weaker ones.

DTIC QUALITY INSPECTED 3

Accession For		6
NTIS GRA&I	<input checked="" type="checkbox"/>	
DTIC TAB	<input type="checkbox"/>	
Unannounced	<input type="checkbox"/>	
Justification		
By		
Distribution/		
Availability Codes		
Avail and/or		
Dist	Special	
A-1		

**Mesoscale Frontogenesis: An Analysis
of Two Cold Front Case Studies**

by
William J. Spendley Jr.

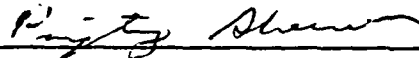
A thesis submitted to the Graduate Faculty of
North Carolina State University
in partial fulfillment of the
requirements for the Degree of
Master of Science

Department of Marine, Earth, and Atmospheric Sciences

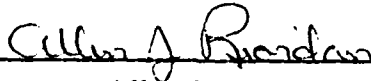
Raleigh
1993



Gerald F. Watson



Ping Tung Shaw



Allen J. Riordan

Chairman of Advisory Committee

ACKNOWLEDGEMENTS

ii

The author would like to thank the United States Air Force for funding my education and providing this outstanding opportunity. I would also like to recognize the efforts of several individuals who provided invaluable assistance to me. I would like to extend my sincere appreciation to Steve Chiswell for his computer knowledge and expertise and to thank him for the programs and subroutines which made this research possible. He solved every problem that I asked him. I would like to thank my peers for being there for me during the difficult times. I want to extend a very heartfelt thanks to my girlfriend, Shannon Werndli, who I love very much and bore the burden of my long hours at the office. Without her, the completion of my research would not have been possible. I owe Dr. Allen J. Riordan a great deal. I would like to thank him for instilling me with confidence, teaching me, guiding me, encouraging me, working with me, and supporting me all the time. It is clear to me after completing my research that I selected an outstanding scientist and person to be my advisor. I would also like to especially thank him for the recommendation which ultimately led to my selection as an instructor at the United States Military Academy.

TABLE OF CONTENTS

iii

List of figures.....	iv
1. Introduction.....	1
2. Literature review.....	3
3. Research goals and objectives.....	12
4. Data sources.....	14
5. Methodology.....	16
6. Synoptic overview case 1.....	20
7. Synoptic overview case 2.....	24
8. Mesoscale analysis case 1.....	28
9. Mesoscale analysis case 2.....	43
10. Frontogenetical forcing.....	56
11. Diabatic frontogenesis.....	81
12. Dynamical forces.....	90
13. Summary and conclusions.....	99
14. Future research.....	104
References.....	106

LIST OF FIGURES

iv

	<u>Page</u>
Figure 1. Location of PAM Stations.....	15
Figure 1.1. Confluence term 1900 UTC 7 March 1986.....	19
Figure 1.2. Confluence term 1900 UTC 7 March 1986.....	19
Figure 2. NMC surface analysis 0900 UTC 7 March 1986.....	21
Figure 3. Same as figure 2 except for 1200 UTC 7 March 1986.....	21
Figure 4. Same as figure 2 except for 1500 UTC 7 March 1986.....	21
Figure 5. Same as figure 2 except for 1800 UTC 7 March 1986.....	21
Figure 6. 850 mb analysis for 1200 UTC 7 March 1986.....	23
Figure 7. Vertical cross-section 1200 UTC 7 March 1986.....	23
Figure 8. NMC surface analysis for 1200 UTC 21 February 1986.....	25
Figure 9. Same as figure 8 except 1500 UTC 21 Feb 1986.....	25
Figure 10. Same as figure 8 except for 1800 UTC 21 Feb 1986.....	25
Figure 11. Same as figure 8 except for 0000 UTC 22 Feb 1986.....	25
Figure 12. Same as figure 8 except for 0300 UTC 22 Feb 1986.....	25
Figure 13. Same as figure 6 except for 1200 UTC 21 Feb 1986.....	25
Figure 14. Vertical cross-section for 0000 UTC 22 Feb 1986.....	28
Figure 15. Mesoscale surface analysis for 1200 UTC 7 Mar 1986.....	33
Figure 16. Same as figure 15 except for 1500 UTC 7 Mar 1986.....	33
Figure 17. Meteogram for PAM 34 from 15-1800 UTC 7 Mar 1986..	35
Figure 18. Same as figure 17 except for 17-2000 UTC 7 Mar 1986...	35
Figure 19. Meteogram for PAM 39 from 15-1800 UTC 7 Mar 1986..	36
Figure 20. Meteogram for PAM 31 from 20-2300 UTC 7 Mar 1986..	36
Figure 21. Meteogram for PAM 10 from 19-2200 UTC 7 Mar 1986..	37
Figure 22. Same as figure 15 except 1800 UTC 7 Mar 1986.....	37

Figure 23. IR satellite imagery for 1501 UTC 7 Mar 1986.....	38
Figure 24. Same as figure 15 except for 2200 UTC 7 Mar 1986.....	40
Figure 25. Meteogram for PAM 45 from 20-2300 UTC 7 Mar 1986..	42
Figure 26. IR satellite imagery for 2101 UTC 7 Mar 1986.....	42
Figure 27. Same as figure 15 except for 1200 UTC 21 Feb 1986.....	44
Figure 28. Radar summary for 1335 UTC 21 Feb 1986.....	44
Figure 29. Visible satellite imagery at 1430 21 Feb 1986.....	46
Figure 30. Same as figure 15 except for 1500 UTC 21 Feb 1986.....	47
Figure 31. Same as figure 15 except for 1800 UTC 21 Feb 1986.....	47
Figure 32. Same as figure 15 except for 2300 UTC 21 Feb 1986.....	49
Figure 33. Meteogram PAM 47 from 03-0600 UTC 22 Feb 1986.....	49
Figure 34. Same as figure 15 except for 2200 UTC 21 Feb 1986.....	50
Figure 35. Same as figure 15 except for 0300 UTC 22 Feb 1986.....	50
Figure 36. Radar summary for 0235 UTC 22 Feb 1986.....	52
Figure 37. Total adiabatic frontogenesis for 1900 UTC 7 Mar 1986..	61
Figure 38. Confluence term for 1900 UTC 7 Mar 1986.....	61
Figure 39. Geostrophic frontogenesis for 1900 UTC 7 Mar 1986.....	65
Figure 40. Divergence field for 1900 UTC 7 Mar 1986.....	65
Figure 41. Vorticity field for 1900 UTC 7 Mar 1986.....	66
Figure 42. Total adiabatic frontogenesis for 2000 UTC 7 Mar 1986..	66
Figure 43. Shear term 2000 UTC 7 Mar 1986.....	68
Figure 44. Geostrophic frontogenesis for 2000 UTC 7 Mar 1986.....	68
Figure 45. Divergence field for 2000 UTC 7 Mar 1986.....	70
Figure 46. Vorticity field for 2000 UTC 7 Mar 1986.....	70
Figure 47. Total adiabatic frontogenesis for 2300 UTC 7 Mar 1986..	71

Figure 48. Divergence field for 2200 UTC 7 Mar 1986.....	71
Figure 49. Divergence field for 2300 UTC 7 Mar 1986.....	72
Figure 50. Shear term for 2300 UTC 7 Mar 1986.....	72
Figure 51. Confluence term for 0200 UTC 22 Feb 1986.....	75
Figure 52. Total frontogenesis for 0200 UTC 22 Feb 1986.....	75
Figure 53. Divergence field for 0200 UTC 22 Feb 1986.....	77
Figure 54. Vorticity field for 0200 UTC 22 Feb 1986.....	77
Figure 55. Divergence field for 0300 UTC 22 Feb 1986.....	78
Figure 56. Vorticity field for 0300 UTC 22 Feb 1986.....	78
Figure 57. Total diabatic heating for 1600 UTC 7 Mar 1986.....	87
Figure 58. Diabatic Frontogenesis for 1600 UTC 7 Mar 1986.....	87
Figure 59. Shear term for 1600 UTC 7 Mar 1986.....	88
Figure 60. Confluence term for 1600 UTC 7 Mar 1986.....	88
Figure 61. Total frontogenesis for 1600 UTC 7 Mar 1986.....	89
Figure 62. Geostrophic winds for 2100 UTC 7 Mar 1986.....	93
Figure 63. Mesoscale surface analysis for 2100 UTC 7 Mar 1986.....	93
Figure 64. Dynamic force balance at 2100 UTC and selected parcel trajectories from 20-2200 UTC 7 Mar 1986.....	95
Figure 65. Same as Fig. 64 except for 0400 UTC 22 Feb 1986.....	97

1. INTRODUCTION

Surface fronts have been observed and studied as important meteorological phenomena since the turn of the century. Many of these studies have revealed the importance of fronts to associated cloud and precipitation patterns, cold air outbreaks, severe weather development and rapid local changes in the weather. These phenomena are related to rapid changes in meteorological variables across and along frontal boundaries.

The ability to accurately forecast frontal conditions requires a detailed knowledge of their movement and structure on all scales of motion. Unfortunately, forecast models mainly exist for synoptic and larger scales with their utility for mesoscale systems largely unproved (Smith et al., 1986). If the routinely available automated guidance is used exclusively, the result is that early clues to significant development of frontal features on smaller scales is often overlooked.

Making accurate local forecasts depends strongly on an analysis and understanding of frontal systems on the mesoscale. Several different types of frontal-like boundaries examined at the mesoscale have been identified in previous studies. These include pressure-jump lines, gust fronts, radar thin lines, arc cloud lines, sea breezes, and gravity currents. Intersecting arc cloud lines which can produce severe thunderstorms exemplify the importance of mesoscale frontal structures.

Forecasters also face the difficulty of forecasting the behavior of fronts moving over mountains and complex terrain. Fronts are often observed to be deformed, slowed down, and blocked when crossing steep topography. Flow over irregular topography also generally produces a spectrum of mesoscale waves important to the transfer of heat, energy, and momentum from smaller scales to larger scales and vice versa.

One of the main objectives of the Genesis of Atlantic Lows Experiment (GALE) conducted in 1986 was to describe the airflow, mass, and moisture fields in east coast winter storms with a special emphasis on mesoscale processes. On 22 February and 7 March 1986, two cold fronts passed through the Portable Automated Mesonet (PAM) network in eastern North and South Carolina during GALE. This dense network of automated surface stations provided the rare temporal and spatial resolution commensurate with studying fronts and frontogenesis at the meso- β level. The current research attempts to capitalize on this special observation system and to study two fronts which had crossed the Appalachian Mountains.

2. LITERATURE REVIEW

Surface fronts have been recognized and studied as important features of atmospheric structure since the early part of the twentieth century. The history of the theory that mid-latitude cyclones are driven primarily by latent heat release in ascending air, known as thermal theory, was replaced by the polar-front cyclone model of the Bergen school following World War I (Bjerknes 1919, Bjerknes and Solberg, 1921,1922). They proposed that available potential energy provided by the temperature contrast between polar and tropical air masses at the polar front was the initial source for cyclogenesis.

The polar-front theory has also been referred to as the Wedge Model of fronts, and frontal surfaces were considered to be sloping material surfaces with zero-order discontinuities in temperature, density, and along-front wind components. J. Bjerknes (1919) concluded that the extratropical cyclone contained two principal lines of convergence which meet at the low pressure center and marked the boundary of warm air or the "warm sector".

Further development of this cyclone model by Bjerknes and Solberg (1922) and Bergeron (1928) provided the empirical background for the revolutionary wave theory of cyclones. These authors explained that the boundary surface separating tropical and polar air masses is the seat of shearing instability which gives rise to wave disturbances, and is the source of solenoidal energy

transformed into kinetic energy as the storm intensifies. For theoretical purposes, they treated the front as a zero-order discontinuity in temperature. In the absence of upper air data, it was assumed from cloud observations that this discontinuity extended to the upper atmosphere.

With the introduction of upper air soundings in the 1930's and the direct observation of fronts in the free atmosphere, no evidence of abrupt discontinuities was discovered. It became apparent that frontal structure was more complex and diffuse than first postulated by scientists of the Norwegian School. Bjerknes and Palmen (1937), Palmen (1948), and Palmen and Newton (1948) studied the three-dimensional aspects of frontal structure and discovered the existence of sloping transition-zone boundaries extending to the upper levels rather than abrupt discontinuities.

At this time, the zone model of fronts, otherwise referred to as baroclinic instability theory, also came into existence (Charney, 1947). Fronts were thought of as regions of pronounced temperature gradients which formed in response to wave amplification. Thus, it was realized around this time that cyclogenesis and frontogenesis were inseparable processes. Until the late 1940's and early 50's, minor modifications and refinements to the cyclone model appeared, but the basic features remained the same. Baroclinic theory did not replace polar-front theory.

The baroclinic theory was also connected to the development of quasi-geostrophic theory. Meteorologists first applied this theory to compute vertical motion fields and to determine rates of cyclone development. It was also applied theoretically to studies of baroclinic instability originating with Charney (1947) and Eady (1949).

Another area pertinent to frontal research was the isolation of kinematic processes which lead to the intensification of the gradient of potential temperature. Bergeron (1928) and Pettersen (1936) determined that horizontal deformation fields concentrate potential temperature contrast with respect to a point if the angle between the axis of dilatation in the wind field and the isentropes is less than 45° . The first quantitative description of this phenomenon was founded by Pettersen (1940) and Miller (1948). Pettersen (1935) showed that frontogenesis was favored near the axis of dilatation in a deformation field, and Pettersen and Austin (1942) discovered the importance of cyclonic wind shear as a frontogenetical process.

Until 1953, frontogenesis studies examined only the field of horizontal motion, since the lack of data resolution in the vertical prevented a complete assessment of the three-dimensional frontal structure. Finally, in 1953 the US Air Force and US Weather Bureau set up a dense network of radiosonde stations for the first time, and with it came a new opportunity for a detailed three-dimensional investigation of frontal structure and behavior. Sanders (1955) used

this opportunity to present tilting and convergence contributions to frontogenesis as fields rather than as single point calculations, and to verify the findings of Reed and Sanders (1953) who had established the importance of the tilting term in upper level frontogenesis. Newton (1954) discovered that different frontogenetic processes are important at different levels. In particular, Newton noted the importance of divergence at the surface and the tropopause.

All of these quantitative studies were conducted at the synoptic scale due to the temporal and spatial resolution afforded by the data networks. Even in the modern era, a lack of spatial and temporal resolution in data coverage has hindered the understanding of frontogenetic processes at the mesoscale level.

In addition, up until this time diabatic effects were assumed to be negligible. The contribution of the physical process is, however, contained in the Miller (1948) frontogenesis formulation. On the mesoscale, this process may be relatively important.

Many different forms of Petterssen's and Miller's frontogenesis equations are used extensively even today. Kinematic approaches to the study of frontogenesis are useful for physically describing the processes. With the advent of quasigeostrophic theory, major advances have been made since the late 1960's in the understanding of frontogenetic processes in baroclinic waves.

It was about this time that a diagnostic approach for determining vertical motions was implemented. A diagnostic equation developed

by Sawyer (1956) and Eliassen (1962) applied quasi-geostrophic theory and related the ageostrophic circulation to patterns of geostrophic deformation acting on the cross-and along-front thermal contrasts. Frictional and diabatic processes were included. This diagnostic approach is based on a set of physical approximations later formalized in semi-geostrophic theory (Hoskins, 1975).

Stone (1966), Williams and Plotkin (1968), Williams (1968), and Hoskins and Bretherton (1972) were among the first to conduct dynamical investigations of frontogenesis using quasi- and semi-geostrophic theory. Until this time, kinematic approaches contributed to the understanding of frontogenetical processes, but were unable to isolate and explain the dynamical forcing mechanisms responsible for the creation and dissipation of fronts. The studies cited above attempted to isolate and explain the interactions between the wind and thermal fields and the diabatic and frictional processes. For example, Hoskins and Bretherton (1972) discovered that ageostrophic contributions to frontogenesis become important to the formation of a discontinuity when the relative vorticity at the earth's surface is of a magnitude comparable to the Coriolis parameter. This and other simplified semi-geostrophic models, with idealized initial conditions imposed, indicated that dissipation and surface friction were required to offset frontogenetic forcing by the vertical stretching of vorticity near the surface in order to achieve a balanced state. Hoskins and West (1979) also relied upon dissipative effects to limit frontal development in their three-dimensional

simulations of cold fronts using the semi-geostrophic system of equations.

However, as the work of McWilliams and Gent (1980) and Blumen (1980) suggest, semigeostrophic equations may fail to simulate important ageostrophic effects on frontal dynamics. It was discovered that the ageostrophic contribution could be of even greater importance than dissipation in balancing frontogenetic growth by opposing the unbounded vorticity stretching characteristic of the semi-geostrophic models of frontogenesis.

Ross and Orlanski (1982) went a step further than semi-geostrophic theory and sought to investigate this ageostrophic phenomenon by applying a complete primitive equation set. They discovered that a phase shift occurs between a line of maximum surface convergence and the maximum vertical component of relative vorticity at the surface. This is induced by the contribution of positive ageostrophic vorticity to the divergence field which leads to vorticity shrinking and inhibits frontogenetic growth. This is a significant finding because progress in describing the dynamic balances which characterize mature fronts has been limited in spite of major advances in the understanding of frontogenetic processes.

The effects of diabatic heating as a forcing mechanism for frontogenesis is another area of research requiring emphasis in the future. Sawyer (1956) and Eliassen (1959) showed that condensational heating can intensify the vertical circulation across

the front. Hoskins and Bretherton (1972) prescribed the latent heat release in a semi-geostrophic model of frontogenesis and found that weak heating strengthens frontogenesis and produces larger vertical velocities. Hoskins (1974) included latent heat release proportional to the vertical divergence at low levels in a two-dimensional numerical model with friction and also found that the field of rising motion is intensified. Ross and Orlanski (1978) addressed the surface heating effect in terms of its ability to erode low-level capping inversions.

Williams, Chou and Cornelius (1981) included large-scale condensation and a convective adjustment parametrization in a time-dependent, two-dimensional numerical model, and found that latent heat release is predominately due to large-scale precipitation rather than cumulus convection. They found that this latent heat release may contribute to the development of intense baroclinic zones above the planetary boundary layer which act to strengthen the front aloft and not at the surface. They also discovered that this heating intensifies the vertical circulation with the strongest vertical motion occurring in the mid-troposphere above the surface front.

Bannon and Mak (1984) studied diabatic quasi-geostrophic frontogenesis and showed that only surface heating can directly alter the surface temperature field and that condensational heating can have an indirect effect through induced ageostrophic surface convergence. They also verified previous findings of Williams et al. (1981) that condensational heating greatly intensifies frontogenesis

aloft and strengthens the cross-frontal circulation, in addition to the fact that the heating increases static stability near the cloud base and decreases it near the cloud top. Segal et al. (1992) assessed the thermal impact of differential cloud shading across a cold front at the surface and concluded that it may provide a pronounced contribution to frontogenesis for weak and moderate cold fronts.

It is apparent from the major research findings cited above that during the past half century, synoptic meteorologists have expanded the knowledge of the dynamics and structure of fronts. In addition, models such as the semi-geostrophic frontogenesis model of Hoskins and Bretherton have been successfully developed and applied by researchers. However, no one comprehensive conceptual model has taken over as a totally suitable replacement for the polar-front cyclone model, and one which will provide the framework and frontal symbology for operational and research meteorologists.

Unfortunately, a comprehensive model integrating the research findings over the past half-century with the widely accepted polar-front cyclone model does not exist. Synoptic analysis techniques have not evolved in parallel with the increased understanding of cyclone structure and dynamics. Operational and research meteorologists often interpret observational data through the Bergen School viewpoint, sometimes incorrectly forcing "non-classic" developments into the Bergen School mold and not exploring discrepancies with the Norwegian cyclone model (Mass, 1991). In spite of impressive gains in attempting to modify and improve upon the Cyclone model,

there is still no comprehensive picture of the three-dimensional structure and evolution of midlatitude cyclones that draws together the collective insights of the past 70 years. Meteorologists are still faced with a confusing array of unconnected ideas regarding cyclone and frontal structure and development.

The ideas recommended by Mass (1991) focus on the continued emphasis of conducting more numerical and observational studies. The integration of research findings from current, past, and future studies to achieve an improved conceptual model may eventually lead to new or improved analysis techniques.

3. RESEARCH GOALS AND OBJECTIVES

Since cold fronts have been studied from the turn of the century, many research findings have been added to the great body of knowledge governing frontal structure and behavior. However, due to the complex nature of the front, a continued need exists to increase our understanding of this distinct atmospheric feature, especially on the mesoscale.

In past studies of fronts, shortfalls have existed in the description and explanation of diabatic heating effects on frontogenesis. In many instances, the diabatic heating effect has been neglected due to the difficulty in computing it. The lack of mesoscale observational case studies, on the other hand, can be attributed to the infrequent availability of dense observational networks. However, important mesoscale processes occur which govern cold frontal structure and behavior.

This study will focus on the use of surface observations from the Portable-Automated-Mesonet (PAM) network which provided the spatial and temporal resolution required to permit an investigation of mesoscale- β surface frontogenesis for two case studies. The study will include an examination of diabatic effects on surface frontogenesis at selected times. In addition to enhancing our understanding of the structure and behavior of surface cold fronts at short time and space scales, the results of this research may aid

weather forecasters with local forecasts under operational conditions. The specific research objectives of this study are to:

A) Conduct a comparative analysis of two case studies with a three-dimensional depiction of the structure and evolution of the two cold fronts.

B) Compare and contrast the evolution of the two cold fronts with classic frontal theory.

C) Evaluate kinematic mesoscale- β surface frontogenesis for both cases by comparing and contrasting the evolution of dominant frontogenetical processes.

D) Explain the dynamical forces at the surface responsible for the evolution of surface frontogenesis for each case.

E) Document the diabatic contributions of surface heating to frontogenesis at selected times for both cases.

Since this study examines fronts on the mesoscale level and after crossing the Appalachian Mountains, one would anticipate that the evolution of the two fronts would deviate from classic theory. One might expect disorganization initially and then possible reorganization downstream. Understanding this non-classical development is one of the major goals of this research. It is hoped that the compilation of similar studies in this region could provide the groundwork for the eventual development of a conceptual model of fronts passing through North Carolina.

4. DATA SOURCES

Data used for this study were obtained from the Genesis of Atlantic Lows Experiment (GALE). Data were collected from three main geographical regions with both standard and special measuring systems.

The Regional GALE area was approximately 1000 km wide from the ridge of the Appalachian mountains to 500 km off shore, and extended 1500 km from Florida to New Jersey. Special observing systems in this area provided data used in the present research, and included standard surface stations, and rawinsonde sites with an increased frequency of observations.

The Inner GALE area included the Portable-Automated-Mesonet (PAM) II surface observing stations and ships, buoys, and the Cross-Chain Loran Atmospheric Sounding System (CLASS) rawinsonde sites (Dirks et. al.,1988). The inner GALE area was approximately 500 km wide, centered on the coast of North and South Carolina, and extended 1,000 km from Georgia to Virginia. This area of concentrated observation systems was especially important to the research, because Meso- β frontal processes could be resolved.

Surface measurements from PAM II stations were the single most important data for the successful completion of the proposed study. The PAM II network was designed to provide high temporal - and spatial-resolution measurements and consisted of 5-minute

average values of pressure, temperature, dewpoint temperature, wind velocity and precipitation for 50 stations in North and South Carolina, and Virginia (Dirks et. al., 1988). Fig. 1 shows the location of these stations within the network. The average station spacing of 68 km permitted the resolution of meso- β structure on the order of 140 km.

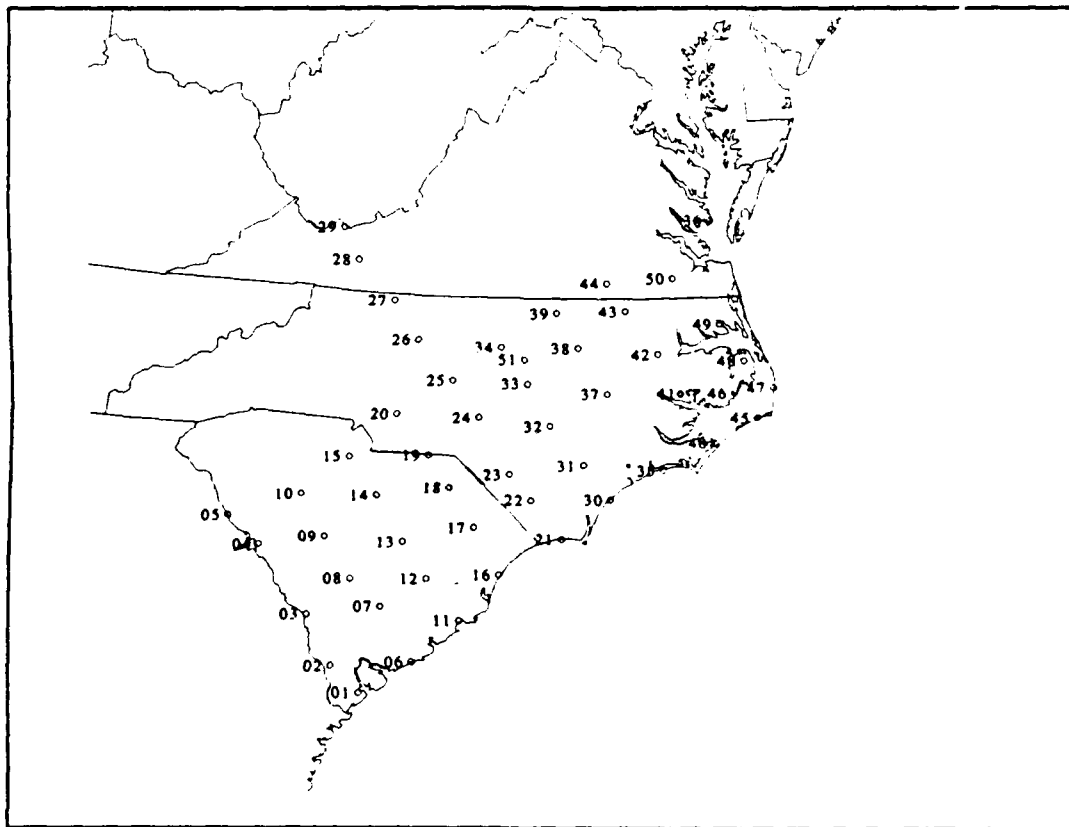


Figure 1. Location of the 50 stations within the PAM data network.

The regular National Weather Service surface hourly data were also used in this study. Vertical soundings taken at 3 to 6-hourly intervals enhanced the usual temporal frequency. National Weather Service stations within the PAM II network improved the resolution of mesoscale level processes. In addition, the National Weather Service stations surrounding the PAM network were useful in extending subjective and objective analyses beyond the PAM network boundaries.

5. METHODOLOGY

GEMPAK version 5.0 Meteorological and Analysis Software was used to plot all observations and gridded data fields, as well as to contour all fields with the exception of mesoscale surface analysis and vertical cross-sections. For example, surface maps were generated by GEMPAK which plotted the temperature, surface potential temperature, dewpoint temperature, altimeter setting, and wind direction and speed. Mesoscale surface analysis of altimeter setting (every 2 mb), surface potential temperature (every 2 K), and frontal position were done by hand and for each hour of the analysis period. GEMPAK was also used to plot sounding data for the 1200 and 0000 UTC times, and then several vertical cross-sections perpendicular to the cold fronts were constructed by hand.

GEMPAK software was used to analyze all other fields including gridded and contoured frontogenesis, vorticity, divergence, vertical velocity, and gridded vector fields. Data were first interpolated to a

30 x 30 grid with a mean grid spacing of 37.2 km in the east-west direction and 36.2 km in the north-south direction. A two-pass Barnes Objective Analysis scheme with a convergence parameter of 0.3 was employed (Barnes, 1964, 1973). The purpose of this interpolation was to provide a grid of regularly spaced data for the finite-difference calculations of horizontal derivatives used to compute quantities mentioned above. The interpolation, however, did not reduce the resolvable wavelength scale which was determined by the station spacing of the original observations.

A small sample of each GEMPAK derived quantity computed was cross checked. Derived quantities were computed by hand for specific points using appropriate finite-difference formulas. Each of these quantities was compared to the values generated by GEMPAK for validation.

Hourly surface data which included the on-the-hour PAM observation and the routine National Weather Service data were used for mesoscale diagnostic computations. Also considered was a time smoothed value of PAM data over a specified interval and based on an average of 5-minute observations. However, the single 5-minute averaged observation is more nearly compatible with the National Weather Service observation. It was necessary to test whether noise and variability in the 5-minute averaged observation, especially in the winds could interfere with discernible meteorological signals. Several diagnostic fields were computed using the regular 5-minute averaged data and the data with 10, 15,

20, 25, and 30-minute smoothing applied. Very little variability was detected between all of the fields seen in Figs. 1.1 & 1.2. Therefore, it was decided that the top-of-the-hour PAM observation would be used without further temporal smoothing.

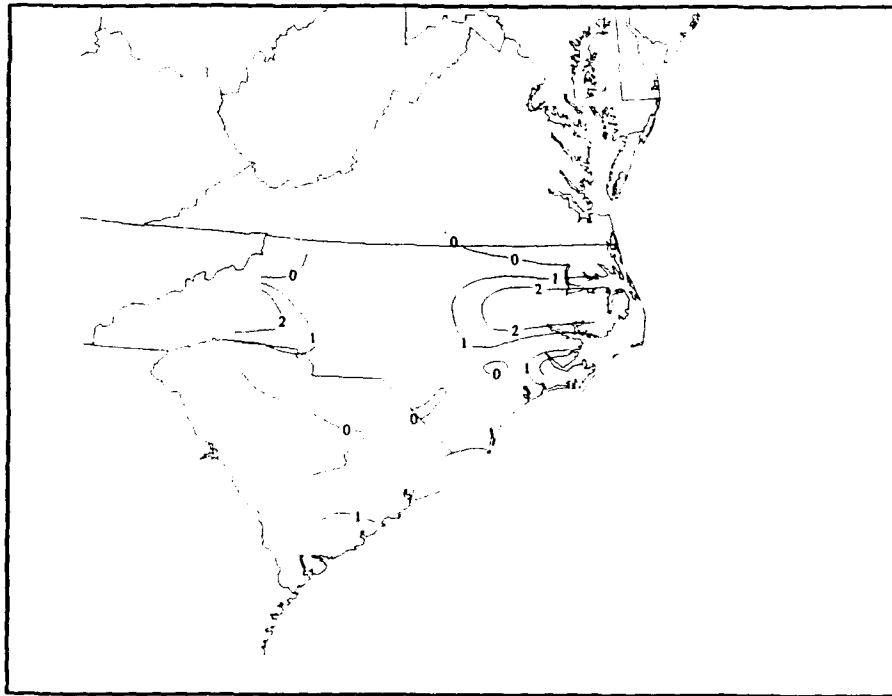


Figure 1.1. Confluence term frontogenesis for 1900 UTC 7 March 1986 using 5-minute averaged values. Units in $10^{-9} \text{ k m}^{-1} \text{ s}^{-1}$.

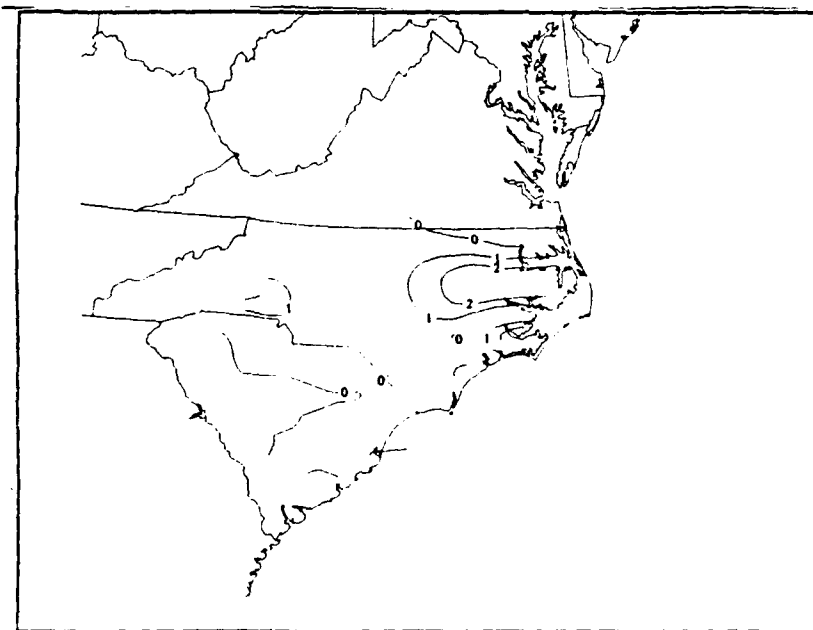


Figure 1.2. Confluence term frontogenesis for 1900 UTC 7 March 1986 using 20-minute time averaging. Same units as fig. 1.1.

6. SYNOPTIC OVERVIEW CASE 1

A series of NMC surface analyses beginning with 0900 UTC on 7 Mar 86 shows the major pressure centers, primary synoptic scale frontal features, and their movement. The 0900 UTC NMC analysis in Fig. 2 depicts a deep low pressure center off the Nova Scotia coast with a central pressure of 976 mb and a strong area of high pressure (1036 mb) over the midwestern United States. A strong pressure gradient between these centers was well established along the northern portion of a cold front which extended southwestward from central New England to the mid-Atlantic seaboard and then westward through northern Virginia and across the Appalachians. The 1200 UTC analysis in Fig. 3 shows that the front has moved southward slowly with an average speed of 3 m s^{-1} . In fact, the portion of the cold front approaching the Appalachians appeared to be quasi-stationary. The pressure gradient across the cold front is no longer depicted as a first order discontinuity (isobars show less bending they did at 0900 UTC) and the gradient appears to be weaker.

The cold front moved more rapidly over the next three hours, but the portion of the front moving across the Appalachians appears to move at a relatively slower speed. By 1800 UTC (Fig. 4), the front has crossed the mountains and approached the piedmont of North Carolina. Nine hours later at 0300 UTC, Fig. 5 shows that the front

has moved off the coast of North Carolina and extends back in an east-west line through the Gulf Coast states. In this sequence of analyses, it is clear that the portion of the front east of the mountains has moved a much greater distance southward than the portion west of the mountains which appears to have had its progress impeded. Additionally, subtle anticyclonic curvature of the analyzed frontal boundary can be detected along this portion beginning at about 1800 UTC. Such curvature is indicative of slow movement. The end result is a corresponding change in the frontal orientation from northeast-southwest to a nearly east-west orientation at the end of the period.

The 850mb analysis for 1200 UTC 7 March 1986 shown in Fig. 6 indicates northwest flow over the eastern United States and the Atlantic behind a trough positioned well off the coast (not shown in Fig. 2). The trough provided upper level support for a deep surface low off the Nova Scotia coast and an associated strong cold front which passed through the mid Atlantic seaboard 24-36 h earlier. A secondary cold front, which is the feature of interest, was also associated with the same deep low but did not have a distinct trough at 850mb. Its shallow nature is depicted in Fig. 7 which is a vertical cross section taken perpendicular to the front from Flint, Michigan (FNT) to Charleston, South Carolina (CHS). This figure shows the secondary front underlying the subsiding cold air aloft associated with the primary front offshore, and the merging of the

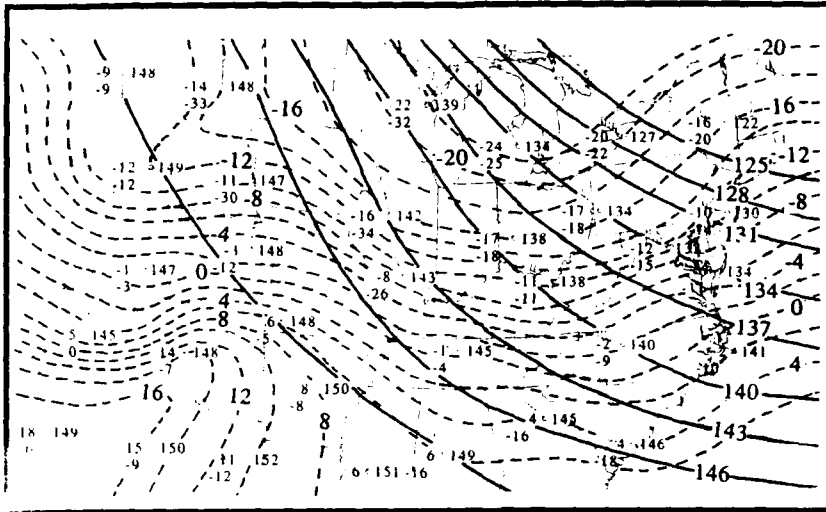


Figure 6. 850 mb analysis for 1200 UTC 7 March 1986. Dashed lines are isotherms analyzed every 2°C. Solid lines are isoheights analyzed every 3 dm.

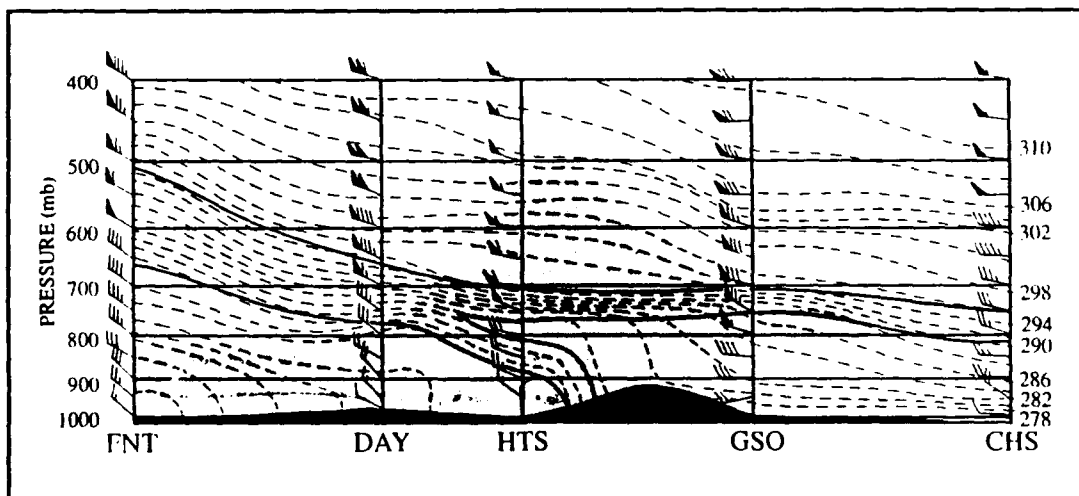


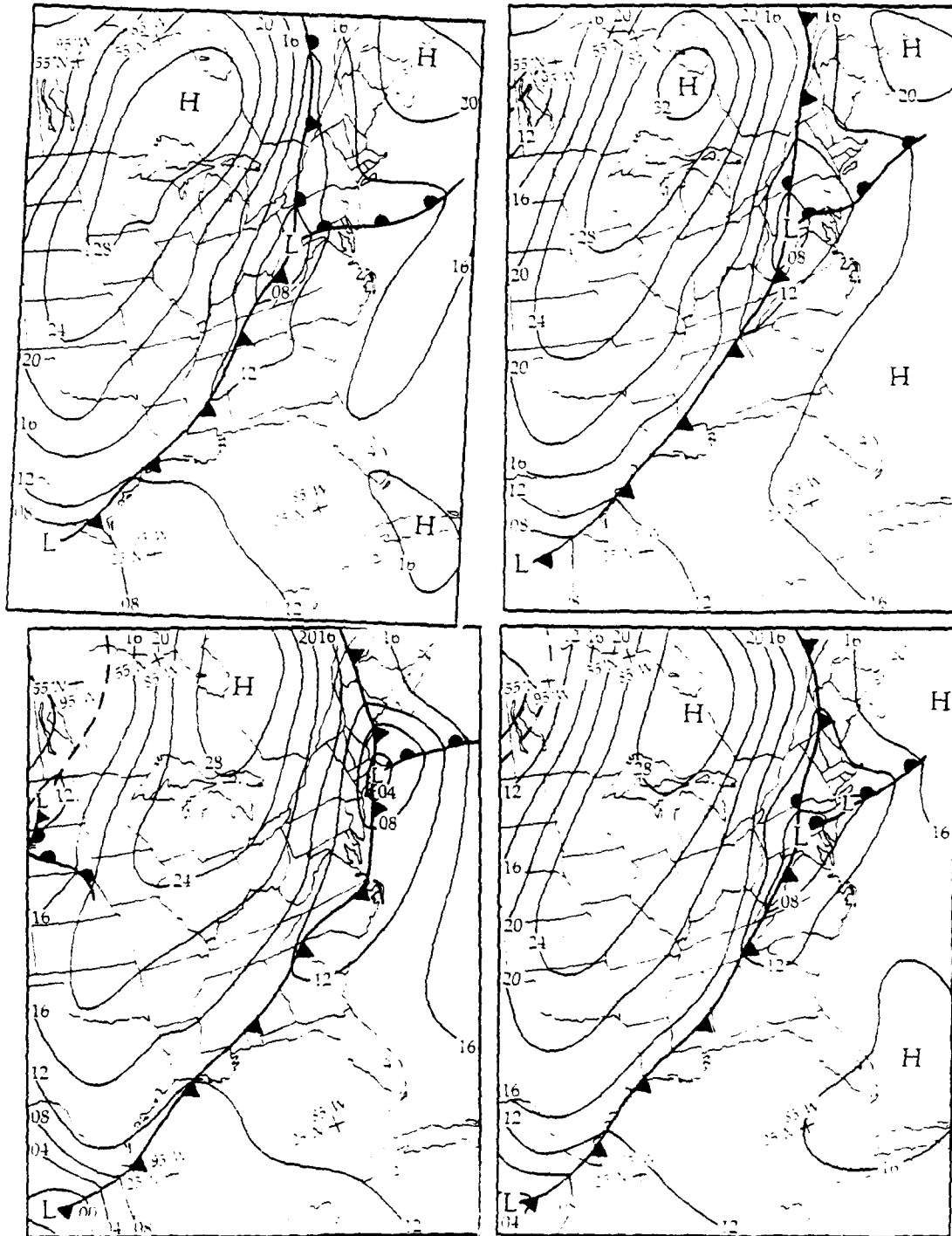
Figure 7. Vertical cross-section taken perpendicular to the front from Flint (FNT), Michigan to Charleston (CHS) South Carolina at 1200 UTC 7 March 1986. Dashed lines are isentropes analyzed every 2 K. Winds are plotted every 50 mb with full (half) barbs representing 5 m s^{-1} (2.5 m s^{-1}). Flags represent 25 m s^{-1} . Relative humidity of greater than 80% indicated by the shaded region in gray. Frontal zones marked with solid black lines.

two upper level frontal structures at 750 mb northwest of Huntington, West Virginia (HTS).

7. SYNOPTIC OVERVIEW CASE 2

A three-hourly sequence of NMC surface analyses depict the major synoptic features, frontal characteristics and movement. The 1200 UTC 21 February analysis in Fig. 8 shows a 1032 mb high pressure center located just north of the Great Lakes. A weak 1004 mb low-pressure center in central West Virginia is analyzed with a warm front extending from the low due east to the mid-Atlantic seaboard and off the coast. The cold front of interest extends southward from the wave and across the region west of the Appalachians and through Alabama, Mississippi, and the gulf coast. The cold front is oriented northeast-southwest. The pressure gradient behind the front is noticeably stronger than in advance of the front with values of 4 mb per 100 km and 1.5 mb per 100 km, respectively.

The front moved slowly for the first six hours ending 1800 UTC (See Fig. 9 & 10). From the analysis, it appears that as in case study #1, the portion of the front in the Appalachians moved relatively slower than the northern portion of the front. By 0000 UTC on the 22nd, the cold front had crossed the mountains and its northern portion is offshore. Anticyclonic curvature is noticeable along the front over western North and South Carolina (See Fig. 11). The 0300



Figures 8, 9, 10, & 11. Clockwise from top left are the NMC surface analyses for 1200, 1500, 1800, and 0000 UTC 21-22 February 1986. Labels and lines are the same as Figs. 2-6.

NMC analysis in Fig. 12 shows that a noticeable decrease in the pressure gradient has occurred behind the front in comparison to 1500 UTC (Fig. 9). At this time, the magnitude of the pressure gradients were 4 mb per 100 km and 1-1.5 mb per 100 km respectively.

The 850mb analysis for 1200 UTC 21 February 86 in Fig. 13 shows a front which extended from western New York through the Ohio Valley west of the Appalachians through Kentucky, Tennessee and into eastern Texas. The figure shows an extensive cold air mass over the Great Lakes that extends southwest to the Texas panhandle with a corresponding strong temperature gradient along the air mass' leading edge. Unlike case study #1, the 850 mb analysis implies the existence of a strong surface front. A vertical cross section taken perpendicular to the front from Dayton, Ohio (DAY) to Wilmington, North Carolina (ILM) shows the cold front to be autonomous. The front does not merge with the remains of any upper level frontal boundaries which had passed the station over the previous 24 h as was the situation for case 1 (See Fig. 14).

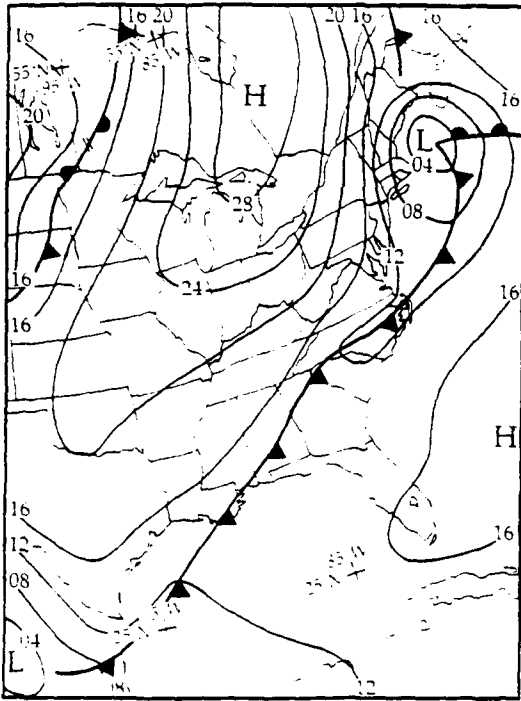


Figure 12. NMC surface analysis for 0300 UTC 22 February 1986.

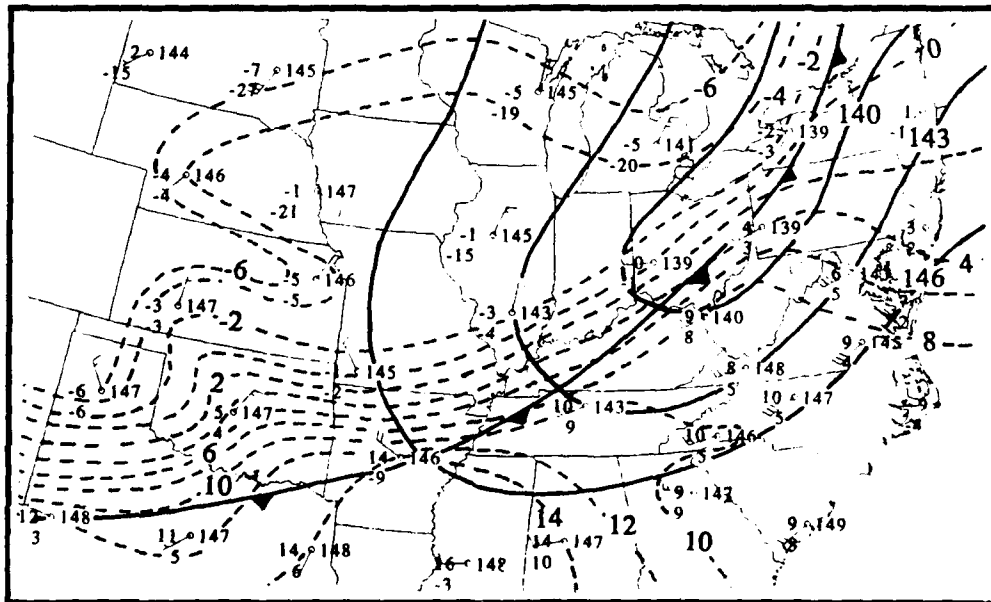


Figure 13. Same as Fig. 6 except for 850 mb analysis for 1200 UTC 21 February 1986.

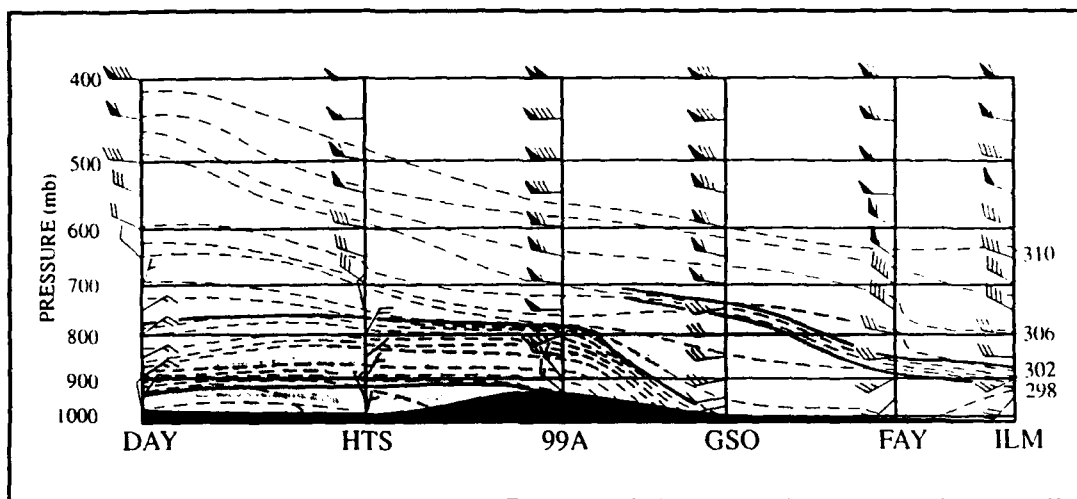


Figure 14. Same as Fig. 7 except for vertical cross-section taken perpendicular to the front from Dayton (DAY) Ohio to Wilmington (ILM) North, Carolina 0000 UTC 22 February 1986.

8. MESOSCALE ANALYSIS CASE 1

The synoptic scale analysis and overview above could not depict the details of frontal structure which became evident after the completion of a mesoscale surface analysis. As discussed above, the analyses used the PAM and National Weather Service hourly data, and some ship and buoy data. The mesoscale analyses greatly improve our understanding of the characteristics and behavior of the cold front of 7 March 1986.

The analysis was based as much as possible on the characteristics of fronts according to the classic polar-front cyclone

model of fronts first postulated by the Norwegian school. Case 1 was compared to this classic model as a point of reference for its comparison with case 2. According to the classic model, fronts are first-order discontinuities between air masses with different densities. Subsequently, cold fronts are placed along the warm side of the thermal gradient. According to the model, when a cold front passes a station, a rapid decrease in temperature occurs.

According to the classic model, the position of the cold front at the surface is coincident with the trough position. A characteristic of the low pressure trough is a distinct cyclonic wind shift that occurs as a result of the first order discontinuity in the pressure gradient field across the trough. As a trough passes a station, a rapid increase in pressure and abrupt cyclonic wind shift occur. Since the position of a trough is coincident with a classic front, a station simultaneously experiences a rapid increase in pressure, an abrupt drop in temperature and a distinct cyclonic wind shift.

To aid in the initial placement of the front in the mesoscale subjective hand-analyses, the surface front location was based on all three characteristics. However, where all three characteristics were not in phase, the Norwegian frontal symbol was placed where the cyclonic wind shift occurred. It is important to understand that some portions of the wind shift line did appear as a classic front (when aligned with the edge of the thermal gradient), while other sections did not. Therefore, the Norwegian frontal symbol used for this analysis is by strict convention a wind shift line which is how it will

be referred to in future discussion. This wind shift line was often a separate and distinct feature from the prefrontal troughs depicted in the mesoscale analysis.

In order to refine and enhance the accuracy of the mesoscale analysis, GEMPAK was used to generate meteograms from the 5-minute PAM II station data centered around the times when the stations experienced the passage of the wind shift line. The position of the wind shift line was then modified to ensure consistent agreement with the meteograms. The same characteristics of classic cold fronts mentioned previously was applied to the meteograms of 5-minute data to determine whether individual PAM stations experienced a classic cold front passage, a trough passage, or simply the passage of a wind shift line. However, since the 5-minute data provided finer temporal resolution than the hourly data, it became necessary to quantify the characteristics associated with a classic cold front passage and distinguish them from those identified with a trough passage as follows:

Criteria for trough passage:

- A wind direction change of at least 30° in 5 minutes with the occurrence of wind regimes lasting a minimum of twenty minutes preceding and following the change in direction.
- An increase in pressure of at least 0.3 mb in 5 minutes.

Additional criterion for determining classic frontal passage:

- A decrease in temperature of at least 1°C in 5 minutes.

An additional criterion was also established for weaker trough passages which was:

- A wind direction change of at least 30° in 5 minutes without well established wind regimes preceding or following the change.

After applying the above mentioned criteria to the 5-minute data, it is not surprising that meteograms provided additional evidence that the evolution of both cold fronts (case 1 and 2) deviated from the classic model.

It should be mentioned that an algorithm developed by Ronald Dunig for correcting and reducing the pressure data recorded at PAM II stations during GALE was used to compute the altimeter settings for the surface pressure analysis.

A series of mesoscale surface analysis beginning with 1200 UTC 7 March 1986, reveal interesting and unique features of the wind shift line and its deviation from the classic polar-front cyclone model. The 1200 UTC mesoscale analysis shows extensive ageostrophy in the wind field north of the line where the wind vectors cross the isobars at greater than 90 degree angles at some locations (See Fig. 15). A comparison of the analyzed pressure field to the computed geostrophic field will be presented later. The comparison substantiates the ageostrophy and augments the credibility of the mesoscale analysis.

The 1200 UTC analysis also shows the front to be weak to moderate before it crosses the mountains. The temperature gradient averaged 4°C per 100 km behind the front. The component of the pressure gradient perpendicular to the front was relatively weak and diffuse (2 mb per 100 km).

The pressure field best illustrates a nonclassic feature of the front. There is no indication of sharply kinked isobars at the wind shift line as postulated by the classic model. In fact, the 1200 UTC analysis also shows the existence of a well-established prefrontal trough, especially in western North Carolina, which is a further deviation from classic theory. This trough persists until 2200 UTC at which time the wind shift line appears to come in phase with it.

To more clearly illustrate the existence of a multiple line structure, the 1500 UTC analysis (Fig. 16) is shown with the location of PAM stations 34 and 39 near Greensboro, North Carolina. The prefrontal trough is just north of these stations at this time, while the wind shift line is well to the north of both stations (in southern Virginia). One would expect the trough to pass through the two stations within the hour, and the wind shift line, which is a separate and distinct feature, should pass through a few hours later.

The meteograms for PAM station 34 from 14-1700 UTC (Fig. 17) provides evidence for the existence of a trough and separate wind shift line. PAM 34 experienced a significant cyclonic wind shift and trough passage at 1535 UTC. The extremely small increase in

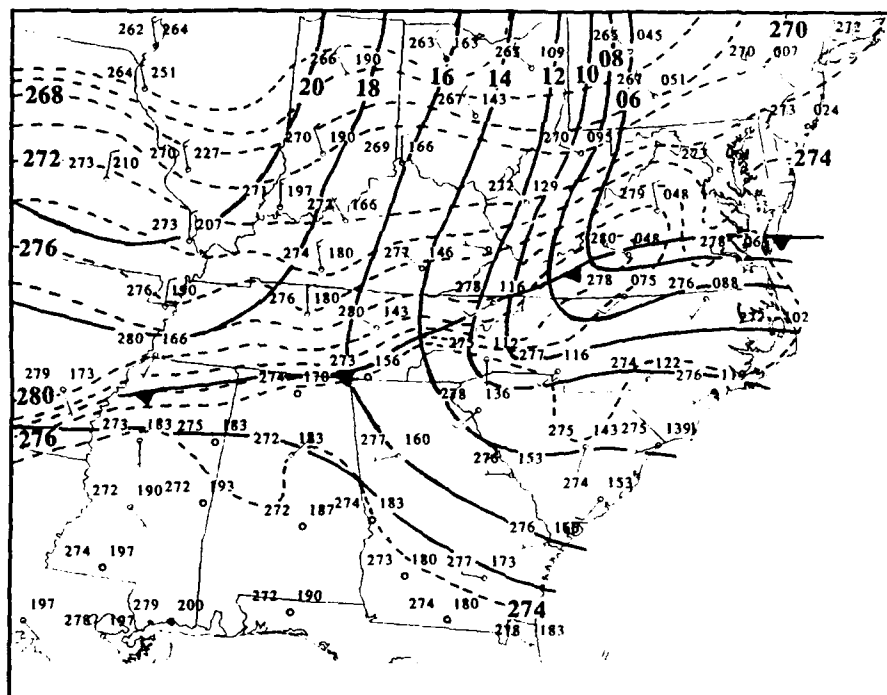


Figure 15. Mesoscale surface analysis for 1200 UTC 7 March 1986. Dashed lines are isentropes analyzed every 2 K. Solid lines are lines of equal altimeter setting analyzed every 2 mb and labeled every line with the leading "9" or "10" omitted.

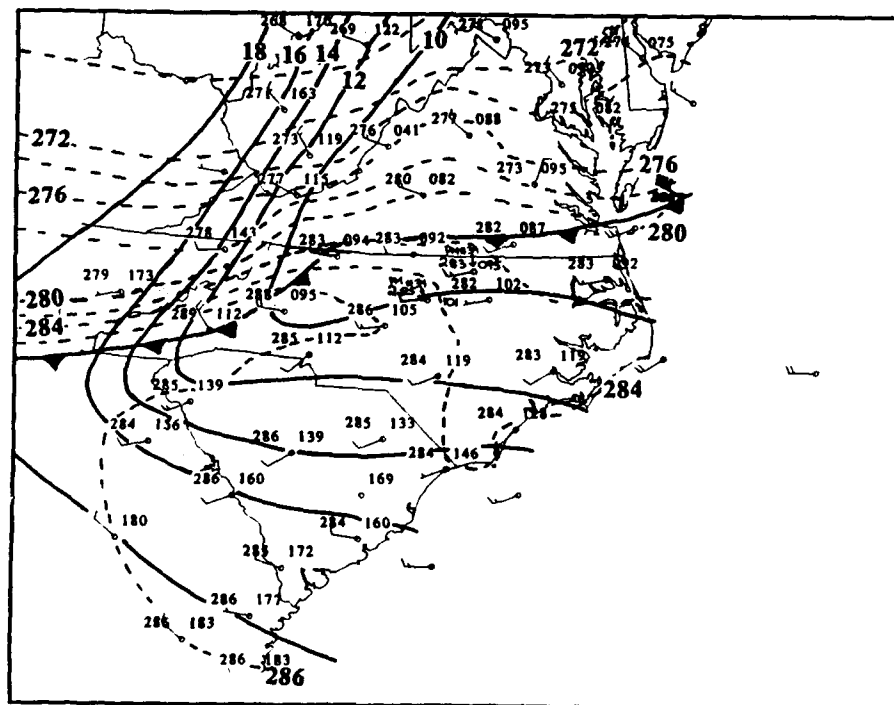


Figure 16. Same as Fig. 15 except for mesoscale surface analysis for 1500 UTC 7 March 1986.

the altimeter setting showed that the prefrontal trough was weak and supported not bending the isobars sharply in the mesoscale analysis. The abrupt cyclonic wind shift at 1835 UTC for PAM station 34 shows the passage of the separate and distinct wind shift line at 1835 UTC (Fig. 18) .

The meteogram for PAM station 39 revealed an interesting phenomenon related to this trough. This station should have experienced trough passage sometime after 1500 UTC as shown by Fig. 16. Instead of showing a distinct trough passage according to the established wind criteria, the meteogram in Fig. 19 reveals a meandering wind pattern from 15-1630 UTC. Alternate backing and veering winds prevailed for many other stations throughout the PAM network (See Fig. 20 & 21). The meandering winds suggest the possibility of the same trough line passing given PAM stations several times or multiple trough passages.

The nonclassic nature of the frontal system is further substantiated by the evolution of a strong temperature gradient ahead of the wind shift line between 1500 and 1800 UTC. At 1500 UTC (Fig. 16), the strong thermal gradient is located behind the wind shift line over the northern two thirds of Virginia. A weak thermal gradient is located south of the wind shift line across central North Carolina at this time. By 1800 UTC (Fig. 22), however, a strong thermal gradient is located across central North Carolina south of the wind shift line. By comparison of the 1500 UTC analysis in Fig. 16 and the IR satellite imagery at 1501 UTC in Fig. 23, it is evident that

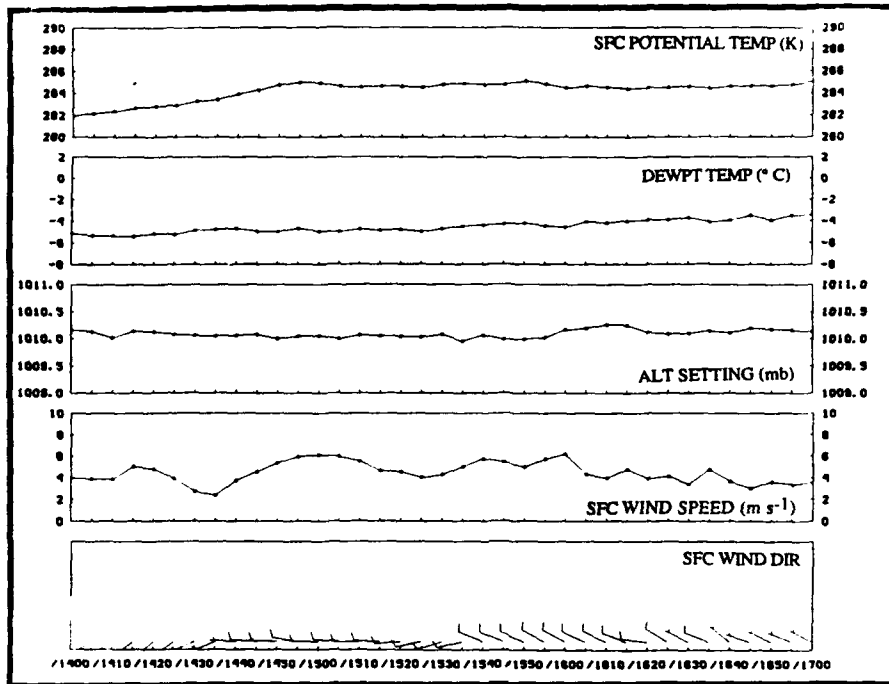


Figure 17. Meteogram for PAM station 34 from 15-1800 UTC 7 March 1986.

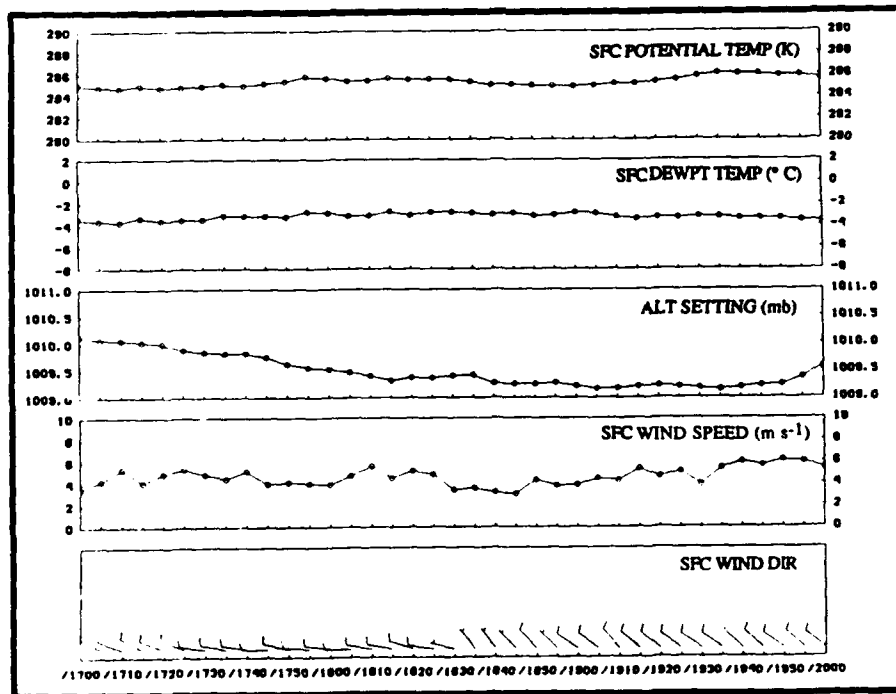


Figure 18. Same as Fig. 17 except for 17-2000 UTC 7 March 1986.

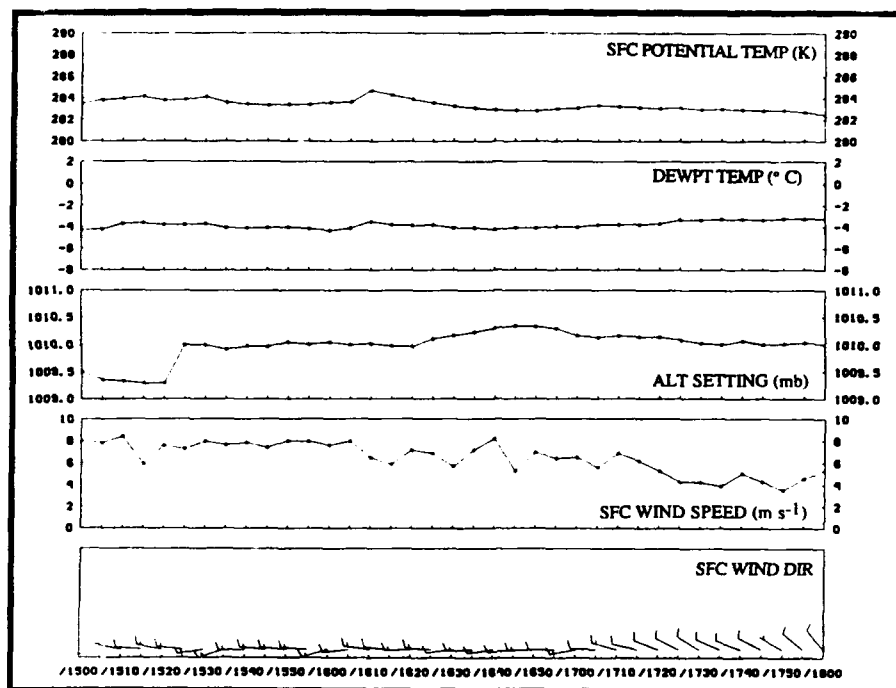


Figure 19. Same as Fig. 17 except for PAM station 39 from 15-1800 UTC 7 March 1986.

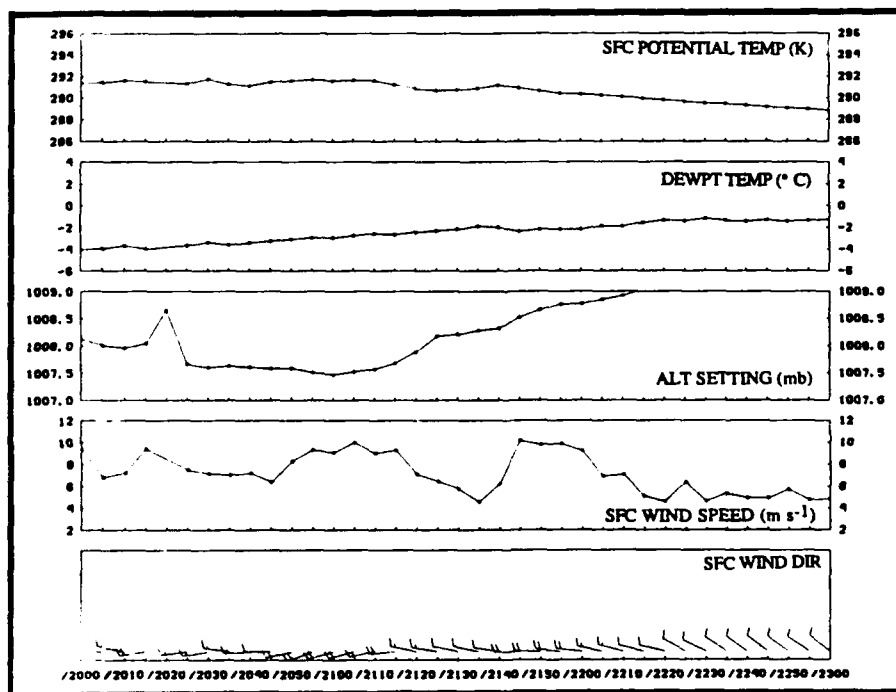


Figure 20. Same as Fig. 17 except for PAM station 31 from 20-2300 UTC 7 March 1986

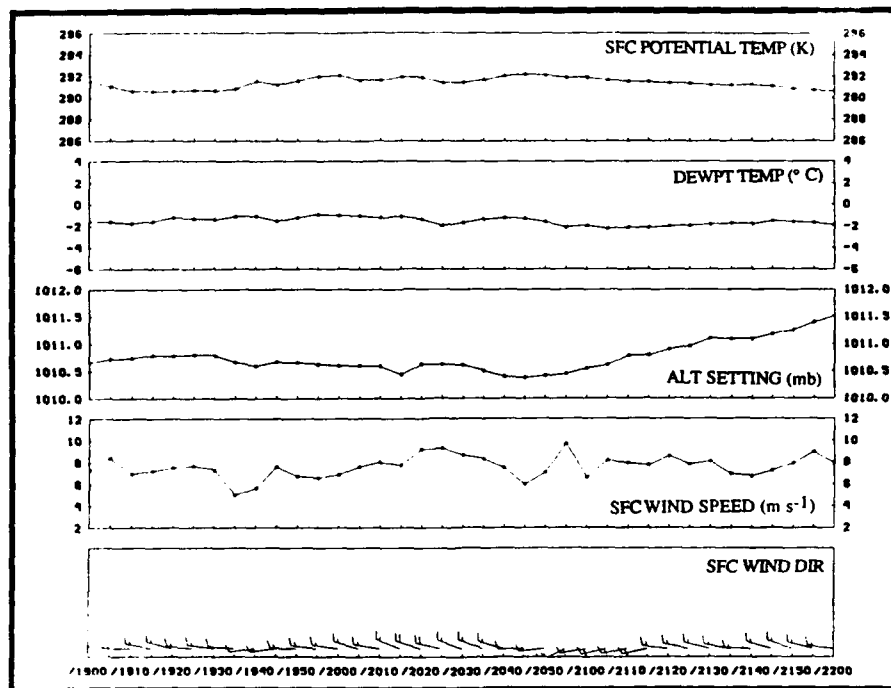
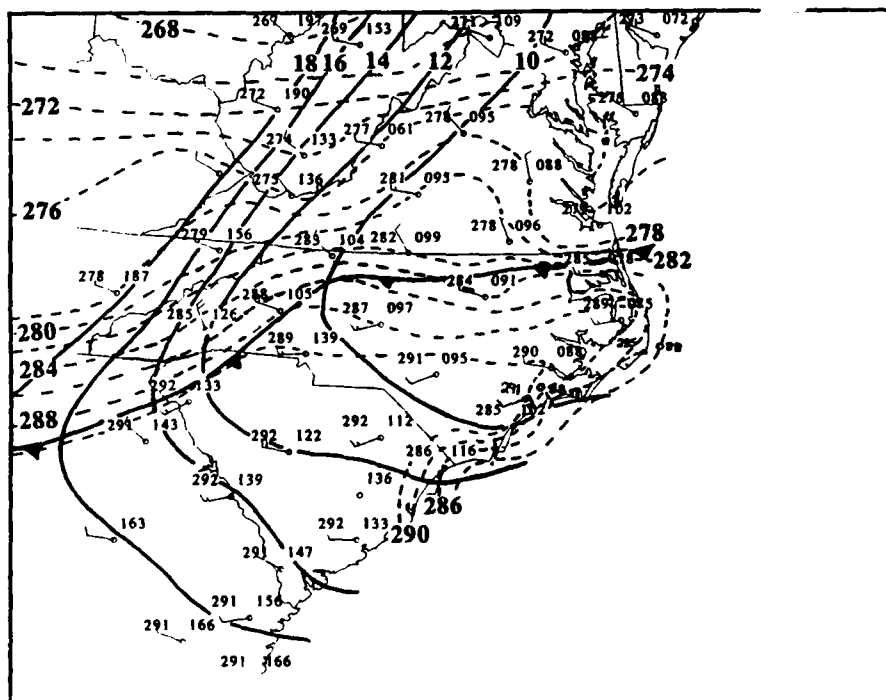


Figure 21. Same as Fig. 17 except for PAM station 10 from 19-2200 UTC 7 March 1986.



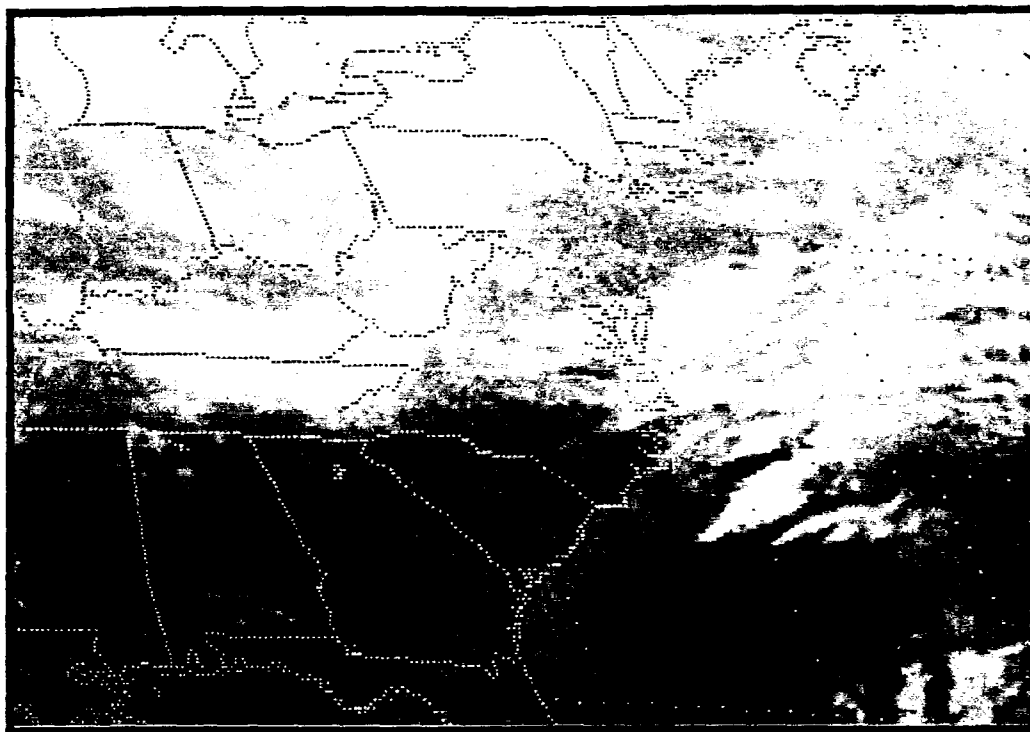


Figure 23. IR satellite imagery for 1501 UTC 7 March 1986.

while the wind shift line lay east-west across southern Virginia, the leading edge of a cloud mass which encompassed the northern third of North Carolina and southern Virginia was much further south. It is reasonable to suppose that surface under the cloud-free area to the south received a larger amount of solar insolation and was heated at a greater rate than the surface under the cloud layer to the north. This differential cloud shading process was the most likely cause for the shift in the leading edge of the strong temperature gradient south of the wind shift line. It will be shown later that the diabatic heating effect in this case was an important frontogenetic process.

Another important feature associated with the eastern portion of the wind shift line is depicted on the 2200 UTC mesoscale analysis in Fig. 24. This strong baroclinic zone was most likely established by differential heating across the coastline which had occurred during the time of maximum solar insolation contrasted with the advection of cold air from the Atlantic shelf waters off the Virginia coast. Garratt et al., 1988 determined the importance of the differential heating process in establishing sharply defined surface cold fronts traveling along a coastline. The authors referred to this phenomenon as summertime "cool changes" in southeastern Australia.

The advection of a pool of cold air off the Virginia capes by the onset of northeasterly winds reinforced the temperature gradient north of the extreme eastern portion of the wind shift line. The NOAA operational Sea Surface Temperature analysis for 4 March 1986 indicates temperatures below 7°C along the coast from extreme northeast North Carolina northward and extending eastward a distance of approximately 80 km. This cold water is probably the source of the cold air.

The 2200 UTC analysis (Fig. 24) shows the resultant enhanced baroclinicity, convergence, and also curvature along the portion of the wind shift line in extreme east central North Carolina. Garratt et al., 1988 determined the importance of differential friction between the land and sea to produce curvature for fronts traveling along a coastline in southeastern Australia.

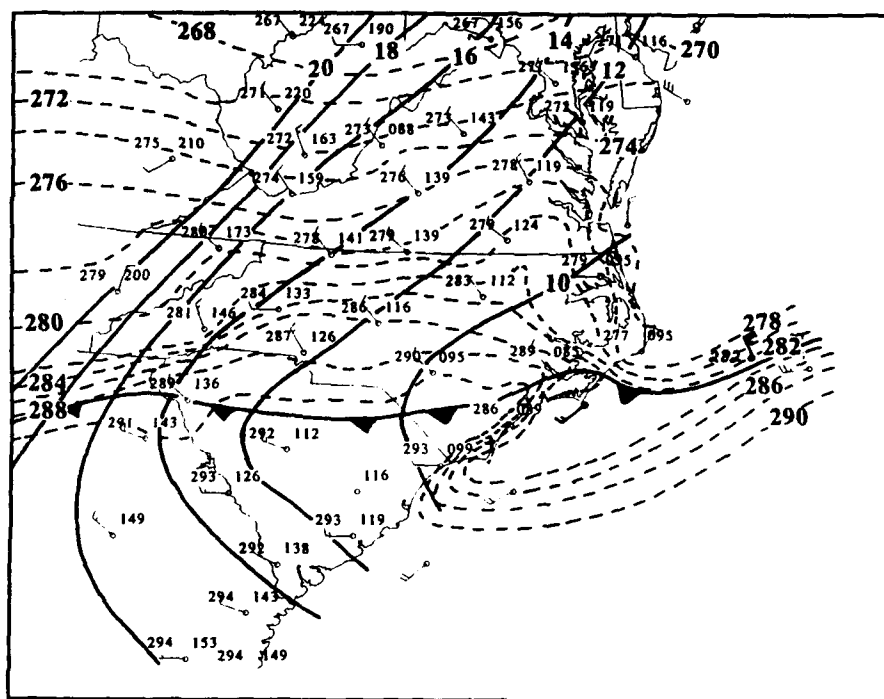


Figure 24. Same as Fig. 15 except for mesoscale surface analysis for 2200 UTC 7 March 1986.

It is interesting to note that only 8 of 51 stations experienced classic frontal passage according to the established criteria and all were located in extreme eastern North Carolina and southeastern Virginia as seen in Fig. 1. The meteogram for PAM station 45 in Fig. 25 is representative of the other stations and shows a simultaneous rapid drop in temperature of 2 K, an increase in altimeter of 1 mb, and a cyclonic wind shift of 120° in a 5-minute period at 2120 UTC. All eight PAM stations experienced strong post-frontal northeasterly winds confirming the possibility of enhanced convergence and increased baroclinicity along the coast of North Carolina which are favorable conditions for cyclogenesis.

The IR satellite imagery from 2101 UTC in Fig. 26 substantiates possible cyclogenesis off the coast of North Carolina. This imagery shows some curvature in enhanced cloudiness across the southern half of North Carolina and suggests that precipitation associated with the front is confined primarily off the coast of extreme North Carolina in the form of rain and rainshowers. The tops were estimated to be 30,000 ft from the IR imagery.

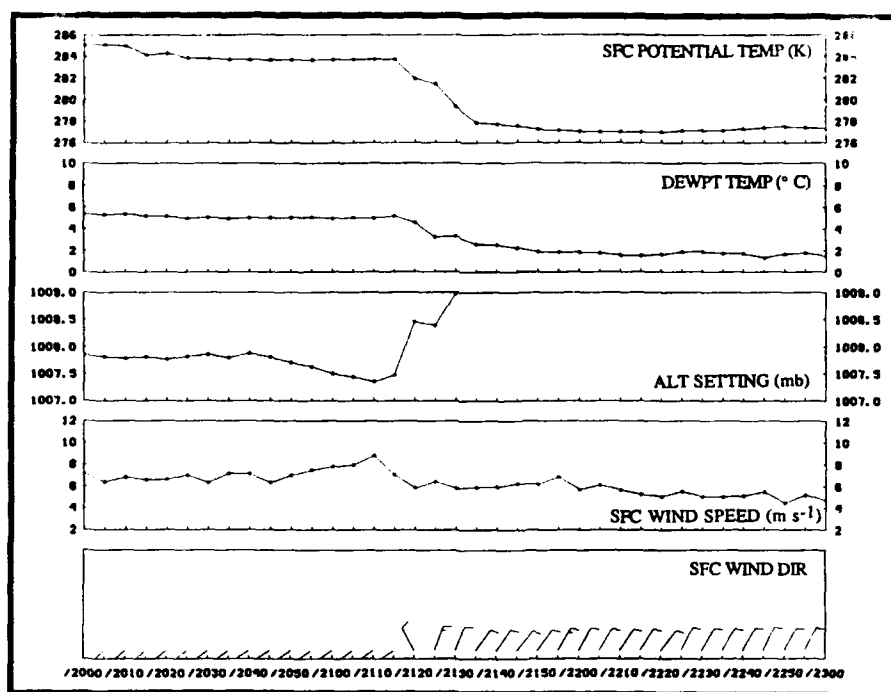


Figure 25. Same as Fig. 17 except meteorogram for PAM station 45 from 20-2300 UTC 7 March 1986.

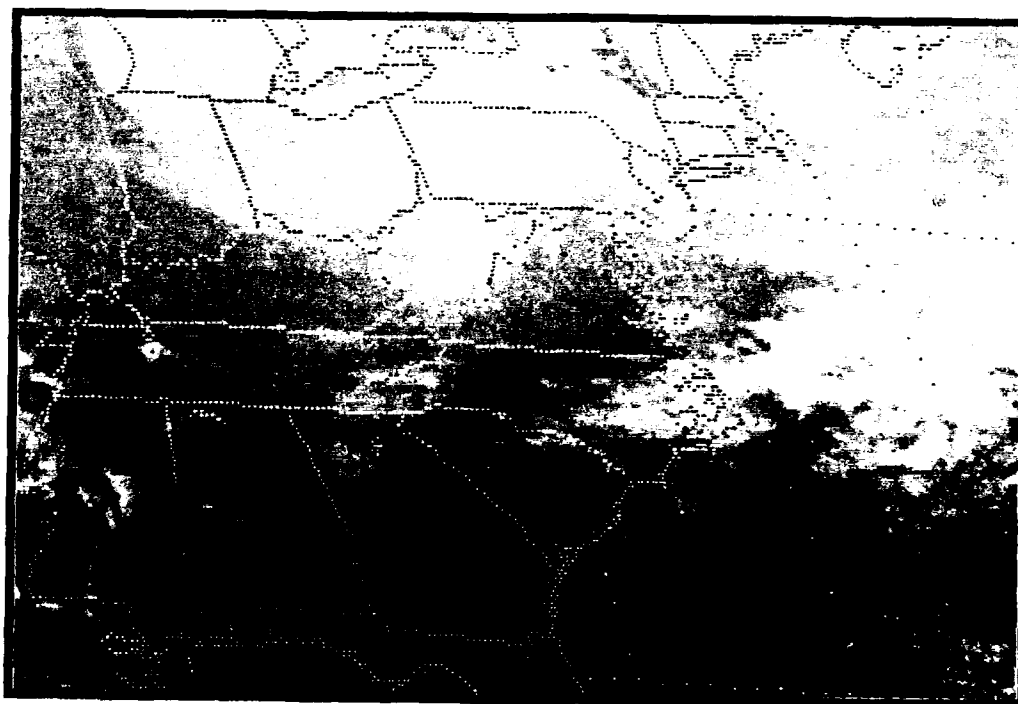


Figure 26. IR satellite imagery for 2101 UTC 7 March 1986.

9. MESOSCALE ANALYSIS CASE 2

A comparison of the mesoscale analysis of case study 2 to case study 1 reveals both distinct similarities and differences between the two. Unlike the front of case 1, that of case 2 initially exhibits a surface structure which closely resembles the classic model, especially at the beginning of the analysis period. The 1200 UTC mesoscale analysis in Fig. 27 shows a pressure trough coincident with a cold front characterized by a strong post-frontal temperature gradient of 8.5°C per 100 km. In case 1, the magnitude of the post frontal temperature gradient was less than half this value. Recall that the cold front was clearly out of phase with a well established pre-frontal trough, and lacked a sharp pressure change across the frontal boundary. On the other hand, the 1200 UTC 21 February 1986 analysis for case 2 shows a very sharp change in the pressure field at the front as indicated by the kinking of the isobars. The synoptic scale analysis (Fig. 8) also shows a sharp pressure trough at the front.

Frontal case 2 also shares some characteristics similar to that of case 1. The wind field is highly ageostrophic with surface winds crossing isobars at angles approaching 90° , mainly west of the line. As in case 1, the front was relatively dry with very little precipitation in North Carolina. The 1335 UTC radar summary in Fig. 28 shows one isolated rain shower in eastern Arkansas and Mississippi, and otherwise precipitation was

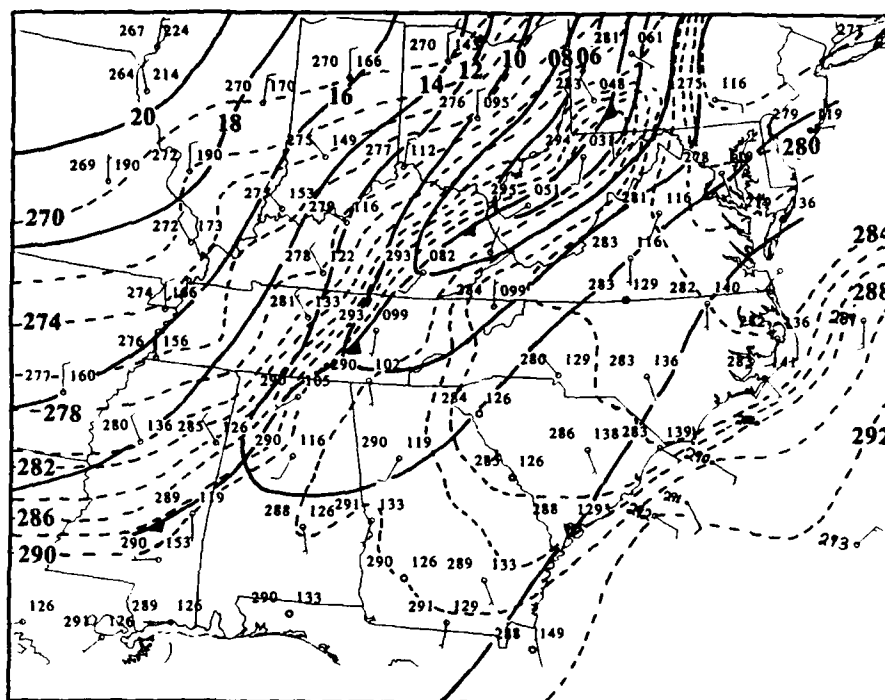


Figure 27. Same as Fig. 15 except mesoscale surface analysis for 1200 UTC 21 February 1986.

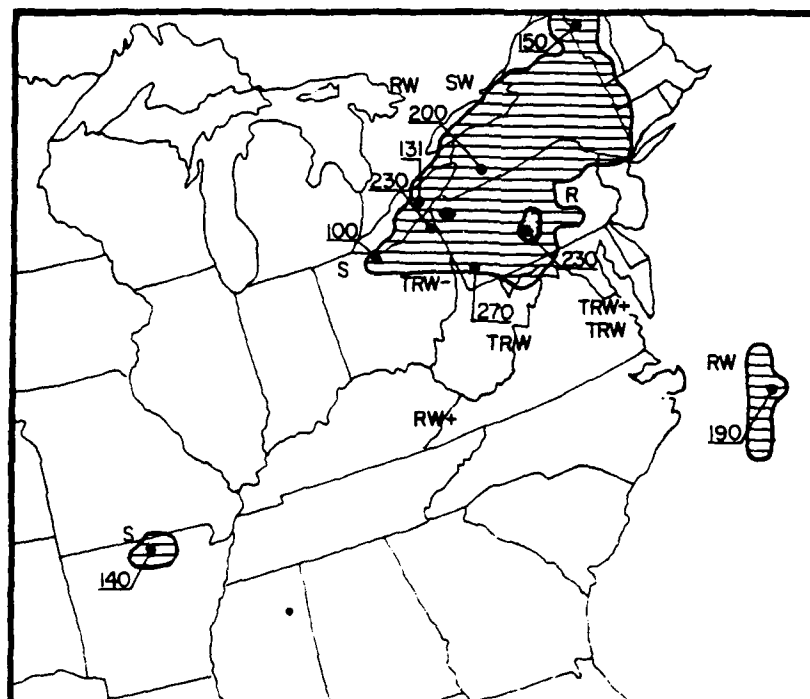


Figure 28. Radar summary for 1335 UTC 21 February 1986. Precipitation areas are hatched. Maximum tops labeled in thousands of feet. Letter symbols indicate precipitation type followed by intensity.

confined to the warm and occluded fronts associated with the low pressure center in West Virginia. The 1200 UTC mesoscale analysis shows a strong temperature gradient offshore, but unlike case 1 the temperature gradient is directed offshore, that is, cold land, warm sea. It will be shown near the end of the analysis period that the interaction of the eastern portion of the cold front in case 2 with the strong baroclinic zone off the coast is remarkably similar to case 1. The importance of the semi-permanent along-shore baroclinic zone to frontogenetical processes for both cases will be discussed later.

The possible importance of diabatic heating as a frontogenetical process and a cause of nonclassic frontal behavior for case #1 was mentioned earlier, and this process is also justifiably important for this case. The diabatic heating, however, is confined to a smaller geographic area than for case #1. The cloud cover associated with the wind shift line in case #2 near the time of maximum solar insolation was far more extensive than it was for case #1. Visible satellite imagery for 1430 UTC 21 February 86 in Fig. 29 shows almost the entire eastern third of the United States under cloud cover. Cloud free areas were located in extreme northwestern South Carolina and southwestern North Carolina. Cloud shading and differential surface heating in these limited areas led to the evolution of a strong temperature gradient east of the front over northwestern South Carolina from 1500 UTC to 1800 UTC seen in Fig. 30 & 31. Recall that in case #1 strong diabatic heating occurred over the entire southern two thirds of North Carolina.

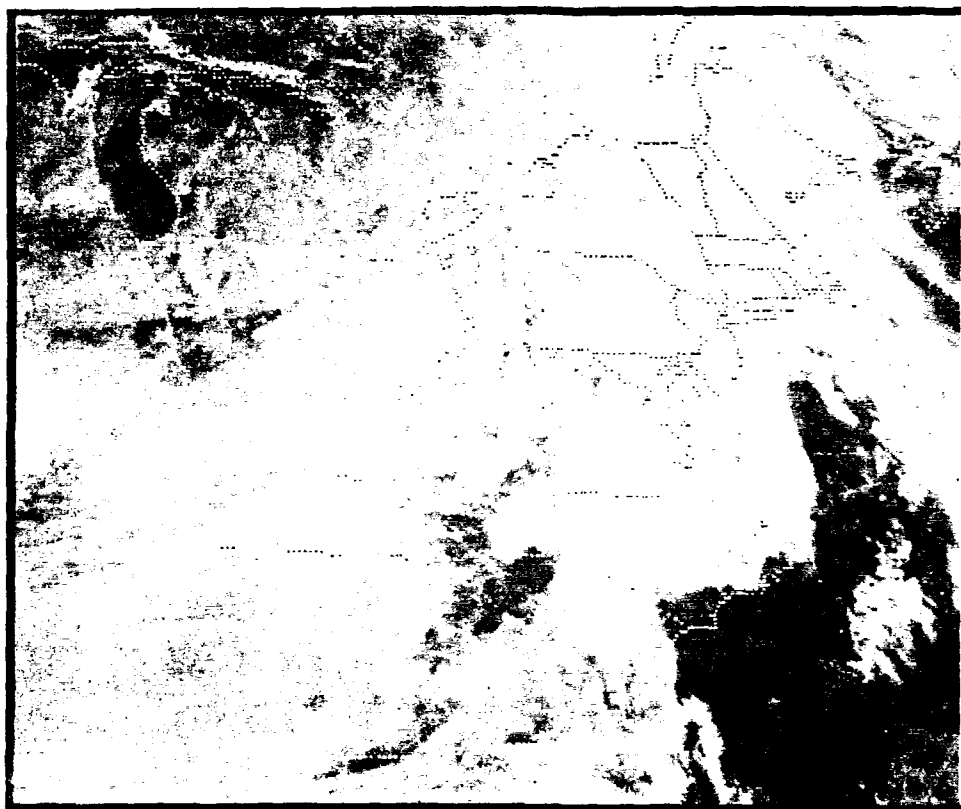


Figure 29. Visible satellite imagery at 1430 21 February 1986.

It was mentioned previously that the front in case #2 behaved according to classic theory at the beginning of the analysis period. The 1500 UTC mesoscale surface analysis in Fig. 30 shows the first sign of deviation from the classic model. At this time, the surface trough was beginning to drift out-of-phase with the wind shift line. By 1800 UTC, the phase shift is more noticeable and anticyclonic curvature along the slow moving portion of the wind shift line along the Appalachians mimics the anticyclonic curvature depicted in the mesoscale analysis for case #1 (See Fig. 31). The line continues to move slowly across the Appalachians with no

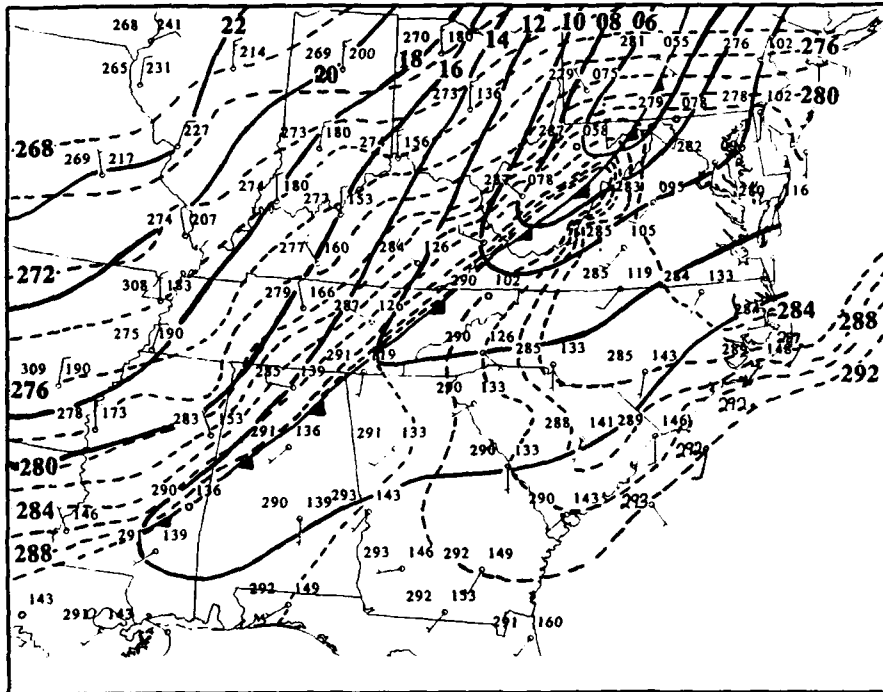


Figure 30. Same as Fig. 15 except mesoscale surface analysis for 1500 UTC 21 February 1986.

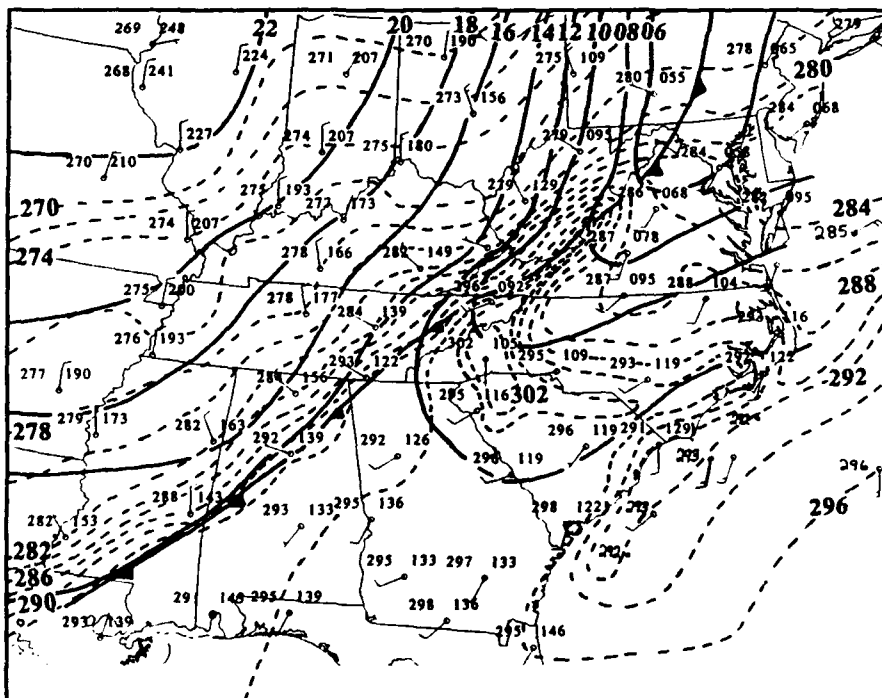


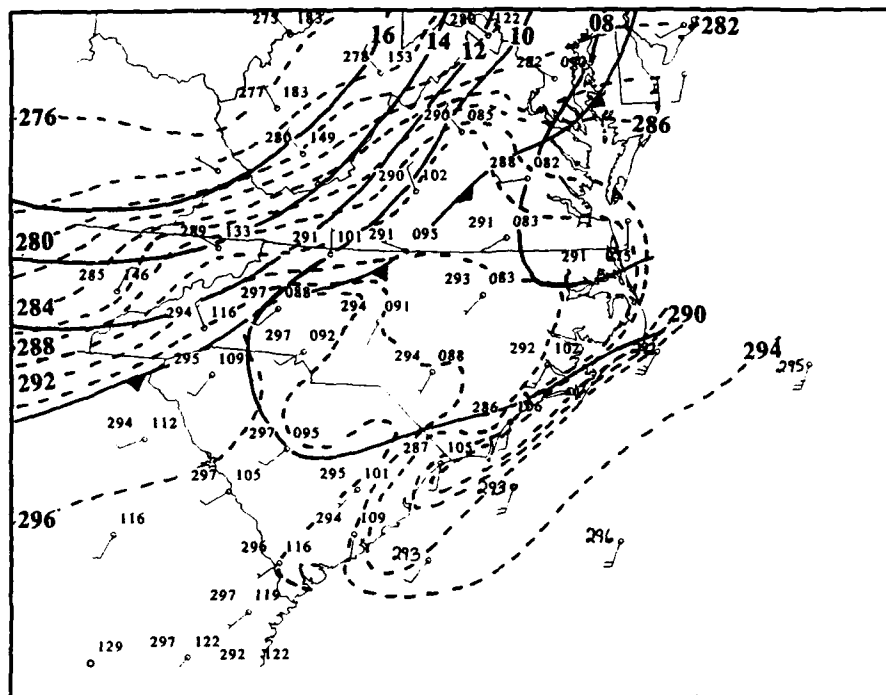
Figure 31. Same as Fig. 15 except mesoscale surface analysis for 1800 UTC 21 February 1986.

substantial change in the pressure or temperature gradients. The pressure trough moves further to the east. At 2300 UTC, the wind shift line has reached the leeside of the Appalachians and continues to move eastward (See Fig. 32).

When the wind shift line reaches the PAM data network, meteograms show a noticeable difference in the pre-frontal trough passage for this case as compared to case 1. PAM stations show a more distinct pre-frontal trough passage and don't exhibit the extensive backing and veering oscillations of the winds seen in case 1. Fig. 33 illustrates this point.

A visual comparison of the temperature and pressure gradients in the 2200 UTC mesoscale analysis in Fig. 34 to those five hours later shown in Fig. 35 reveal that the wind shift line, unlike that of case 1 has undergone a considerable degree of modification. The sharp near-kinking of the isobars evident at 1200 UTC (Fig. 27) was replaced 21 hours later by a weak and diffuse pressure field without a significant pressure change across the line. At the same time, the magnitude of the post-frontal temperature gradient at 0300 UTC (5°C per 100 km) has been reduced nearly in half. The strong discontinuity in the thermal field no longer exists, and the structure of the line no longer fits the classic polar front paradigm.

As mentioned previously, another important process affecting the behavior of the wind shift line is the strengthening of the eastern portion by the pre-existing baroclinic zone off the coast. This



portion was enhanced and showed striking similarity to the behavior of the wind shift line in case 1. According to the mesoscale surface analysis, 34 PAM stations showed the passage of the wind shift line. However, meteograms indicate that only 4, including PAM stations 45, 46, 47, and 48, experienced classic frontal passage according to the established criteria. The meteogram for PAM 47 in Fig. 33 is representative of the other three stations and shows an abrupt cyclonic wind shift at 0435 UTC on the 22nd followed by the passage of the front approximately one hour later. As in case 1, the four PAM stations experiencing classic frontal passage were all located in the same region of northeastern North Carolina near the coast (See Fig. 1), and all experienced strong post-frontal northeasterly flow. PAM station #45, 46, 47, and 48 also happened to be four of the eight stations in case #1 to experience similar effects.

The 0235 UTC 22 February 1986 radar summary in Fig. 36 shows an enhanced area of precipitation in the form of rainshowers which extended further inland than the precipitation which occurred in this area for case 1. The precipitation provides evidence consistent with enhanced baroclinicity, convergence, and frontogenesis due to differential heating across the coastline, just as in case 1.

Hakim (1992) determined the importance of the differential heating across the coastline in the formation of a somewhat similar "side-door" front which made landfall in the mid-atlantic coast in April 1987. In fact, the density difference across this front resulted

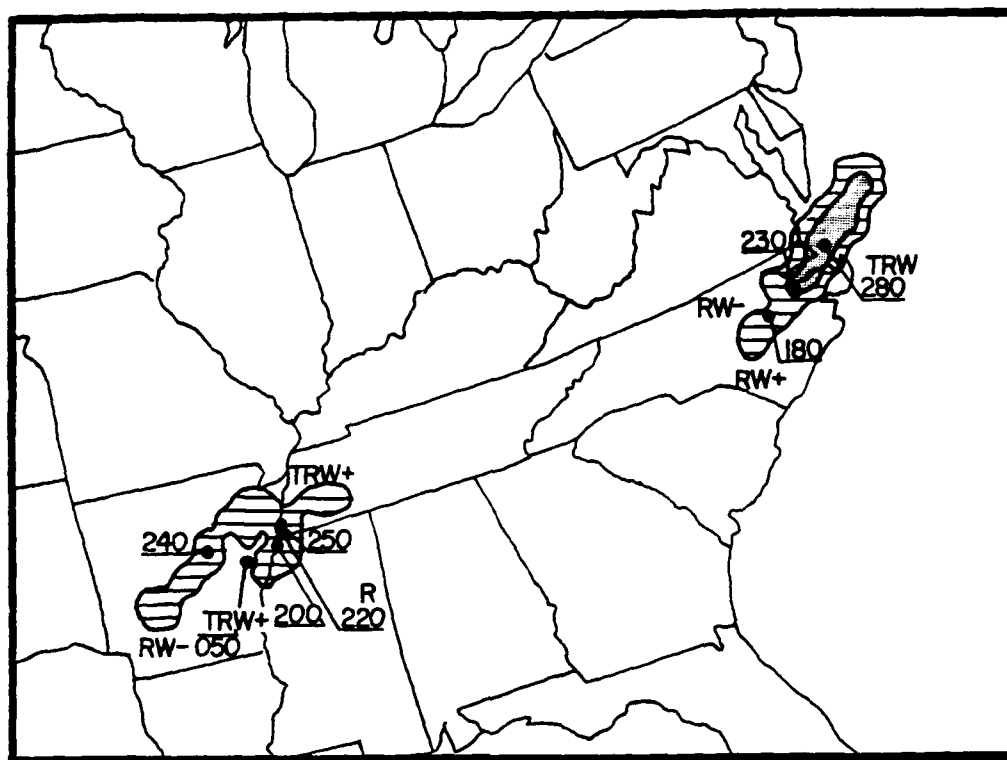


Figure 36. Same as Fig. 28 except radar summary for 0235 UTC 22 February 1986.

in the propagation of a density current several hundred kilometers inland. These currents are produced when a high density fluid and low density fluid come into contact in the presence of gravity as a restoring force. The denser of the two fluids will flow in a shallow current beneath the less dense fluid. Density currents possess large horizontal density differences, a low-level wind speed maximum in the cold air and a limited region of relative advected flow in the cold air towards the surface cold front (Garratt and Physick, 1986). For a given frontal speed c and post-frontal fluid speed U , density currents exhibit positive-front relative-flow, $U - c > 0$ (Smith and Reeder, 1988). Hakim observed positive-front relative-flow of

approximately $3-7 \text{ m s}^{-1}$. In addition, the speed of propagation of density currents that he computed using Seitter (1986) compared quite well with his analyzed surface velocity. Therefore, Hakim's data showed good agreement with density current theory. Some observed intense summertime "cool change" mesoscale fronts in southeastern Australia also showed characteristics resembling density currents (Garratt, 1988).

Similar computations in this research indicate a lack of positive-front relative-flow behind the eastern portion of the wind shift lines. Analyzed surface front propagation speeds along the North Carolina coast for the two cases are 8 m s^{-1} based on an isochrone analysis from 1800 - 2100 UTC. Post-frontal fluid speeds were determined from surface wind speeds at those PAM stations showing distinct frontal passage. Most meteograms showed post-frontal speeds of approximately 8 m s^{-1} , a speed nearly equal to that of the front. Although positive-front relative-flow did not seem to exist for the two cases, the values for the frontal and post-frontal wind speeds are so close that the possibility of density currents can not be ruled out.

The meteograms for the PAM stations experiencing distinct frontal passages showed similar characteristics to fronts of other observational studies which closely resembled density currents. The meteogram for PAM station 47 in case 1 shows a 2 K temperature drop, a 1.0 mb pressure jump, and a 60° wind direction change in 5 minutes around the time of frontal passage.

The magnitude of these abrupt changes compare favorably with the results of other studies. Garratt (1988) observed a 60° wind shift, a 1.5 mb pressure rise, and a 2 K temperature fall in a 5-minute period associated with an active surface cold front which passed through Melbourne, Australia in 1983. It is impressive that these fronts showed distinct frontal passage even on the mesoscale.

10. FRONTOGENETICAL FORCING

The frontogenetical function as defined by Miller (1948) is the increase in the three-dimensional gradient of a scalar property S with time in a moving air parcel, thus

$$F = \frac{d}{dt} |\nabla S| \quad (1)$$

Using surface potential temperature θ for the scalar property, and considering only the horizontal x,y plane, one can write the frontogenetical function for the surface:

$$F_h = \frac{d}{dt} |\nabla_h \theta| \quad (2)$$

where $\nabla_h \theta$ is the absolute magnitude of the potential temperature gradient in the x,y plane and $\frac{d}{dt}$ is the time rate of change following the motion of an air parcel (Lagrangian). To examine the individual terms of the frontogenetical equation in the x,y plane, a short derivation is presented to show their origin. Starting with following equation:

$$F_h = \frac{d|\nabla_h \theta|}{dt} = N_\theta \cdot \frac{d(\nabla_h \theta)}{dt} \quad (3)$$

$$\text{where } N_\theta = \frac{\nabla_h \theta}{|\nabla_h \theta|}$$

Expanding the right hand side of eq. (3) yields:

$$F_h = N_\theta \cdot \nabla_h \left(\frac{d\theta}{dt} \right) - N_\theta \cdot \left(\frac{\partial \theta}{\partial x} \nabla_h u + \frac{\partial \theta}{\partial y} \nabla_h v \right) \quad (4)$$

After rearranging terms in eq. (4), the following equivalent expression is obtained:

$$N_\theta \cdot \frac{d(\nabla_h \theta)}{dt} = N_\theta \cdot \left[\frac{\partial(\nabla_h \theta)}{\partial t} + \mathbf{V} \cdot \nabla(\nabla_h \theta) \right] \quad (5)$$

Setting eq. (4) equal to eq. (5) and solving for the local time derivative results in an expression for the local (Eulerian) surface-based frontogenesis. That is,

$$\frac{\partial|\nabla_h \theta|}{\partial t} = N_\theta \cdot \left[-\mathbf{V} \cdot \nabla_h(\nabla_h \theta) + \nabla_h \frac{d\theta}{dt} - \frac{\partial \theta}{\partial x} \nabla_h u - \frac{\partial \theta}{\partial y} \nabla_h v \right] \quad (6)$$

$$\frac{\partial |\nabla_h \theta|}{\partial t} = -\frac{\nabla \theta}{|\nabla \theta|} \cdot \left[\hat{i} \left(u \frac{\partial^2 \theta}{\partial x^2} + v \frac{\partial^2 \theta}{\partial x \partial y} + \frac{\partial u}{\partial x} \frac{\partial \theta}{\partial x} + \frac{\partial v}{\partial x} \frac{\partial \theta}{\partial y} - \frac{\partial}{\partial x} \left(\frac{d\theta}{dt} \right) + \right. \right. \\ \left. \left. \hat{j} \left(u \frac{\partial^2 \theta}{\partial x \partial y} + v \frac{\partial^2 \theta}{\partial y^2} + \frac{\partial v}{\partial y} \frac{\partial \theta}{\partial y} + \frac{\partial u}{\partial y} \frac{\partial \theta}{\partial x} - \frac{\partial}{\partial y} \left(\frac{d\theta}{dt} \right) \right) \right] \quad (7)$$

Total surface frontogenesis (parcel following or Lagrangian) can be expressed as the sum of the confluence, shear, and diabatic heating terms as:

$$\text{Confluence} = -\frac{\nabla \theta}{|\nabla \theta|} \cdot \left[\hat{i} \left(\frac{\partial u}{\partial x} \frac{\partial \theta}{\partial x} \right) + \hat{j} \left(\frac{\partial v}{\partial y} \frac{\partial \theta}{\partial y} \right) \right] \quad (8)$$

$$\text{Shear} = -\frac{\nabla \theta}{|\nabla \theta|} \cdot \left[\hat{i} \left(\frac{\partial v}{\partial x} \frac{\partial \theta}{\partial y} \right) + \hat{j} \left(\frac{\partial u}{\partial y} \frac{\partial \theta}{\partial x} \right) \right] \quad (9)$$

$$\text{Diabatic term} = -\frac{\nabla \theta}{|\nabla \theta|} \cdot \left[\hat{i} \left(\frac{-\partial}{\partial x} \left(\frac{d\theta}{dt} \right) \right) + \hat{j} \left(\frac{-\partial}{\partial y} \left(\frac{d\theta}{dt} \right) \right) \right] \quad (10)$$

The remaining terms in eq. (7) are advection terms.

At times, diabatic heating does not contribute significantly, and it is reasonable to neglect it. In these instances, total frontogenesis is simply the sum of the individual contributions of the confluence and shear terms above and is referred to as total adiabatic frontogenesis.

For the most part, this current research involved an examination of total adiabatic surface frontogenesis. At selected times, however, the mesoscale analysis showed the importance of differential surface

heating due to cloud shading as a potentially significant contributor to total frontogenesis. The diabatic term in the frontogenetical expression represents the effect of horizontal variation in diabatic heating (Bluestein, 1986).

Another important forcing term to total frontogenesis is the confluence term. This process represents the kinematic effect of confluence (diffluence) on the thermal gradient. A negative contribution acts to increase frontogenesis, whereas a positive contribution acts to decrease frontogenesis. The confluence term also represents the thermodynamic effect of a horizontal gradient in temperature advection (Bluestein, 1986). Cold advection in the cold air and warm air advection in the warm air on opposite sides of the frontal boundary sharpens the temperature gradient.

Shear is a type of deformation that contributes to total surface frontogenesis. It represents a two dimensional rotation of the thermal gradient into, or out of, the direction normal to the front. In effect, creating a positive or negative contribution, respectively, to frontogenesis.

The formation of a front is called frontogenesis, and the decay of a front is called frontolysis. Frontogenesis relates only to the potential temperature gradient and not on the other characteristics of a front based on the additional criteria established by classic theory (ie., cyclonic wind shift).

With these definitions in mind, kinematic total observed adiabatic frontogenesis and total geostrophic frontogenesis were computed for the two cases. To compute geostrophic frontogenesis, the geostrophic winds obtained using the equations of motion in a sigma-coordinate system (see section 12) were used in the frontogenetical equation in lieu of the observed (real) winds. In order to satisfy one of the objectives of the study which was to resolve meso- β scale frontogenesis and compare and contrast individual terms, the fronts were examined in detail when they reached the data-dense PAM network. All frontogenesis values appearing in this document are in units of $10^{-9} \text{ K m}^{-1} \text{ s}^{-1}$.

Divergence, $\nabla \cdot \mathbf{V}$ and the vertical component of relative vorticity $\frac{\partial v}{\partial x} - \frac{\partial u}{\partial y}$ were also computed for the two cases using GEMPAK software and integrated into the description of frontogenetical forcing. These computed quantities are in units of 10^{-5} with units of s^{-1} .

At 1900 UTC, the wind shift line for case 1 entered the northern third of the PAM network. Total observed adiabatic frontogenesis reflected positive values concentrated in a band along the eastern portion of the wind shift line (See Fig. 37). The confluence term contributed about 75 % of the total frontogenesis maximum value of 4 (See Fig. 38). It is interesting to note a near lack of frontogenetic or frontolytic forcing along the central portion of the wind shift line. Another region of positive frontogenesis with a

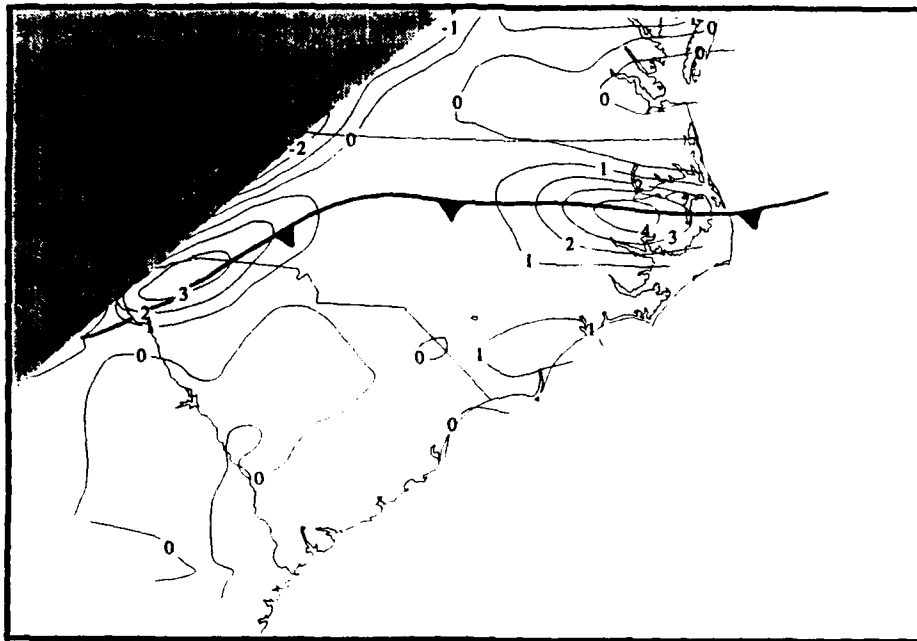


Figure 37. Total adiabatic frontogenesis for 1900 UTC 7 March 1986. Units in $10^{-9} \text{ K m}^{-1} \text{ s}^{-1}$.

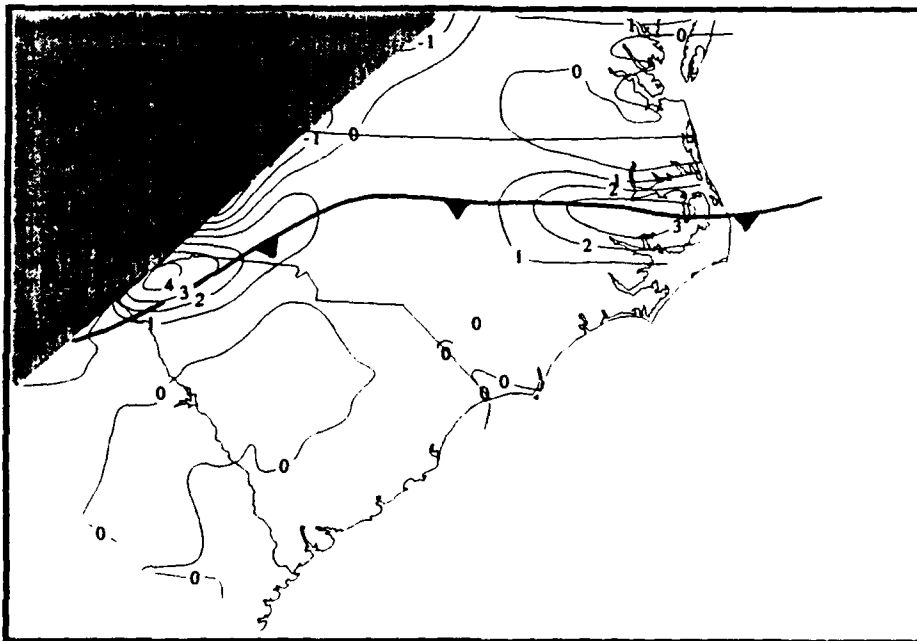


Figure 38. Confluence term at 1900 UTC 7 March 1986.

maximum of 3 was located along the western portion of the line over northwestern South Carolina. The confluence term also dominated frontogenetical forcing in this area.

Total geostrophic frontogenesis appears to be dominant north of the wind shift line and just east of the mountains (Fig. 39), and this is a recurrent theme for the first several hours for case 1. One must be careful in accepting this field as completely accurate because it is well outside the data dense PAM network. However, it appears to be reasonable when one considers that the thermal field is located well behind the wind shift line and that there is a considerable amount of horizontal shear in the geostrophic wind field across the area. The strong positive geostrophic frontogenesis over this region with a maximum value of 14 indicates its possible importance in maintaining the thermal gradient at this location after it crossed the mountains.

Total geostrophic frontogenesis for this time shows two other areas with less importance to frontogenetic forcing (See Fig. 39). A small area of positive frontogenesis (max value of 4) was located along the eastern portion of the wind shift line and another area (max value of 12) was located over northwestern South Carolina. These regions generally coincide with the maxima calculated from the actual winds (Fig. 37).

It is important to note that geostrophic frontogenesis was not computed based on geostrophic winds determined from the gradient of altimeter setting which is essentially a sea level pressure field. Instead, geostrophic winds were computed from the gradient of the Exner function (Pielke, 1984) in the sigma (terrain following) coordinate system. A complete description of the dynamic forces and geostrophic winds calculated in this coordinate system can be found in section 12 of this thesis.

The divergence field showed a strong convergence maximum of -8 over extreme eastern North Carolina due south of the wind shift line with significant convergence extending into southeastern North Carolina (See Fig. 40). It appears that the convergence to the south was associated with the pre-frontal trough. Another area of convergence was located along the wind shift line in the western edge of the PAM network extending into northwestern South Carolina with a maximum value of -6.

A cyclonic vorticity maximum of 6 was located along the eastern portion of the wind shift line (Fig. 41). A cyclonic vorticity maximum of 9 was also located along the border of North Carolina and northwestern South Carolina. Another area of positive vorticity was located over the sandhills of North Carolina quite possibly associated with the pre-frontal trough.

By 2000 UTC, the wind shift line and the frontogenetic region over eastern North Carolina advanced southward approximately 10

to 15 km. The magnitude of total observed frontogenesis along the eastern portion of the wind shift line doubled in magnitude (Fig. 42).

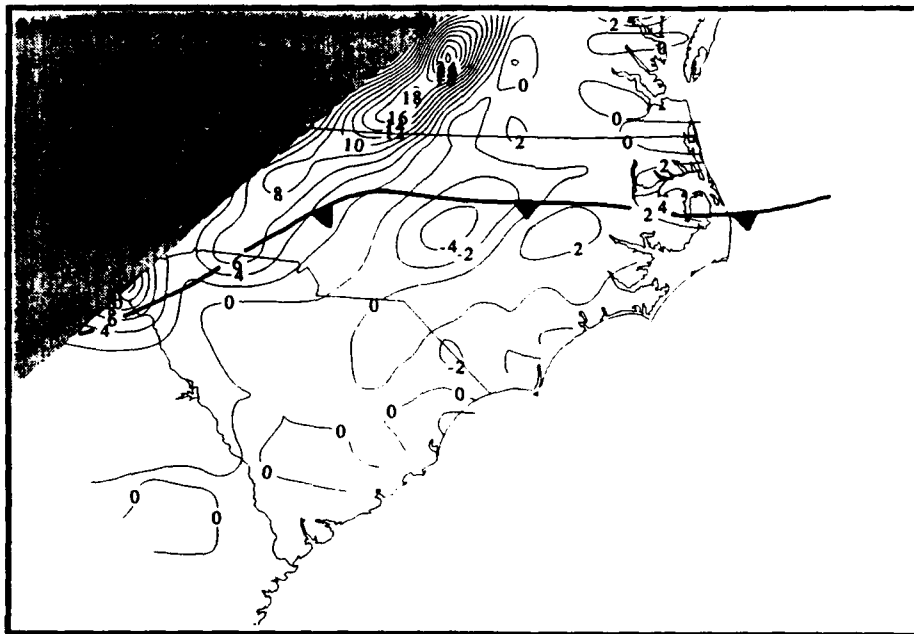


Figure 39. Total geostrophic frontogenesis for 1900 UTC 7 March 1986. Units same as Fig. 37.

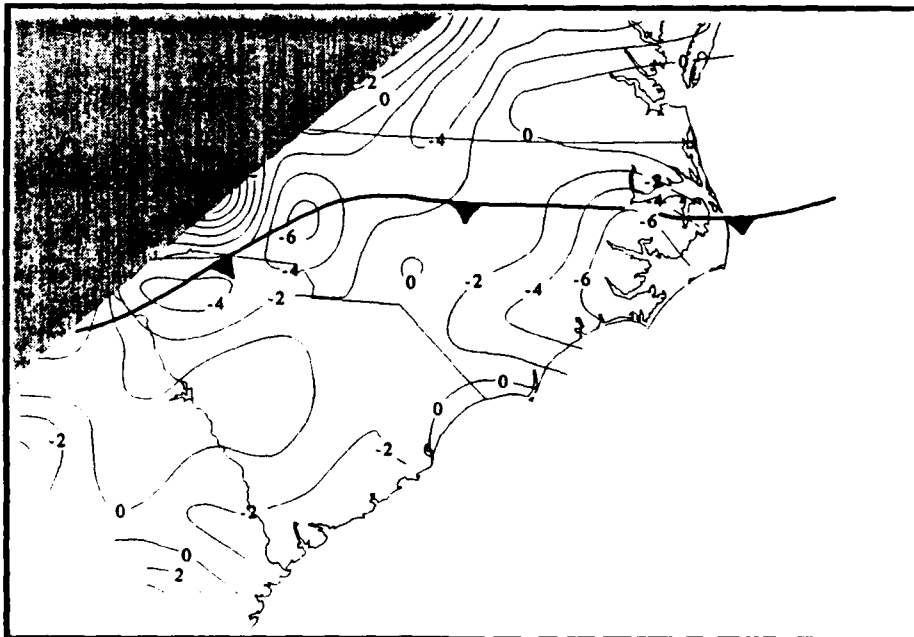


Figure 40. Divergence field for 1900 UTC 7 March 1986. Units in 10^{-5} s^{-1} .

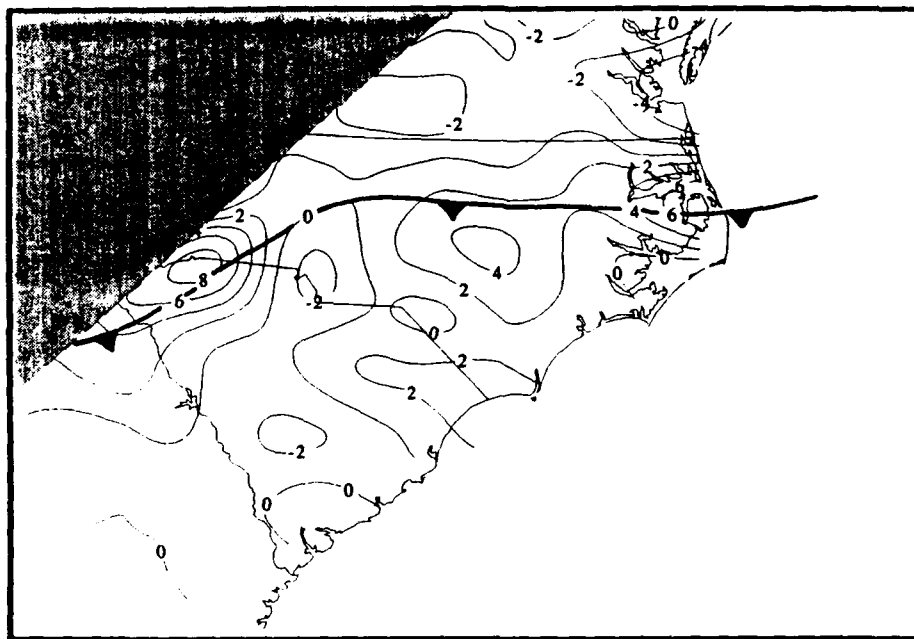


Figure 41. Vorticity field for 1900 UTC 7 March 1986. Units in 10^{-5} s^{-1} .

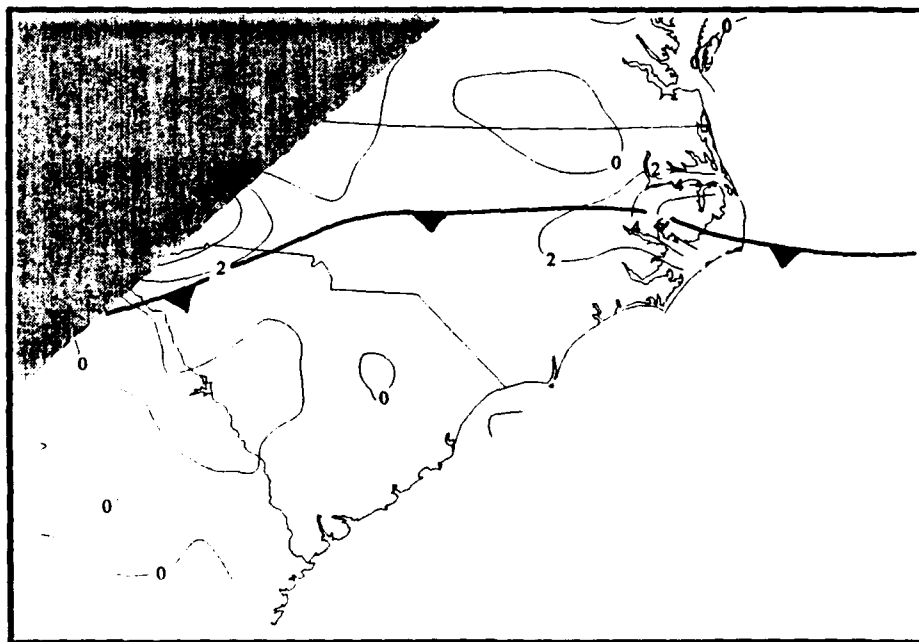


Figure 42. Total adiabatic frontogenesis for 2000 UTC 7 March 1986.

This increase shows that frontogenesis is stronger than it was during the past hour with a subsequent increase in the strengthening of the thermal gradient. The increase in frontogenesis can be attributed to a near doubling of the confluence term coupled with a modest contribution of the shear term (Fig. 43). Significant positive frontogenesis driven primarily by confluence continued to occur along the extreme western portion of the wind shift line.

Positive total geostrophic frontogenesis continued to be important just east of the mountains. A maximum of 3 which was located along the wind shift line nearest the North Carolina coast continued its contribution to frontogenetic forcing (Fig. 44). A maximum value of 2 was also located in extreme northwestern South Carolina along the extreme western portion of the wind shift line.

Convergence occurred along the entire wind shift line with a maximum of 9 found once again along the eastern portion of the line (Fig. 45). Another smaller area of convergence (max value of 6) occurred over northwestern South Carolina along the extreme western portion of the line. Significant convergence was again noted in southeastern North Carolina south of the wind shift line.

One cyclonic vorticity maximum (4) was located along the eastern portion of the wind shift line, while another significant maximum was found along the extreme western portion of the line (max value of 10). Another maximum was located over southeastern

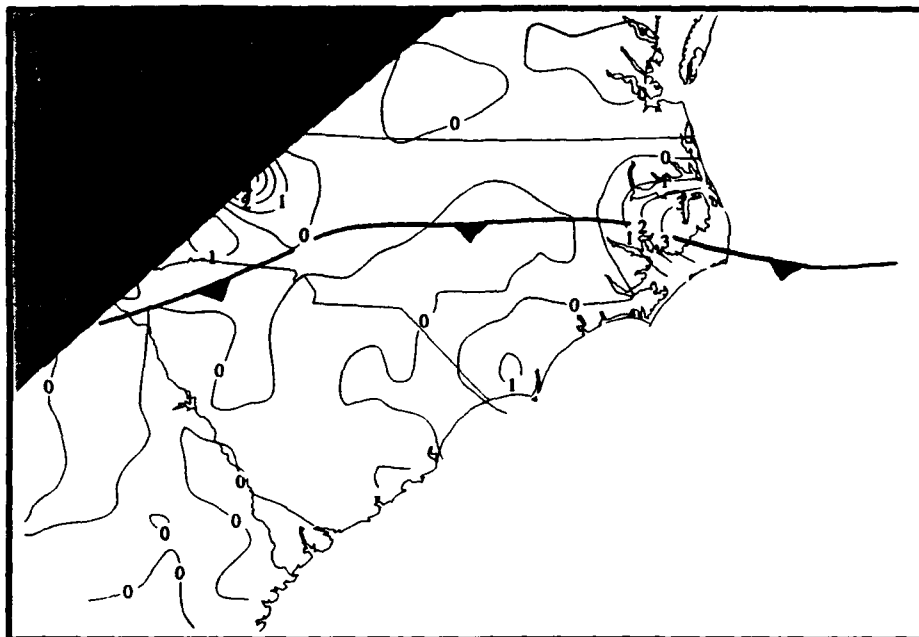


Figure 43. Shear term 2000 UTC 7 March 1986.

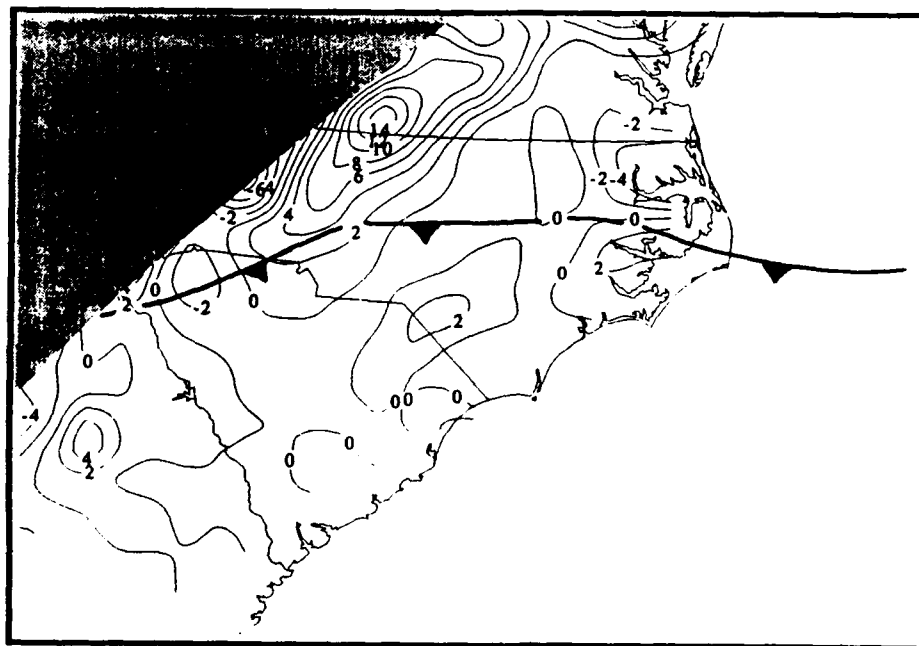


Figure 44. Total geostrophic frontogenesis for 2000 UTC 7 March 1986.

North Carolina (5) (Fig. 46). It is important to note that the credibility and representativeness of the values for the diagnostic computations along the extreme western portion of the front are questionable. This area is outside the dense PAM data network, and it is in close proximity to the mountains where the winds at measurement sites are not necessarily representative of the entire region. A closer examination of the frontogenesis, vorticity, and divergence fields from 1900 to 2000 UTC show multiple irregularities of the diagnostic values in space and time. The portion of the wind shift line over central and eastern North Carolina, on the other hand, is located within the dense PAM data network. The diagnostically computed fields here show coherent and consistent spatial and temporal continuity. Further description of frontal evolution will therefore focus on the diagnostic fields within the PAM network.

By 2300 UTC, maximum total frontogenesis decreased significantly to 2.5 (Fig. 47). This indicated weaker positive frontogenesis as compared to the strong frontogenesis depicted at 2000 UTC. The decrease can be attributed to the confluence term halving its value from the previous hour to 2. This appeared to be associated with a significant corresponding decrease in the convergence maximum (from 12 to 5) in eastern North Carolina from 2200 to 2300 UTC (Fig. 48 & 49). The shear term also decreased by about half to a value of 1 (Fig. 50). Positive cyclonic vorticity had

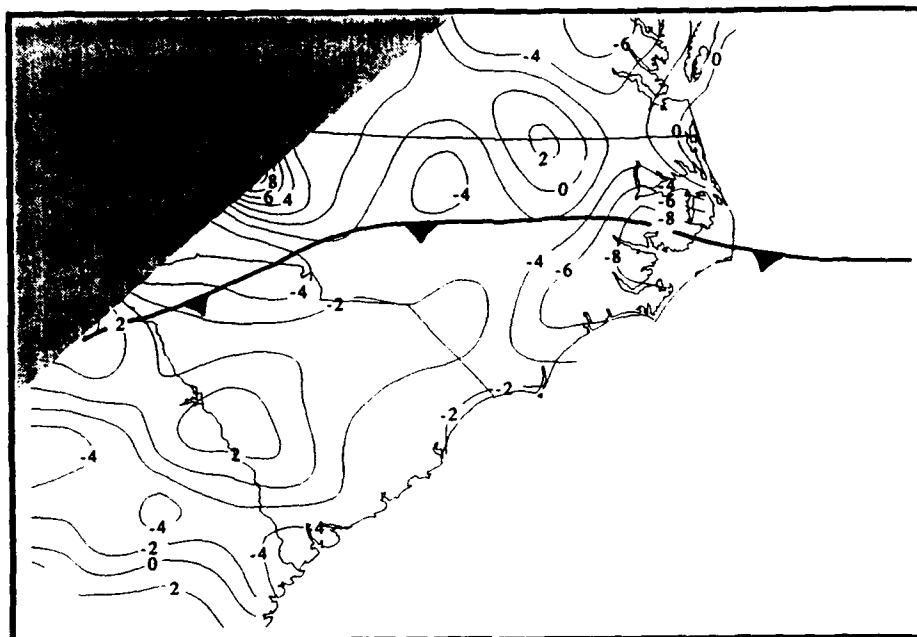


Figure 45. Divergence field for 2000 UTC 7 March 1986.

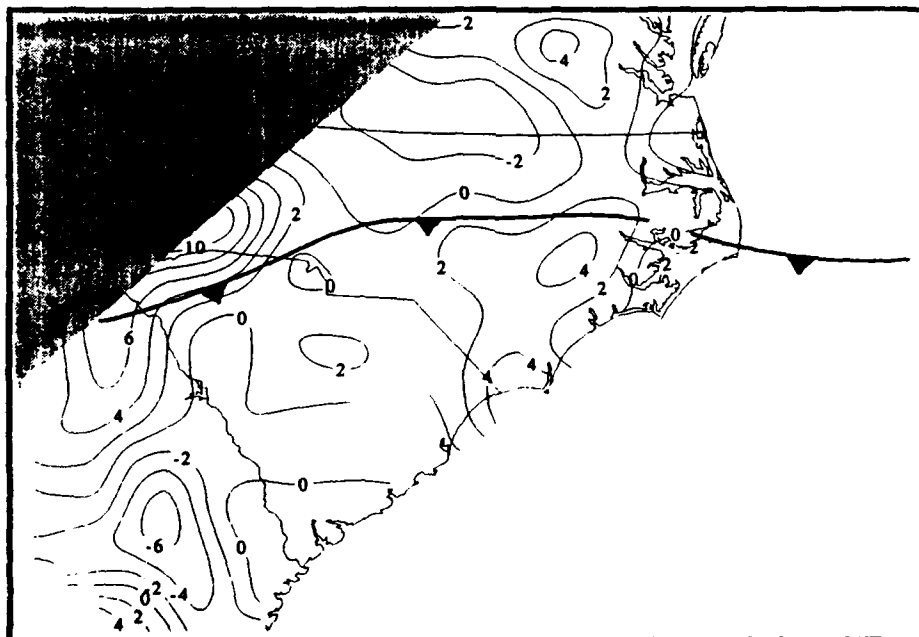


Figure 46. Vorticity field for 2000 UTC 7 March 1986.

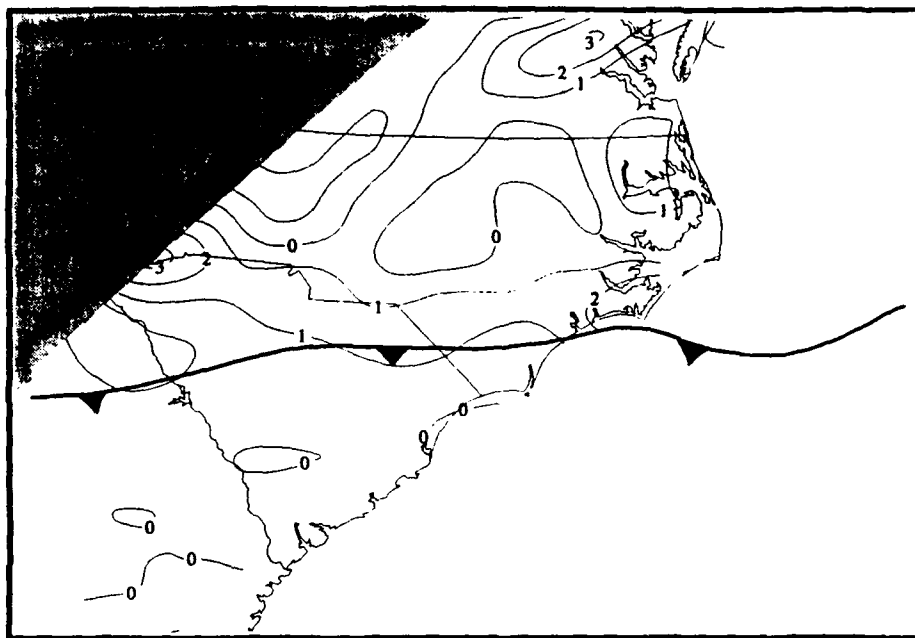


Figure 47. Total adiabatic frontogenesis for 2300 UTC 7 March 1986.

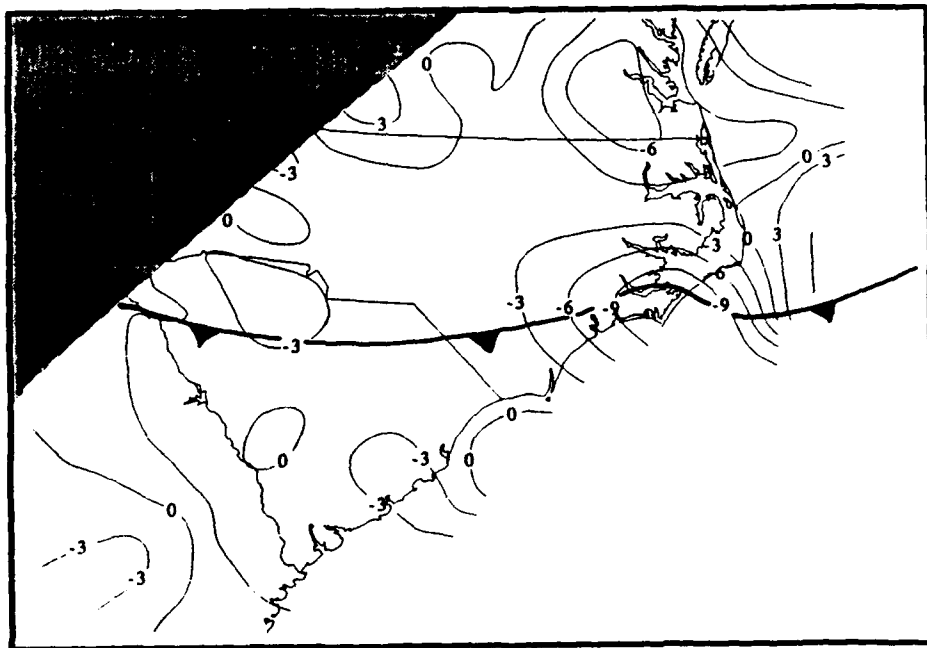


Figure 48. Divergence field for 2200 UTC 7 March 1986.

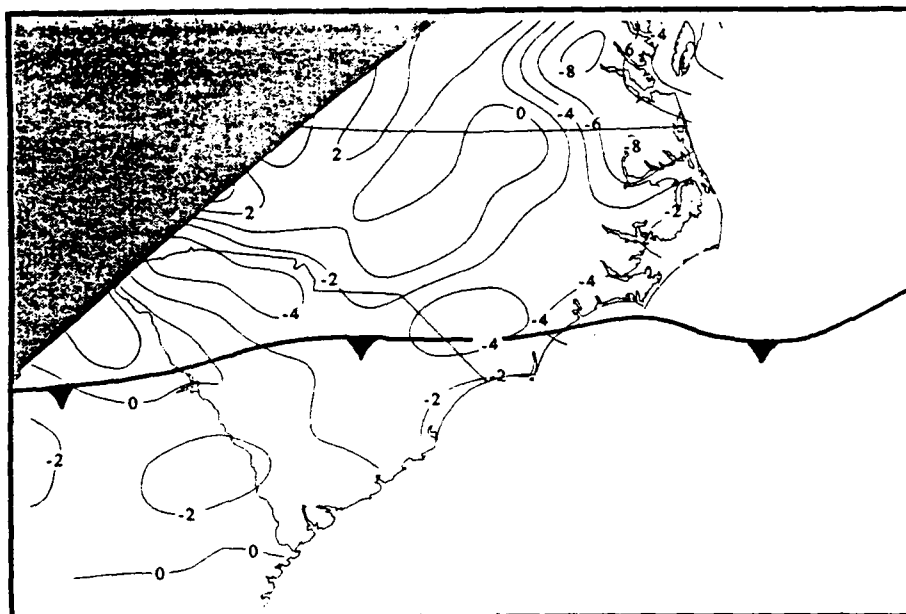


Figure 49. Divergence field for 2300 UTC 7 March 1986.

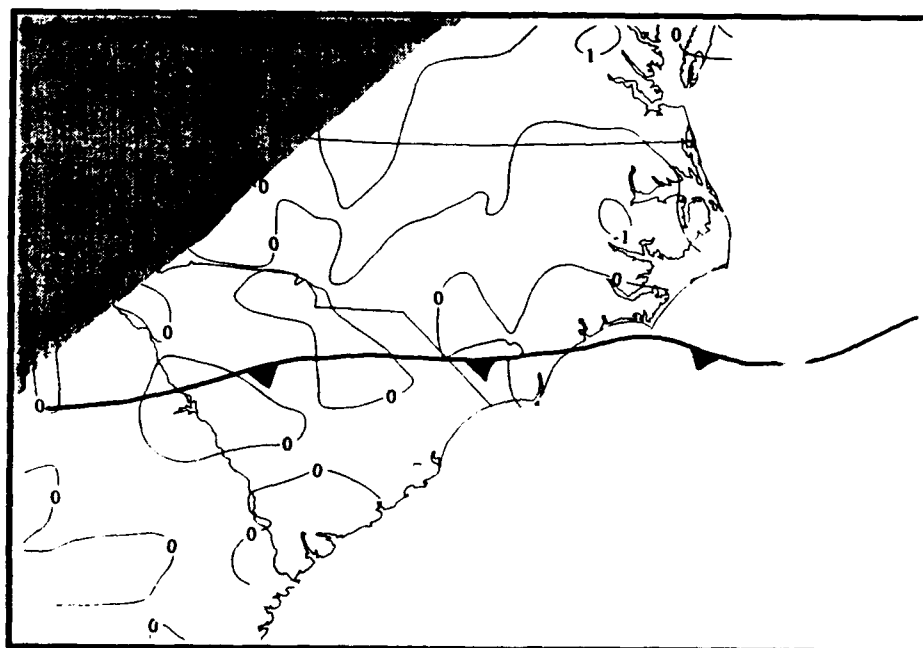


Figure 50. Shear term for 2300 UTC 7 March 1986.

also weakened over the previous several hours with a maximum value of 3 depicted over eastern North Carolina.

It is clear from this description of vorticity and the other diagnostically computed fields above that several important and recurring themes and trends have been established for case 1. The evolution of frontogenesis in the dense PAM data network for case 1 showed the existence of a positive frontogenetic maximum located along the eastern portion of the wind shift line as the primary feature of interest. The eastern portion of the wind shift line experienced positive frontogenesis for the entire period with the frontogenesis becoming stronger at the beginning of the period and weaker at the end. The initial strengthening was most likely associated with the zone of pronounced temperature gradient over the cold Atlantic shelf waters reinforcing the temperature gradient north of the eastern portion of the wind shift line. Confluence was the major frontogenetical forcing mechanism. Geostrophic frontogenesis appeared to be most important in maintaining the strength of a portion of the front which remained behind in the foothills east of the mountains. The frontogenetical forcing in this case was located well behind the wind shift line.

Significant positive total adiabatic and geostrophic frontogenesis, cyclonic vorticity and convergence along the eastern portion of the wind shift line indicate its active nature. These diagnostic computations combined with evidence of the meteograms for PAM

stations along northeastern North Carolina substantiate that the eastern portion of the wind shift line typifies a classic cold front.

Total adiabatic frontogenesis was also studied in detail for the cold front in case study #2 and compared to the front in case study #1. At 0200 UTC, the cold front was located in the northern portion of the PAM network and was oriented east-west. The thermal gradient in this case was located further behind the wind shift line as compared to case 1. Furthermore, frontogenetical forcing as seen in Fig. 51 also occurred across the central portion of the PAM network. As a rule, frontogenesis values were considerably less than values for case 1. Recall that the wind shift line for case 2 appeared to experience a considerable degree of modification after crossing the mountains which manifested itself in weaker pressure and temperature gradient fields. The weaker pressure gradient field resulted in a weaker wind field, and when combined with the weaker thermal field explains the lower magnitudes of frontogenesis. As in case 1, the confluence term dominated over the shear term as a frontogenetical forcing term. The maximum value of frontogenesis which was located just behind the extreme eastern portion of the wind shift line was 1 and accounted for over 90 % of the total frontogenesis (Fig. 52). No significant geostrophic frontogenetic forcing occurred in the vicinity of the wind shift line which was a noticeable difference from case 1. However, significant geostrophic frontogenesis did occur behind the wind shift line and east of the mountains as in case 1.

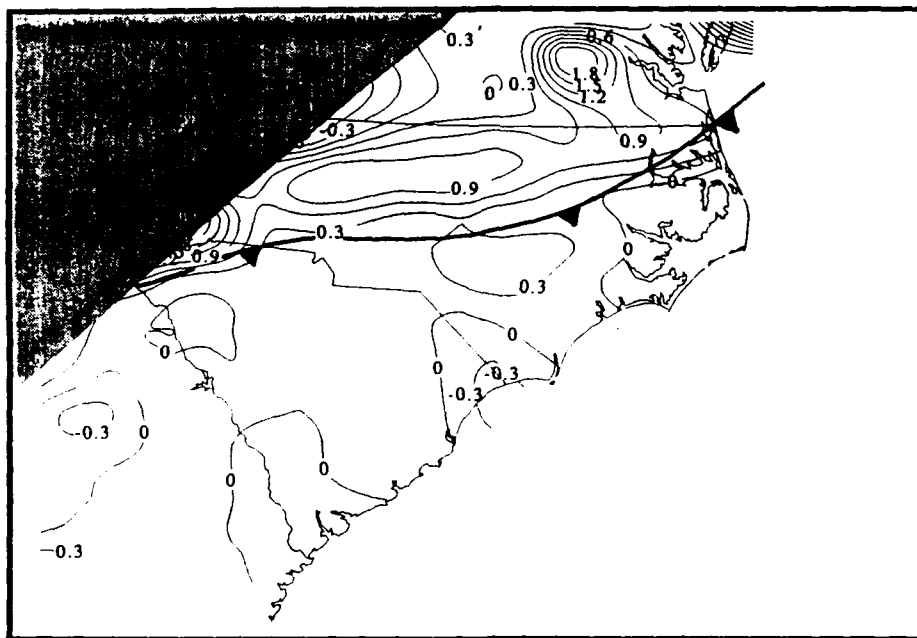


Figure 51. Confluence term for 0200 UTC 22 February 1986.

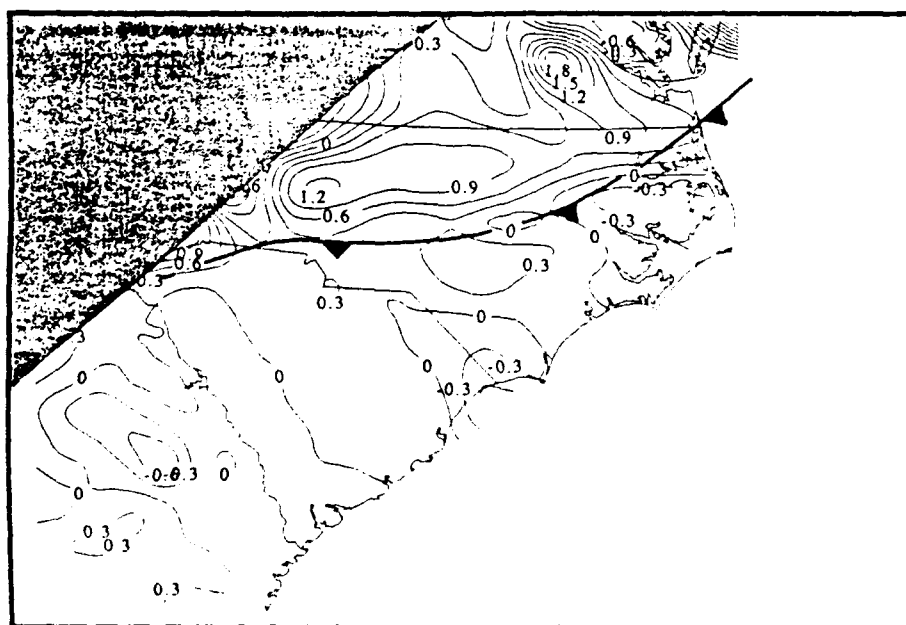


Figure 52. Total adiabatic frontogenesis for 0200 UTC 22 February 1986.

Significant convergence occurred uniformly across the entire wind shift line, whereas in case 1, maximum convergence occurred primarily in extreme eastern North Carolina. The meteograms confirmed that 29 out of 33 PAM stations experienced an abrupt wind shift from southwest-northwest through northeast, which substantiates the uniform convergence across the state. A convergence maximum of 5 was located along the extreme eastern portion of the wind shift line (Fig. 53). An area of positive cyclonic vorticity (maximum value of 3) was located along the eastern portion of the wind shift line as in case 1 (Fig. 54).

Three significant changes to frontogenesis occurred. The confluence term increased from near 0 to 3.5 from 1900 to 2000 UTC indicating stronger positive frontogenesis along the eastern portion of the wind shift line. The increase can be attributed to the strengthening of the thermal gradient behind the wind shift line as it acted on the pre-existing baroclinic zone over the cold Atlantic waters. A convergence maximum in this region (Fig. 55) superimposed on this thermal gradient is associated with the frontogenesis here.

An area of positive cyclonic vorticity occurred over extreme eastern North Carolina. The vorticity maximum of 5 was located along the eastern portion of the wind shift line (Fig. 56). Significant convergence continued to occur along the entire wind shift line with a maximum of 5 located along the eastern portion. Another

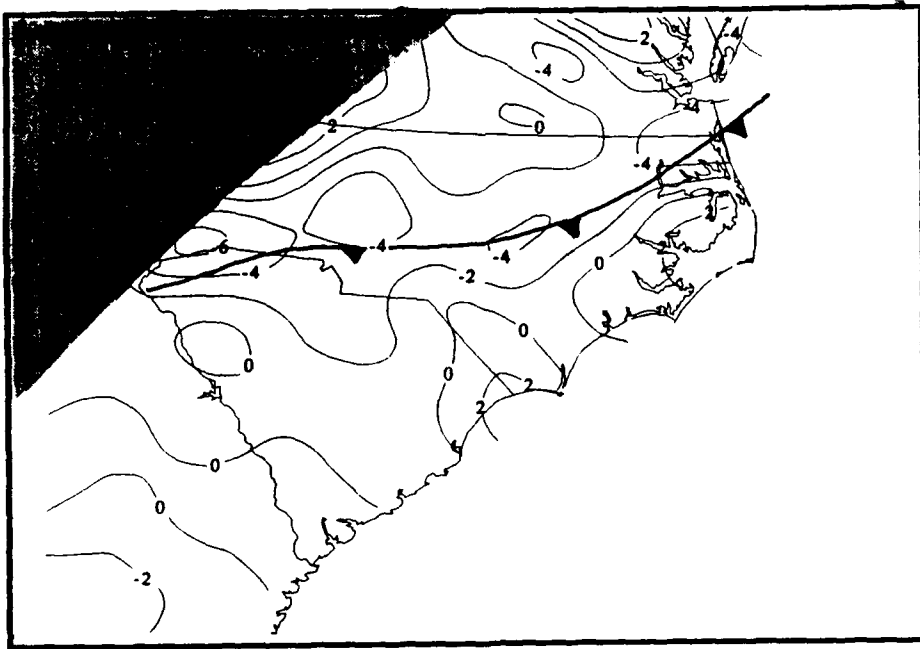


Figure 53. Divergence field for 0200 UTC 22 February 1986.

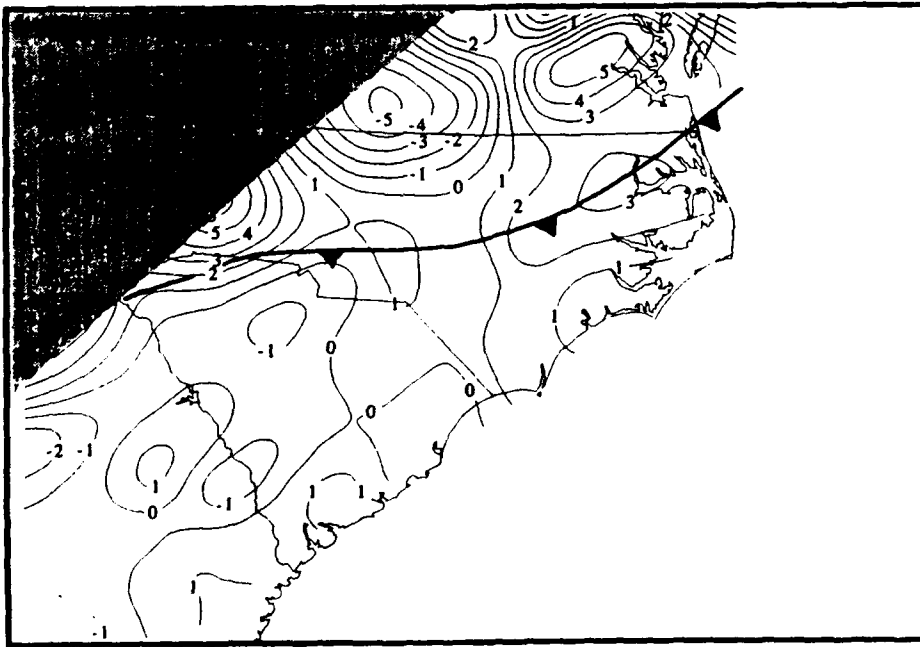


Figure 54. Vorticity field for 0200 UTC 22 February 1986.



Figure 55. Divergence field for 0300 UTC 22 February 1986.

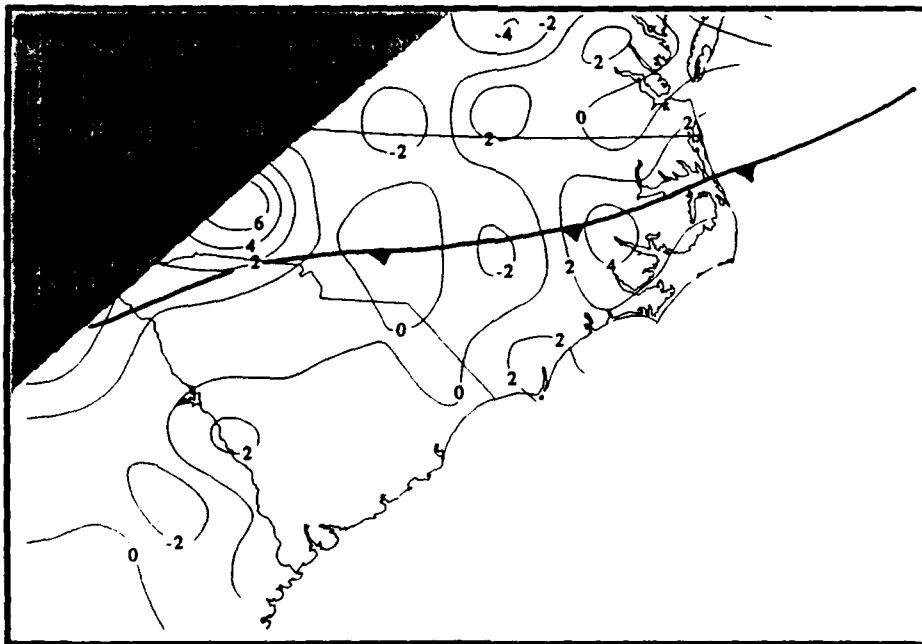


Figure 56. Vorticity field for 0300 UTC 22 February 1986.

maximum of 6 was located in the western edge of the PAM network across central North Carolina.

It is apparent that frontogenetical forcing for case 2 showed both differences as well as similarities to case 1. As a rule, the magnitudes of frontogenesis for case 2 were less than the magnitudes for case 1. In case 2, it had been shown previously that the wind shift line had been modified considerably by the mountains. The weakened pressure gradient, resultant weak wind field and weakened thermal field resulted in correspondingly lower values of frontogenesis. Diagnostically computed values of divergence and vorticity for case 2 were less than case 1. Positive geostrophic frontogenesis appeared to be important in case 1, but did not contribute significantly in case 2. Convergence was more uniformly distributed along the wind shift line in case 2, whereas in case 1 convergence was concentrated along the eastern portion of the wind shift line. Subsequently, confluent frontogenesis occurred along the entire wind shift line in case 2, while it occurred in a concentrated band along the eastern portion of the line in case 1. Frontogenesis also occurred well behind the wind shift line in case 2 with the exception of the eastern portion.

It appeared that for both cases, geostrophic frontogenesis was important in maintaining the strength of the front after it crossed the mountains. The strongest region of geostrophic frontogenesis was

located well behind the wind shift line. Geostrophic frontogenesis appeared to be more important along the eastern portion of the wind shift line in case 1 than in case 2.

The two cases showed distinct similarities in this region of coastal North Carolina. In both cases, total positive frontogenesis increased along the extreme eastern portion of the wind shift line. The confluence term dominated frontogenetical forcing in both cases. The increase in frontogenesis was most likely related to the enhancement of the thermal gradient behind the wind shift line by the pre-existing baroclinic zone over the cold Atlantic shelf waters. Recall that PAM stations showing distinct frontal passage in both cases were located in northeastern North Carolina and southeastern Virginia. Convergence and positive vorticity maxima along coastal North Carolina provided further evidence that the eastern portions of the wind shift lines were most active and closely resembled fronts according to classic theory.

11. DIABATIC FRONTOGENESIS

Diabatic effects on frontogenesis are difficult to assess, and in many instances the uniformity of surface properties can justify neglecting this physical process. However, in certain cases, diabatic effects can have a pronounced impact on positive or negative frontogenesis. The most important diabatic effect at the surface is surface heating. Bannon and Mak (1984) showed that only surface heating can directly alter the surface temperature field. It was shown by Segal et al. (1992) that the effect of surface heating is particularly important in the case of differential cloud shading across a cold front. In the author's study, the thermal impact of cloud shading across a cold front was evaluated briefly through conceptual, scaling, and numerical approaches. It was determined that the shading effect may have a pronounced contribution to frontogenesis for weak and moderate cold fronts. In a recent paper, Businger et al. (1991) suggested that cloud cover across a Piedmont front resulted in enhanced solar insolation on the warm side of a dry cold front that strengthened frontogenesis. Koch (1984) and Keyser (1986) have conducted related studies. However, according to Segal et al., no general elaboration or quantifications were given in these studies regarding the enhancement of cold front temperature contrast by differential cloud cover, and the studies were primarily qualitative.

Observational case study 1 of the current research substantiated the impact of differential cloud shading across the wind shift line

as a frontogenetic mechanism. The importance of this diabatic effect was previously mentioned for case 2, but the diabatic influence of differential cloud shading was limited to a small geographic area. Recall that the reason for this can be attributed to a much smaller cloud free area in case 2 than in case 1. It could be surmised that the frontogenetic effect would therefore be confined to a small geographic area for case 2, and thus will not be examined in further detail.

As was previously mentioned for case 1, satellite imagery for 1501 UTC (Fig. 23) showed significant cloud cover ahead of the wind shift line which covered the northern third of North Carolina. An extensive cloud free area was located to the south of the leading edge of the cloud mass. This was the situation at the time when the surface was beginning to receive maximum solar insolation with the cloud free area heating up at a significantly greater rate than the area under the clouds. Since the cold front was located well behind the leading edge of the cloud mass, it would be expected that the diabatic effect of differential cloud shading would establish a substantial temperature gradient ahead of the front which, in fact occurred between 1500 and 1800 UTC. In addition, the stronger temperature gradient would result in enhanced frontogenesis.

To initially assess the effect of this differential cloud shading process, diabatic surface heating was computed by hand for select points using the surface mesoscale analysis and an expansion of the

total derivative, $\frac{d\theta}{dt} = \frac{\partial\theta}{\partial t} + \mathbf{V} \cdot \nabla \theta$ assuming that $w = 0$ at the surface. In order to maintain consistency between scales of time, space, and motion, a time scale of two hours was selected based on a regional estimated boundary-layer wind speed obtained from the vertical sounding profiles. For the points selected in this study, Greensboro's (GSO) 1200 UTC sounding was the closest profile. It was used in selecting a representative boundary-layer wind speed of 15 m s^{-1} . Based on this speed, a parcel will travel 54 km in 1 h, the approximate station spacing in the PAM network. The minimum resolveable wavelength is twice the station spacing, namely 120 km. It would thus take a parcel about two hours to travel this distance. With these constraints imposed, $\frac{\partial\theta}{\partial t}$ was calculated for 15-1700 UTC centered at 1600 UTC. The advection term was computed at 1500 UTC and 1700 UTC using a distance of 120 km for the $\nabla\theta$ term. An average of the two advection terms was computed for the two hours and added to the local change to obtain the total diabatic heating for 1600 UTC. Total diabatic heating was computed at two locations in the vicinity of Greensboro and to the south of the cloud edge. Both points yielded values of about 2.0 K per hour.

These values were compared to forecast values of diabatic heating generated by using a 33-layer one-dimensional form of the Jean Francois Luis (1979) parametric model of vertical eddy fluxes in the atmosphere. The model is a surface based radiation model which includes the soil heat flux, sensible heat flux, latent heat flux, net

shortwave and net longwave radiation. The chosen parameterization scheme for the latent and sensible heat fluxes is based on Monin-Obukhov boundary layer similarity theory and Businger flux-profile relationships. GSO's 1200 UTC sounding was used to initialize the model run, since it was the closest station to the two selected points.

Latent and sensible heat fluxes were computed in the model based on several inputs. To compute the fluxes, a roughness parameter of 0.02, a soil depth of 0.12m, a soil heat capacity of $5.5 \times 10^4 \text{ kg s}^{-2} \text{ K}^{-1}$, and a deep soil temperature of 276 K were used. A value of 0.74 was used for the ratio of drag coefficients of heat and momentum in the neutral limit as suggested by Businger et al., (1971). A time scale of one day for the restoring effect of the deep layer of the soil, and a volumetric concentration of soil moisture of 0.1 were additional inputs to the model.

Several parameters were also needed by the model to calculate net shortwave and longwave radiation. The inputs for shortwave radiation were a surface albedo of 0.1, a solar declination angle of -7° , a solar constant of 1395 W m^{-2} . Net longwave radiation was computed based on the Stefan-Boltzmann relationship. The earth was assumed to be a black body emitter, and the atmosphere was assumed to be a grey body emitter. Radiative transfer theory was applied to compute the upward and downward components of short and longwave radiative fluxes for the entire 33-layer 12 km vertical depth in the model.

The model simulation started at 0700 local standard time and generated the forecast surface temperature for a 24-hour period. Diabatic heating was determined by computing the change in surface temperature from 1500 UTC to 1700 UTC centered at 1600 UTC to maintain consistency with the hand calculations performed for the same time. For 1600 UTC, the model results compared favorably to the hand calculations and yielded a value of 2.0 K hr⁻¹.

In addition, GEMPAK software was also used to compute total diabatic heating using the same method as the hand calculations. The contoured pattern of diabatic heating produced by GEMPAK appears to be coherent when comparing it to the 1500 UTC and 1800 UTC mesoscale surface analysis. The higher values of diabatic heating correspond with the cloud free region, while the lower values are located under the cloud mass. The actual magnitudes of the diabatic heating values for the two select points near Greensboro do not agree precisely with the hand-calculated and model-predicted values. GEMPAK values for these two points in Fig. 57 were approximately 3 K per hr which was slightly higher than the value of 2 K hr⁻¹ obtained using the two methods mentioned above.

Having established the importance of differential cloud shading and its effect on diabatic surface heating, diabatic surface frontogenesis was computed to determine its relative importance to total frontogenesis when compared to the other forcing terms of shear and confluence. Diabatic frontogenesis, $\frac{\nabla \theta}{|\nabla \theta|} \cdot \nabla \left(\frac{d\theta}{dt} \right)$ was

computed for 1600 UTC as shown in Fig. 58. The highest values of frontogenesis are located in the region south of the leading edge of the cloud mass. However, it is significant that the diabatic heating term dominates over both the shear term and the confluence term with respect to both magnitude and region of influence (Figs. 59 & 60). The maximum value of diabatic frontogenesis in the cloud free region is 10 as compared to a corresponding maximum value of 6 for the confluence term and 2 for the shear term. In fact, the dominance of the diabatic term in Fig. 58 can be seen when it is compared to total frontogenesis in Fig. 61. The contoured fields look nearly identical. This substantiates the importance of the thermal effect of cloud shading as an important frontogenetic process. This process also explains the strong temperature gradient ahead of the wind shift line, again illustrating its nonclassic nature.

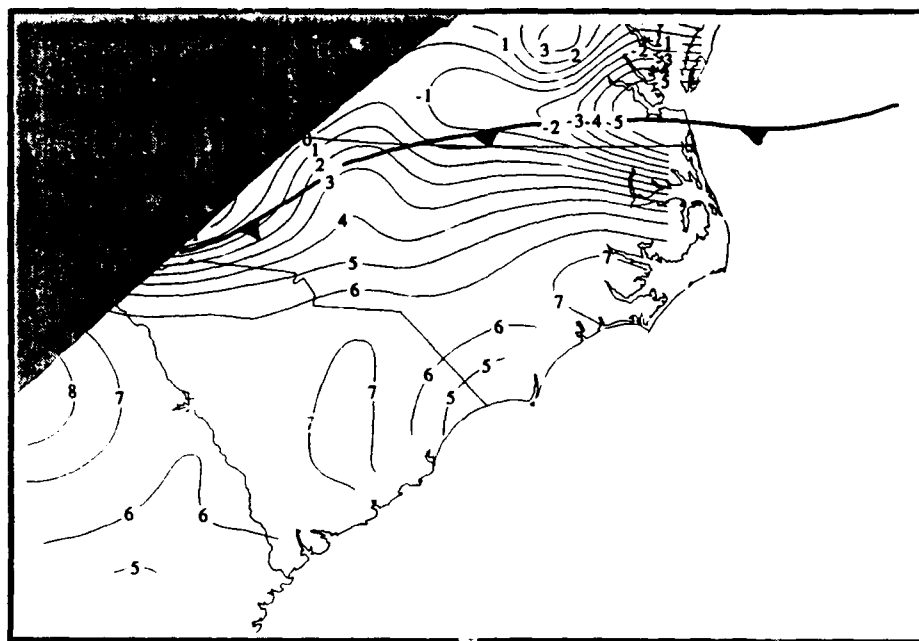


Figure 57. Total diabatic heating for 1600 UTC 7 March 1986. Units in k hr^{-1} .

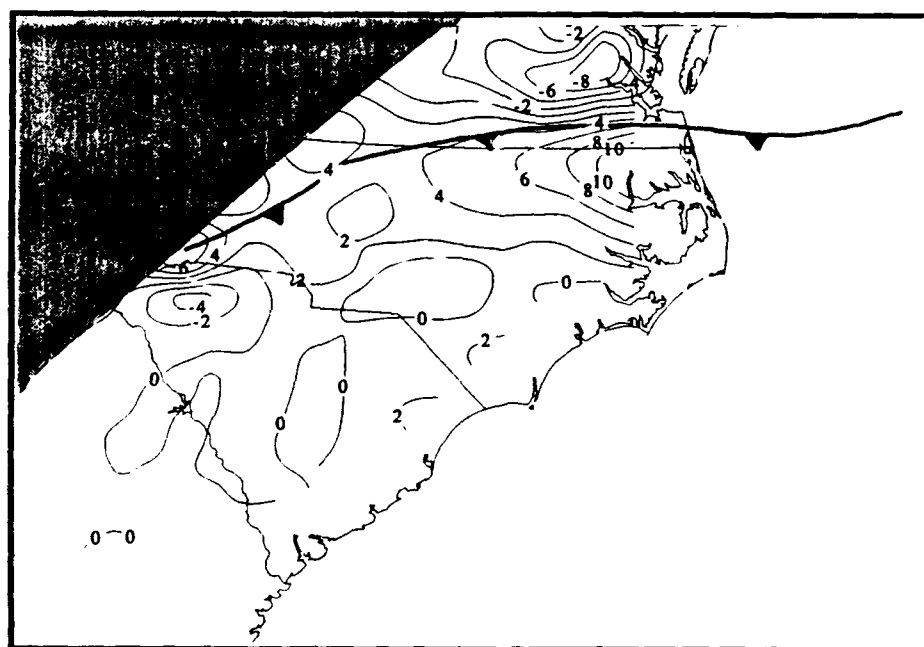


Figure 58. Diabatic Frontogenesis for 1600 UTC 7 March 1986.

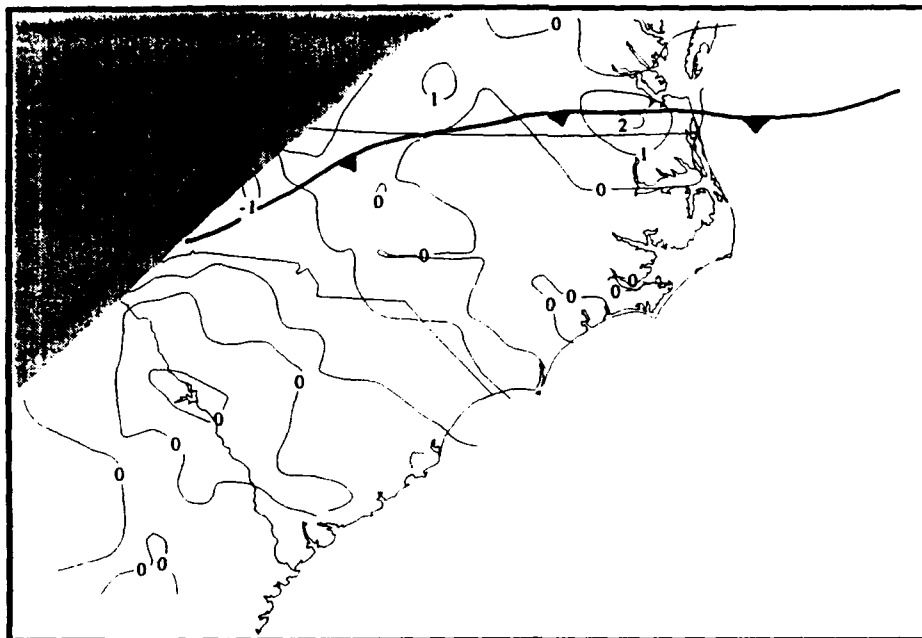


Figure 59. Shear term for 1600 UTC 7 March 1986.

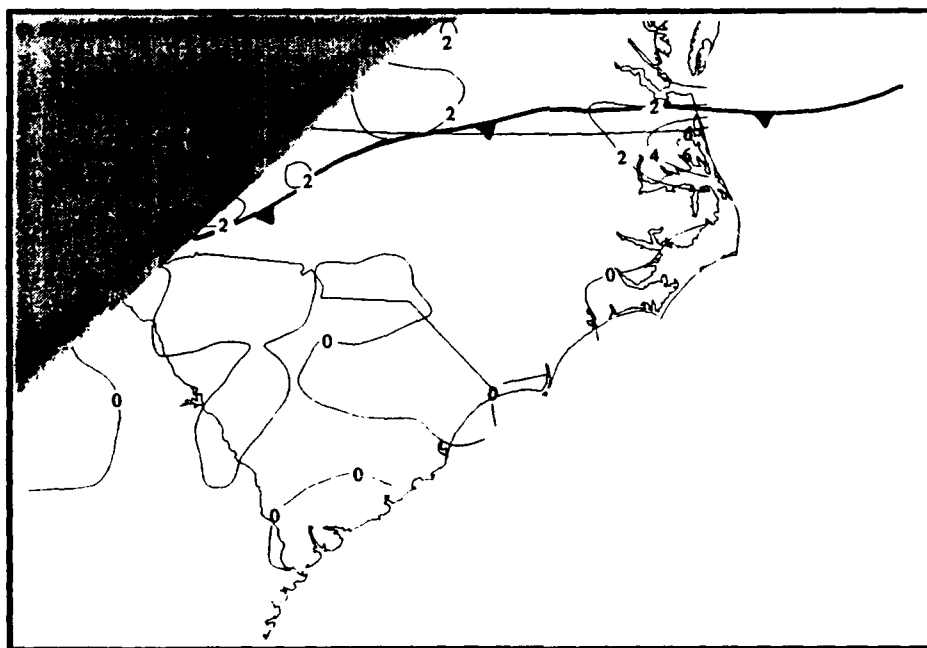


Figure 60. Confluence term for 1600 UTC 7 March 1986.

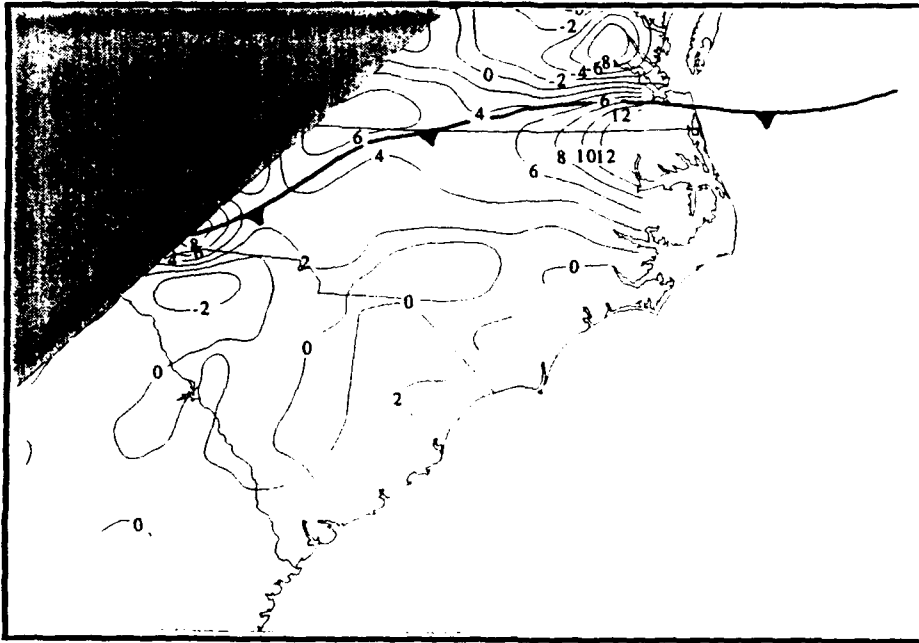


Figure 61. Total frontogenesis for 1600 UTC 7 March 1986 with the shear, confluence, and diabatic terms included.

12. DYNAMICAL FORCES

In order to explain why frontogenesis or frontolysis was occurring for each case, the individual forces acting on air parcels were examined with the aid of the equations of motion. Since the study was primarily surface based, a terrain following coordinate system was used in GEMPAK to compute the individual forces. Pielke and Martin (1981) defined a generalized vertical coordinate:

$$\sigma = S \frac{Z - Z_G}{S - Z_G} \quad \text{where } S \text{ is the height of the 500 mb level, } Z_G$$

is the terrain elevation, and Z is the height above the surface. Pielke (1984) showed that the momentum equations for terrain - following flow could be written in the form:

$$\frac{d u}{d t} = -\theta \frac{\partial \pi}{\partial x} + g \left(\frac{\sigma - S}{S} \right) \frac{\partial Z_G}{\partial x} + f v + F_x \quad (11)$$

$$\frac{d v}{d t} = -\theta \frac{\partial \pi}{\partial y} + g \left(\frac{\sigma - S}{S} \right) \frac{\partial Z_G}{\partial y} - f u + F_y \quad (12)$$

where f is the Coriolis parameter, θ is the potential temperature, g is the acceleration due to gravity. The Exner function is:

$$\pi = \frac{c_p T}{\theta} = c_p \left(\frac{p}{p_0} \right)^{\frac{R}{c_p}}$$

where T is the temperature. The Exner function shows that the scaled argument, π is directly related to the pressure p . The pressure gradient term in the momentum equations above is written as the sum of the π gradient along a σ surface (first term on the right hand side) and the terrain gradient term (second term on the right hand side). (Pielke et al., 1985).

By use of the geostrophic approximation, the momentum equations above reduce to the geostrophic wind equation in the σ coordinate system:

$$v_g = \frac{\theta}{f} \frac{\partial \pi}{\partial x} - \frac{g}{f} \left(\frac{\sigma - S}{S} \right) \frac{\partial Z_G}{\partial x} \quad (13)$$

$$u_g = -\frac{\theta}{f} \frac{\partial \pi}{\partial y} + \frac{g}{f} \left(\frac{\sigma - S}{S} \right) \frac{\partial Z_G}{\partial y} \quad (14)$$

In this sigma coordinate system, at the surface $\sigma = 0$ and the component geostrophic wind equations become:

$$v_g = \frac{\theta}{f} \frac{\partial \pi}{\partial x} + \frac{g}{f} \frac{\partial Z_G}{\partial X} \quad (15)$$

$$u_g = -\frac{\theta}{f} \frac{\partial \pi}{\partial y} - \frac{g}{f} \frac{\partial Z_G}{\partial y} \quad (16)$$

The pressure gradient force was computed through the use of the two geostrophic wind equations above by multiplying the x-

component of the geostrophic wind, U_g , with $-f$ to obtain the x component of the force. Subsequently the x-component of the pressure gradient force was obtained by multiplying the y-component of the geostrophic wind (v_g) by f . GEMPAK was then used to resolve the two components into the pressure gradient force vector.

The geostrophic winds computed from eqs. (16) and (17) are in reasonable agreement with those expected from the pressure field east of the mountains as depicted on the mesoscale surface analyses done by hand. This agreement substantiates the credibility of the analyzed pressure field as is shown in Fig. 62 and 63.

The other force vector quantities which included acceleration terms and the Coriolis and friction forces were also computed in the sigma coordinate system in order to assess the total dynamic force balance for individual air parcels. The Coriolis force was computed simply from the components fv and $-fu$. Total horizontal acceleration was computed by expanding the total derivative of acceleration components into their local and advective changes:

$$\frac{d u}{d t} = \frac{\partial u}{\partial t} + u \frac{\partial u}{\partial x} + v \frac{\partial u}{\partial y} \quad (17)$$

$$\frac{d v}{d t} = \frac{\partial v}{\partial t} + u \frac{\partial v}{\partial x} + v \frac{\partial v}{\partial y}. \quad (18)$$

The local changes were computed as two-hour difference centered at the time of interest, and the total advective change was computed

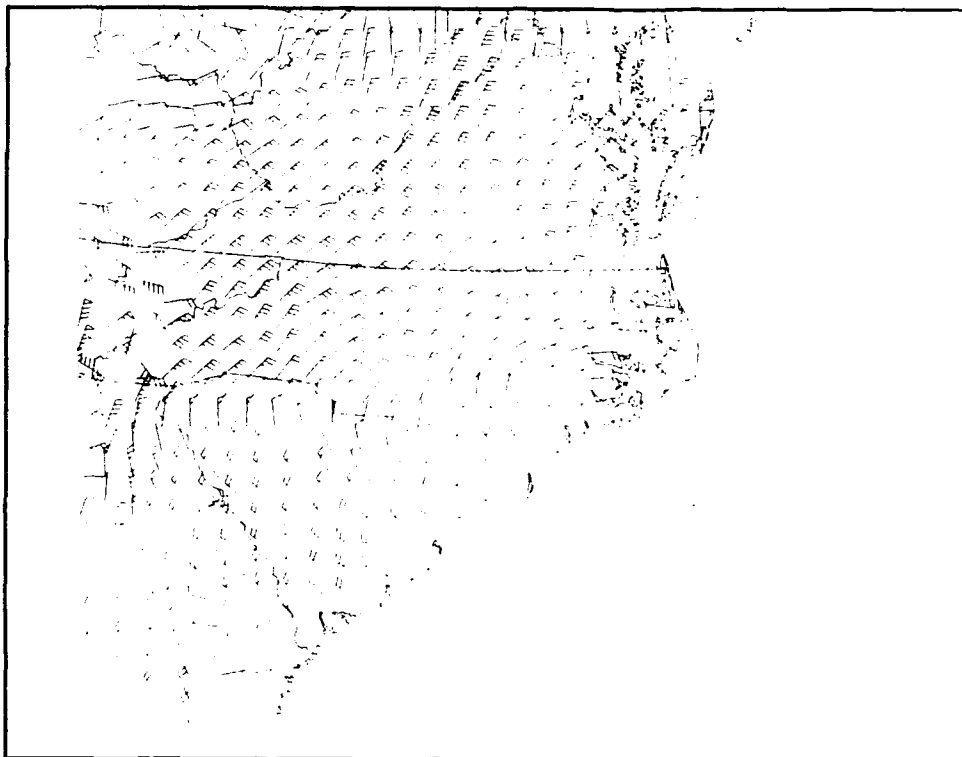


Figure 62. Geostrophic winds for 2100 UTC 7 March 1986. Full (half) barbs indicate wind speeds of 5 m s^{-1} (2.5 m s^{-1}).

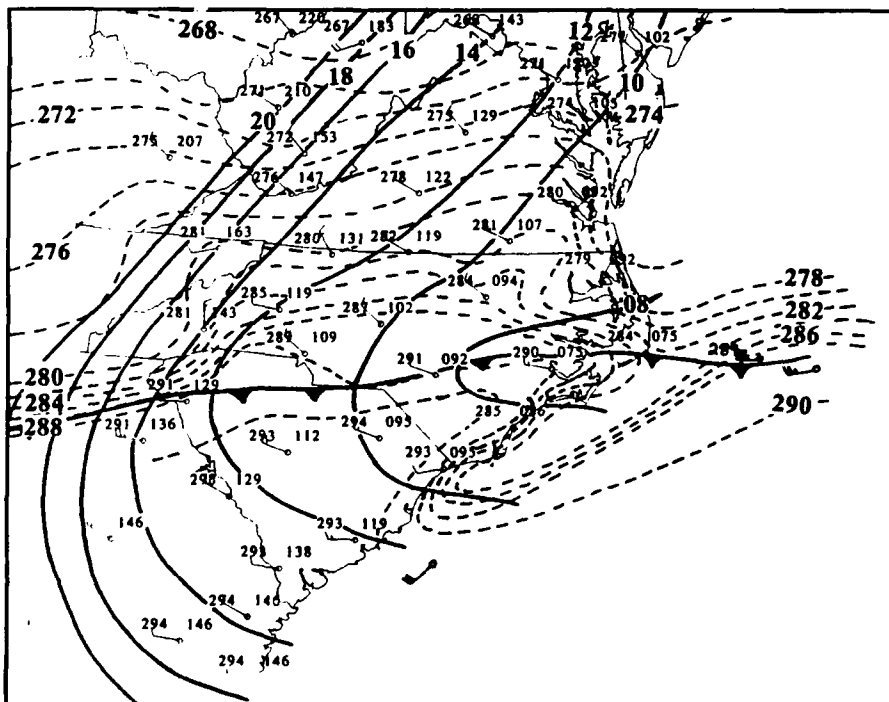


Figure 63. Mesoscale surface analysis for 2100 UTC 7 March 1986.

based on the average of the advective change over the same period. It should be noted that the vertical advection term does not appear in the substantial derivatives above by virtue of the fact that vertical motion, $\frac{d\sigma}{dt} = 0$ on $\sigma = 0$ surface and subsequent vertical acceleration due to the movement of parcels in sloping terrain is already accounted for in the sigma coordinate system. This adequately justifies the use of the expressions above to compute acceleration at the surface using the σ system. The vector subtraction of the pressure gradient force and the Coriolis force from this acceleration yielded the friction force as a residual.

Friction was computed in this way due to the difficulty in calculating this force directly. It is composed of both the friction force resolvable from the observed data, and computational errors arising from the spatial distribution and interpolation of computed quantities inherent in the Barnes Objective Analysis scheme.

In both case 1 and case 2, a surface parcel trajectory analysis was accomplished partially by hand and by GEMPAK. Then the dynamic force balance was computed for individual parcels within the PAM network. In both cases, the pressure gradient and residual friction force were the dominant forces, but were slightly less in case 2 due to the weaker pressure gradient. In most cases, the pressure gradient force was at least twice as large as both the acceleration and the Coriolis force. Since terrain roughness is reasonably uniform

east of the mountains, one expects that friction would be proportional to wind speed. Therefore, parcel accelerations are probably due to changes in the pressure gradient force.

For case 1, the dynamic force balance was determined for 4 parcels at 2100 UTC. Fig. 64 shows the position of the 4 parcels at 2000, 2100, and 2200 UTC with implied trajectories. Arrows indicate the magnitude and direction of the acceleration and individual forces at 2100 UTC. The two parcels north of the front were accelerating to the west southwest. The parcels were moving generally from an area with a stronger pressure gradient field to an area where that field was weaker.

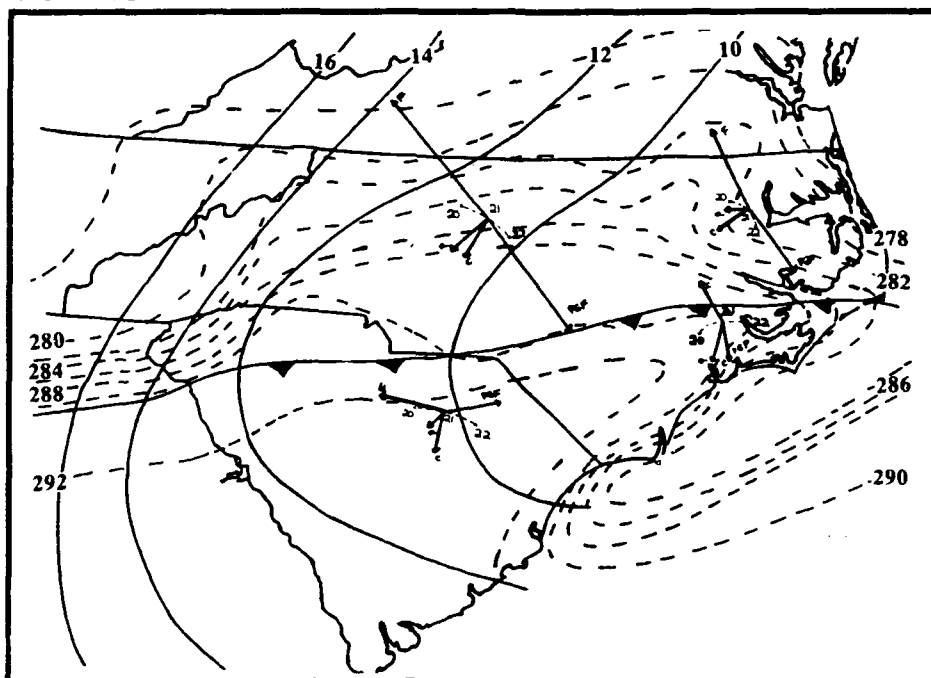


Figure 64. Dynamic force balance at 2100 UTC and selected parcel trajectories from 20-2200 UTC. Individual forces labelled as F-friction, PGF-pressure gradient force, a-acceleration, and C-coriolis. Magnitudes of forces indicated by lengths scaled as $1\text{cm} = 10^{-4} \text{ m s}^{-4}$.

For the two parcels south of the front, the pressure gradient force is smaller as the isobar pattern indicates. In fact, the easternmost parcel has an acceleration, pressure gradient force, and Coriolis force of nearly equal magnitude. In the case of the parcel to the west, the pressure gradient force is nearly twice as large as the Coriolis force. The trajectories of both parcels indicate that the acceleration is to the southsouthwest. Again, the parcels were moving generally toward decreasing pressure gradient force.

To examine the possible effect of the parcel accelerations on frontogenesis, one can look at the two eastern most parcels in particular and compare their motion and acceleration with the superimposed thermal gradient. It appears that based on the two parcel trajectories that the winds at 2100 UTC for the two parcels are convergent. When superimposed on the thermal gradient, this convergence produces positive frontogenesis. Positive frontogenesis was occurring in this region with a maximum value of 7 at this time. Recall that parcel accelerations determine the future wind field. At 2100 UTC, the parcel accelerations are somewhat divergent. One would expect that the resultant future winds for the two parcels would be less convergent with time. The decreased convergence on the superimposed thermal field resulted in a decrease in positive frontogenesis with a value of 6 at 2200 UTC.

For case 2, 3 parcels are depicted in Fig. 6 which shows the force balance and acceleration for each parcel centered at 0400 UTC 22 Feb 86. Again, the pressure gradient force dominates the force balances

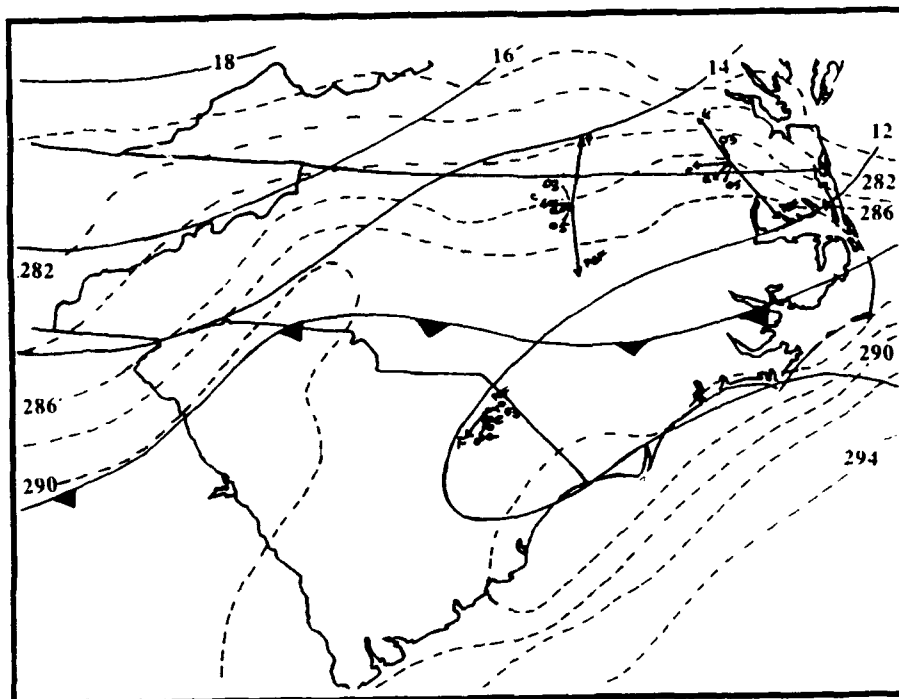


Figure 65. Same as Fig. 65 except dynamic force balance at 0400 UTC 22 February 1986 and parcel trajectories from 03-0500 UTC 22 February 1986.

for these individual parcels with the exception of the parcel south of the wind shift line which is in a region where the pressure gradient is weak. Based on its trajectory this parcel was accelerating slightly to the right.

The parcel trajectories and accelerations were examined to assess the effect on frontogenesis as in case 1. At 0400 UTC, the winds for the westernmost parcel north of the front were northerly and the winds for the parcel south of the front were southwesterly. The winds for the two parcels are therefore convergent at this time. The thermal field associated with the parcel south of the front is weak, while the thermal field north of the front is significantly stronger. When the parcel trajectories for the two parcels are superimposed

on the thermal field, one would anticipate weak positive frontogenesis over the region between the two parcels.. After 0400 UTC, however, the parcel accelerations appear to force the wind field to be less convergent. Therefore, one would expect at least a slight decrease in positive frontogenesis over time. In fact, the maximum value of frontogenesis was approximately 1 at 0400 UTC in the area between the two parcels and decreased to around 0.5 at 0500 UTC.

The dynamic force balance shows which forces are dominant and responsible for parcel accelerations. For the two wind shift lines in these case studies, it is apparent that the main force responsible for parcel accelerations is the pressure gradient force. From the parcel accelerations, the future wind field can be determined. This could ultimately lead to the capability for short range prediction of frontogenesis and frontolysis.

13. SUMMARY AND CONCLUSIONS

Meso- β scale frontogenesis was investigated for two cold front case studies. A comparative analysis of the two cases was conducted, and the evolution of the two fronts was compared to classic frontal theory. Kinematic frontogenesis was evaluated to identify the dominant forcing terms for each case. The diabatic effects of differential cloud shading on solar heating at the surface and its contribution to total frontogenesis was studied. Dynamical force balances for select air parcels in the PAM network for select times were computed to determine dominant forces, resultant accelerations, and their relationship to frontogenesis.

The cold front of case 1 exhibited non-classic features with a multiple line structure including a pre-frontal trough, wind shift line, and front prior to crossing the mountains. The associated thermal and pressure gradients were relatively weak. The mesoscale surface analysis showed the pre-frontal trough to be relatively weak as well. Meteograms showed that many stations experienced backing/veering oscillations rather than an abrupt wind shift at the time of this trough passage.

Significant frontogenesis mainly occurred along the extreme eastern portion of North Carolina, with the confluence term dominating frontogenetical forcing. The divergence and vorticity fields also showed this region to be most active. Positive geostrophic frontogenesis also appeared to be somewhat important along the

extreme eastern portion of the wind shift line. Geostrophic frontogenetical forcing appeared to be quite important in maintaining the strength of the front after it crossed the mountains. This forcing was located well behind the wind shift line and due east of the mountains.

The diabatic effect of surface heating due to differential cloud shading was found to be an important contributor to total frontogenesis at selected times. The mesoscale surface analysis showed the evolution of a strong thermal gradient ahead of the wind shift lines. Diabatic frontogenesis was calculated at a particular time for case 1 and shown to be nearly twice as important as confluence and five times as important as shear to total frontogenesis.

The mesoscale surface analysis for case 1 showed the importance of diabatic heating over the land from 15 to 1800 UTC and the advection of cold air over the Virginia coastal plain in re-establishing the eastern portion of the frontal boundaries which were destroyed after crossing the mountains. Other studies also showed this process to be important, and in some cases resulted in the development of density currents. The enhanced baroclinicity and convergence over eastern North Carolina produced significant frontogenesis at the coast.

Meteograms based on 5-minute PAM data confirmed that only certain stations experienced classic frontal passage. These stations were all located near the coast of northeastern North Carolina and

southeastern Virginia. The stations experienced wind shifts, temperature drops, and pressure jumps at the mesoscale typical of fronts from other case studies and which closely resembled density currents. The meteograms indicate that only the extreme eastern portion of the wind shift line closely resembled fronts of the classic cyclone model.

The dynamical force balances showed that the pressure gradient force appeared to be the dominant factor responsible for the acceleration of individual air parcels. This acceleration occurred as the overall pressure gradient weakened with time and also as the parcels moved eastward into areas with a weaker pressure gradient. The acceleration subsequently determines the future wind field. When the new wind field acts on the thermal field either frontogenesis or frontolysis occurs. This suggests that the availability of a dense mesoscale data network with good temporal and spatial resolution would allow a forecaster to determine the future behavior of frontogenesis fields. This would allow a forecaster to more accurately predict the strengthening or weakening of fronts or temperature gradients, the impact on other sensible weather phenomenon. (eg., precipitation)

The cold front of case 2 showed similarities and differences to the cold front of case 1. Prior to crossing the mountains, the case 2 front differed significantly. This frontal system appeared initially to be classic. The surface trough was coincident with the cold front, and the thermal and pressure gradients were strong.

However, when this front crossed the mountains, it appeared to be significantly altered by the topography and to behave similarly to the front of case 1. Both exhibited non-classic features with a multiple line structure.

The pre-frontal trough for case 2 was more pronounced. Meteograms of most stations showed distinct wind shift associated with trough passage. This trough was also associated with greater convergence through central North Carolina subsequently resulting in somewhat more frontogenetical forcing in this region as compared to case 1.

The overall magnitudes of frontogenesis for case 2, however were significantly smaller than for case 1. The lower magnitudes for case 2 could be attributed to weaker thermal and pressure gradients. The confluence term dominated frontogenetical forcing as it did for case 1. Strongest frontogenesis also occurred along the coast, and divergence and vorticity fields confirmed that this region was active. Positive geostrophic frontogenesis also appeared to be as important as in case 1 for maintaining the strength of the front after it crossed the mountains. The diabatic effect of surface heating due to differential cloud shading for case 2 was limited to a very small geographic area, and therefore was not as important to total frontogenesis.

The advection of cold air over the Virginia coast for case 2 was important in re-establishing the eastern portion of the frontal

boundaries which were destroyed after crossing the mountains. The enhanced baroclinicity and convergence over eastern North Carolina produced significant frontogenesis at the coast just as they did for case 1.

The dynamical force balances showed that the pressure gradient force appeared to be the dominant force responsible for the acceleration of individual air parcels as it was for case 1.

14. FUTURE RESEARCH

Several areas of frontal research require additional emphasis in the future. An important limiting factor to the current research was the absence of a spatially dense radiosonde network to mirror the dense surface-based PAM network during GALE. In spite of the deployment of additional soundings with increased frequency, the radiosonde network could not provide the spatial and temporal resolution required to resolve upper level mesoscale- β frontal processes. Performing diagnostic computations of derived quantities (ie., frontogenesis) at this scale in the upper levels of the atmosphere was not possible. Meteorological field experiments conducted in the future should include the employment of dense surface based networks with equivalently dense upper air networks. This would permit a more complete and thorough three-dimensional analysis of fronts on the Meso- β scale.

Improved horizontal and vertical resolution of data possible in future field experiments should be exploited by conducting numerous observational case studies like those of this current research. These studies should focus on, but not be limited to, a comprehensive evaluation of dynamical forces and resultant accelerations in an attempt to explain the causes of frontogenesis for individual cases. Another area of research requiring further emphasis is the evaluation of diabatic frontogenesis at the surface and upper levels, due to their relative importance as forcing

mechanisms in certain situations. A need exists to develop new and improved methods for accurate computations of diabatic frontogenesis and ultimately total frontogenesis for future observational studies.

A large number of these observational studies, especially at the mesoscale level, should be conducted to increase the understanding of fronts and extend the large body of knowledge which already exists. More frontal studies are needed, particularly for North Carolina, to discover a conceptual frontal model unique to the region. Such data may lead to the eventual modification of the classic polar-front cyclone model of fronts.

REFERENCES

- Bannon, P.R. and M. Mak, 1984: Diabatic quasi-geostrophic surface frontogenesis. *J. Atmos. Sci.*, **41**, 2189-2201.
- Barnes, S.L., 1964: A technique for maximizing details in numerical weather map analysis. *J. Appl. Meteor.*, **3**, 396-409.
- _____, 1973: Mesoscale objective map analysis using weighted time-series observations. *NOAA Technical Memorandum ERL NSSL-62*, Norman, Ok, 60 pp.
- Bergeron, T., 1928: Uberdie dreidimensional verknupfende wetternupfende wetteranalyse. *Geofys. Publ.*, **5**, 1-111.
- Bjerknes, J. 1919. On the structure of moving cyclones. *Geofys. Publ.*, **1(1)**, 1-8.
- _____, and H. Solberg, 1921: Meteorological conditions for the formation of rain. *Geofys. Publ.*, **2(3)**, 1-60.
- _____, and H. Solberg, 1922: Life cycle of cyclones and the polar front theory of atmospheric circulation. *Geofys. Publ.*, **3(1)**, 1-18.
- _____, J. and E. Palmen, 1937: Investigations of selected European cyclones by means of serial ascents. *Geofys. Publ.*, **12(2)**, 1-62.
- Bluestein, H.B., 1986: Fronts and Jet Streaks: A theoretical perspective, In: *Mesoscale Meteorology and Forecasting*, Ray, P.S., Ed., 173-215.

- Blumen, W., 1980: A comparison between the Hoskins-Bretherton model of frontogenesis and the analysis of an intense surface frontal zone. *J. Atmos. Sci.*, **37**, 64-77.
- Bosart, L.F., 1975: New England coastal frontogenesis. *Quart. J. Roy. Meteor. Soc.*, **101**, 957-978.
- Businger, J.A., J.C. Wyngaard, Y. Izumi, and E.F. Bradley 1971: Flux-profile relationships in the atmospheric surface layer, *J. Atmos. Sci.*, **28**, 187-202.
- Businger, S., W.H. Bauman III and G.F. Watson (1991): The development of the Piedmont front and associated outbreak of severe weather on 13 March 1986. *Mon. Wea. Rev.*, **119**, 2224-2251.
- Charney, J.G., 1947: The dynamics of long waves in a baroclinic westerly current. *J. Meteor.*, **4**, 135-163.
- Dirks, R.A., J.P. Kuettner and J.A. Moore, 1988: Genesis of Atlantic Lows Experiment (GALE): an overview. *Bull. Amer. Meteor. Soc.*, **69**, 148-160.
- Eady, E.T., 1949: Long waves and cyclone waves. *Tellus*, **1(3)**, 33-52.
- Eliassen, A., 1959: On the formation of fronts in the atmosphere. The Atmosphere and The Sea In Motion (B. Bolin, Ed.), Rockefeller Institute Press, 277-287.
- _____, 1962: On the vertical circulation in frontal zones. *Geofys. Publ.*, **24(4)**, 147-160.

- Garratt, J.R., 1988: Summertime cold fronts in southeastern Australia-Behavior and low-level structure of main frontal types. *Mon. Wea. Rev.*, **116**, 636-649.
- _____, P.A.C. Howells, and E. Kowalczyk, 1988: The behavior of dry cold fronts traveling along a coastline. *Mon. Wea. Rev.*, **117**, 1208-1220.
- Hakim, G.J., 1992: The eastern United States side-door cold front of 22 April 1987: A case study of an intense atmospheric density current. *Mon. Wea. Rev.*, **120**, 2738-2762.
- Hoskins, B.J. and F.P. Bretherton, 1972: Atmospheric frontogenesis models: Mathematical formulation and solution. *J. Atmos. Sci.*, **29**, 11-37.
- _____, 1974: The role of potential vorticity in symmetric stability and instability. *Quart. J. Roy. Meteor. Soc.*, **100**, 480-482.
- _____, B.J., 1975: The geostrophic momentum approximation and the semi-geostrophic equations. *J. Atmos. Sci.*, **32**, 233-242.
- _____, B.J. and N.V. West, 1979: Baroclinic waves and frontogenesis. Part II: Uniform potential vorticity jet flows-cold and warm fronts. *J. Atmos. Sci.*, **36**, 1663-1680.
- Keshishian, L.G. and L.F. Bosart, 1987: A case study of extended east coast frontogenesis. *Mon. Wea. Rev.*, **115**, 100-117.
- Keyser, D. K., 1986: Diagnosis of the role of vertical deformation in a two-dimensional primitive equation model of upper level frontogenesis. *J. Atmos. Sci.*, **43**, 839-885.

- Koch, S.E., 1984: Role of an apparent mesoscale frontogenetic circulation in squall line initiation. *Mon. Wea. Rev.*, **112**, 2090-2111.
- Luis, Jean-francois, 1979: Parametric model of vertical eddy fluxes in the atmospheric surface layer, *J. Atmos. Sci.*, **28**, 181-189.
- Mass, C.F., 1991: Synoptic frontal analysis: Time for a reassessment? *Bull. Amer. Meteor. Soc.*, **72**, 348-363.
- McWilliams, J.C. and P.R. Gent, 1980: Intermediate models of planetary circulations in the atmosphere and ocean. *J. Atmos. Sci.*, **37**, 1657-1678.
- Miller, J.E., 1948: On the concept of frontogenesis. *J. Meteor.*, **5**, 169-171.
- Newton, C.W., 1954: Frontogenesis and frontolysis as a three-dimensional process. *J. Meteor.*, **11**, 449-461.
- Orlanski, I. and B.B. Ross, 1982: The evolution of an observed cold front. Part II: Mesoscale dynamics. *J. Atmos. Sci.*, **41**, 1669-1702.
- Palmen, E., 1948: On the distribution of temperature and wind in the upper westerlies. *J. Meteor.*, **5**, 20-27.
- _____, and C.W. Newton, 1948: A study of the mean wind and temperature distribution in the vicinity of the polar front in winter. *J. Meteor.*, **5**, 220-226.
- Petterssen, S., 1935: A contribution to the theory of frontogenesis. *Geofys. Publ.*, **11**, No. 6.

- _____, 1936: A contribution to the theory of frontogenesis. *Geofys. Publ.*, **11**, 1-27.
- _____, and J. M. Austin, 1942: Fronts and frontogenesis in relation to vorticity. *Pap. Phys. Oceanogr. Meteor.*, **7(2)**, 1-37.
- _____, 1940: Weather Analysis and Forecasting, Vol 1., Motion and motion systems. 1st ed., McGraw Hill, New York, 428 pp.
- Pielke, R.A., and C.L. Martin, 1981: The derivation of a terrain-following coordinate system for use in a hydrostatic model. *J. Atmos. Sci.*, **38**, 1707-1713.
- _____, 1984: *Mesoscale Meteorological Modeling*, Academic Press, 612 pp.
- _____, M. Segal, R.T. McNider and Y. Mahrer, 1985: Derivation of slope flow equations using two different coordinate representations. *J. Atmos. Sci.*, **42**, 1102-1106.
- _____, and J. Cram, 1987: An alternate procedure for analyzing surface geostrophic winds and pressure over elevated terrain. *Weather and Forecasting*, **2**, 229-236.
- Reed, R.J. and F. Sanders, 1953: An investigation of the development of a mid-tropospheric frontal zone and its associated vorticity field. *J. Meteor.*, **10**, 338-349.
- Ross, B.B. and I. Orlanski, 1978: The circulation associated with a cold front. Part II: Moist case. *J. Atmos. Sci.*, **35**, 445-465.
- Ross, B.B. and I. Orlanski, 1982: The evolution of an observed cold front. Part I: Numerical simulation. *J. Atmos. Sci.*, **39**, 296-327.

- Sanders, F., 1955: An investigation of the structure and dynamics of an intense surface frontal zone. *J. Meteor.*, **12**, 542-552.
- Saucier, W.J., 1983: Principles of Meteorological Analysis, Dover Publications Inc., New York, 433 pp.
- Sawyer, J.S., 1956: The vertical circulation at meteorological fronts and its relation to frontogenesis. *Proc. Roy. Soc. London*, **A234**, 346-362.
- Segal et. al., 1992: On the enhancement of cold front temperature contrast by differential cloud cover. (submitted to *Mon. Wea. Rev.*)
- Seitter, K.L., 1986: A numerical study of atmospheric density current motion including the effects of condensation. *J. Atmos. Sci.*, **24**, 3068-3076.
- Smith, D.L., F.L. Zuckerberg, J.T. Schaefer, and G.E. Rasch, 1986: Forecast problems: The meteorological and operational factors, In: *Mesoscale Meteorology and Forecasting*, Ray, P.S., Ed., 1986, 36-49, AMS, Boston.
- Smith, R.K., and M.J. Reeder 1988: On the movement and low-level structure of cold fronts. *Mon. Wea. Rev.*, **116**, 1927-1943.
- Stone, P.H., 1966: Frontogenesis by horizontal wind deformation fields. *J. Atmos. Sci.*, **23**, 455-465.
- Williams, R.T. and J. Plotkin, 1968: Quasi-geostrophic frontogenesis. *J. Atmos. Sci.*, **25**, 201-206.
- Williams, R.T., 1968: A note on quasi-geostrophic frontogenesis. *J. Atmos. Sci.*, **25**, 1157-1159.

Williams, R.T., L.C. Chou, and C.J. Cornelius, 1981: Effects of condensation and surface motion on the structure of steady-state fronts. *J. Atmos. Sci.*, **38**, 2365-2376.